Investigation on the physical and chemical properties of mortar using Metakaolin and Bagasse ash as a Partial Replacement of Ordinary Portland Cement

Yodit Birhanu Bereda

A Thesis Submitted to

The Department of Materials Science and Engineering
School of Mechanical, Chemical, and Materials Engineering

Presented in Partial Fulfillment of the Requirement for the Degree of Master's in Materials Science and Engineering

Office of Graduate Studies
Adama Science and Technology University

June-2022
Adama, Ethiopia

Investigation on the physical and chemical properties of mortar using Metakaolin and Bagasse ash as a Partial Replacement of Ordinary Portland Cement

Yodit Birhanu Bereda

Advisor: Temesgen Debelo D. (Ph.D.)

Co-advisor: Belay Brhane (Ph.D.)

A Thesis Submitted to

The Department of Materials Science and Engineering

School of Mechanical, Chemical, and Materials Engineering

Presented in Partial Fulfillment of the Requirement for the Degree of Master's in Materials Science and Engineering

Office of Graduate Studies
Adama Science and Technology University

June-2022.G.C
Adama, Ethiopia

DECLARATION

I hereby declare that this Master Thesis entitled "**Investigation on the physical and chemical properties of mortar using Metakaolin and Bagasse ash as a Partial Replacement of Ordinary Portland Cement**" is my original work. That is, it has not been submitted for the award of any academic degree, diploma or certificate in any other university. All sources of materials that are used for this thesis have been duly acknowledged through citation

Yodit Birhanu Bereda	_____	_____
Name of the student	Signature	Date

RECOMMENDATION

I/we, the advisor(s) of this thesis, hereby certify that I/we have read the revised version of the thesis entitled "**Investigation on the physical and chemical properties of mortar using Metakaolin and Bagasse ash as a Partial Replacement of Ordinary Portland Cement**" prepared under my/our guidance by Yodit Birhanu Bereda submitted in partial fulfillment of the requirements for the degree of Mater's of Science in Materials Science and Engineering. Therefore, I/we recommend the submission of a revised version of the thesis to the department following the applicable procedures.

Temesgen Debelo D. (Ph.D.)	_____	_____
Major Advisor	Signature	Date
Belay Brehane (Ph.D.)	_____	_____
Co-advisor	Signature	Date

APPROVAL PAGE

I/we, the advisors of the thesis entitled "**Investigation on the physical and chemical properties of mortar using Metakaolin and Bagasse ash as a Partial Replacement of Ordinary Portland Cement**" and developed by Yodit Birhanu Bereda, hereby certify that the recommendation and suggestions made by the board of examiners are appropriately incorporated into the final version of the thesis.

Temesgen Debelo D. (Ph.D.	_____	_____
Major Advisor	Signature	Date
Belay Brehane (Ph.D.)	_____	_____
Co-advisor	Signature	Date

We, the undersigned, members of the Board of Examiners of the thesis by Yodit Birhanu Bereda have read and evaluated the thesis entitled "**Investigation on the physical and chemical properties of mortar using Metakaolin and Bagasse ash as a Partial Replacement of Ordinary Portland Cement**" and examined the candidate during open defense. This is, therefore, to certify that the thesis is accepted for partial fulfillment of the requirement of the degree of Master of Science in Material Science and Engineering.

_____	_____	_____
Chairperson	Signature	Date
_____	_____	_____
Internal Examiner	Signature	Date
_____	_____	_____
External Examiner	Signature	Date

Finally, approval and acceptance of the thesis is contingent upon submission of its final copy to the Office of Postgraduate Studies (OPGS) through the Department Graduate Council (DGC) and School Graduate Committee (SGC).

_____	_____	_____
Department Head	Signature	Date
_____	_____	_____
School Dean	Signature	Date
_____	_____	_____
Office of Postgraduate Studies, Dean	Signature	Date

ACKNOWLEDGMENTS

First and foremost, I would like to praise and thank God, the Almighty, who has granted me countless blessings, knowledge, and opportunity, so that I have been finally able to accomplish the thesis.

I would like to express my gratitude and sincere to my advisor Dr. Temesgen Debelo for his patience, guidance, and very constructive criticism. His guidance helped me in all the time of research and writing of this thesis. I would like to express my deep gratitude to my co-advisor Dr. Belay Brehane for his timely valuable advice and insightful comments. I would like also to express my deep gratitude to the quality control manager of Habesh Cement Factory Mr. Abraham Tezera and Physical Chemist Mr. Petiros Gadisa for allowing me to conduct my thesis experiments in all possibilities.

My thanks also extend to Mr. Demeke Tesfaye, and all staff members of the Materials Science and Engineering department. I would like to express my gratitude to ASTU for giving me this scholarship in grant number ASTU/SM- R/436/22 and for support by funding my thesis work. I would like to say thanks to Awash Melkasa Aluminum Sulfate Chemical Factory and Wonji Sugar Factories for their support in providing their waste products.

Last but not least, I would like to thank my family, especially my mother W/ro, Ergo Tessema, and my long-time classmates who supported me through their inspiration and advice. Finally, my thanks go to all the people who have supported me to complete the research work directly or indirectly.

Table of Contents

DECLARATION ii
RECOMMENDATION iii
APPROVAL PAGE iv
ACKNOWLEDGMENTS v
LIST OF TABLES ix
LIST OF FIGURES x
LIST OF ACRONYMS AND SYMBOLS xii
ABSTRACT xiii
CHAPTER ONE 1
1. INTRODUCTION 1
1.1. Background of the Study 1
1.2. Statement of the Problem 3
1.3. Objectives 4
1.4. Significance of the Study 4
1.5. Scope of the Study 4
CHAPTER TWO 6
2. LITERATURE REVIEW 6
2.1 Portland Cement 6
2.2 Hydration Reaction of Cement 7
2.3 Supplementary Cementitious Materials 12
2.4 Blended or Composite Cement 23
2.5 Research Gap 25
CHAPTER THREE 26
3. MATERIALS AND METHODS 26
3.1 Materials and Chemicals 26
3.2 Measuring and Characterization Techniques 26
3.3 Experimental Procedures 27
3.3.1 Collection and Pre-treatment of Metakaolin (MK) 27
3.3.2 Collection and Pre-treatment of Bagasse Ash 28
3.3.3 Preparation of Metakaolin (MK)-Blended OPC Mortar Samples 29
3.3.4 Preparation of Bagasse Ash (BA)-Blended OPC Mortar Samples 30
3.3.5 Preparation of MK-BA Blended OPC Mortar Samples 30

3.3.6 Preparation Procedures of the Mortar for all Specimens 31
3.3.7 Blended Cement Pastes Preparation 33
3.4 Mechanical, Physical, and Chemical Property Test 34
3.4.1 Determination of the Flexural and Compressive Strength 34
3.4.2 Chemical analysis with X-ray fluorescence spectroscopy (XRF) 35
3.4.3 Determination of density of samples 35
3.4.4 Determination of Fineness of the samples 36
3.4.5 Setting Time Determination 37
3.4.6 Expansion Test 38
3.4.7 Durability Test 40
3.4.8 Electrochemical Corrosion Measurements 41
CHAPTER FOUR 43
4 RESULTS AND DISCUSSION 43
4.1 Characterization of MK and MK Blended OPC Mortar/paste 43
4.1.1 Mineralogical compositions of Metakaolin (MK) 43
4.1.2 XRD Analysis of Filter Cake-Kaolinite, MK blended paste 44
4.1.3 FTIR Analysis of Filter Cake (Kaolinite), MK, -blended paste 47
4.1.4 Thermal Analysis of filter cake-kaolinite and mortar samples 49
4.1.5 Flexural and compressive strength of MK-Blended OPC-mortar 51
4.1.6 Setting time and Expansion of Mk-Blended OPC-pastes 53
4.1.7 Water absorption and apparent porosity of MK-Blended OPC Mortar . 55
4.1.8 Microstructure characterization of MK and MK-blended mortar 56
4.2 Characterization of BA and BA Blended OPC Mortar/paste 58
4.2.1 Mineralogical Compositions of Bagasse Ash (BA) 58
4.2.2 XRD Analysis of Calcined Bagasse ash 59
4.2.3 Phase Analysis of Hardened 0% and 15% BA Blended Mortar. 62
4.2.4 FTIR Analysis of BA (300℃), BA (600℃), and BA-Blended paste 63
4.2.5 Thermal Analysis of BA and BA-Blended mortar samples 65
4.2.6 Flexural and Compressive Strength of BA-Blended OPC-Mortar 67
4.2.7 Setting time and Expansion of BA-Blended OPC-pastes 69
4.2.8 Water Absorption and Apparent Porosity of BA-Blended OPC Mortar 70
4.2.9 Microstructure Characterization of BA and BA-Blended Mortar 72
4.3 Characterization of Composites MK/BA/OPC blended Mortar/paste 73

4.3.1 XRD Analysis of Composite MK-BA /OPC Paste 73
4.3.2 Thermal Analysis of MK-BA Blended Mortar 74
4.3.3 Flexural and Compressive Strength of MK-BA OPC-Mortar 75
4.3.4 Setting Time and Expansion of MK-BA Blended OPC-Pastes 76
4.3.5 Water Absorption and Apparent Porosity of MK-BA Blended 78
4.3.6 Potentiodynamic polarization curve of MK-BA Blended Mortar..... 79
4.3.7 Microstructure Characterization of Composite Blended Mortar..... 80
CHAPTER FIVE..... 82
5 CONCLUSIONS AND RECOMMENDATION 82
5.1 Conclusion 82
5.2 Recommendation 83
REFERENCE..... 84
Appendix..... 95

LIST OF TABLES

Table 2.1 Composition of the cement clinker (Dunuweera & Rajapakse, 2018) 7
Table 2.2 Mechanical and physical (ES 1177-1:2005) (MESERET). 8
Table 2.3. Annual sugar production capacity and expected BA amount (Tekleab, 2016) 22
Table 2.4 Summary of Literature Review 24
Table 3.1 Mixing proportion of MK-Blended OPC mortars, Cement: Sand = 1: 3... 30
Table 3.2 Mixing proportion of BA-Blended OPC mortars, Cement: Sand = 1: 3. .. 30
Table 3.3 Mixing proportion of MK-BA Blended OPC mortars. 31
Table 3.4 Summary of Experimental Program Used in this Thesis work 42
Table 4.1 Chemical composition of filter cake-kaolinite, MK, and Habesha OPC ... 43
Table 4.2 Chemical composition of Sugarcane Bagasse Ash (BA) 59
Table 4.3 Parametr Obtained from Tafel Plot 79

LIST OF FIGURES

Figure 2.1 Transformation of the raw materials into clinker(P.-C. Aïtcin, 2016). 6
Figure 2.2 Ternary diagram of PC and SCMs (Lothenbach et al., 2011). 13
Figure 2.4. Setting times at standard water of consistency (Ibrahim et al., 2017)..... 19
Figure 2.5 Mortar incorporating propylene fibers (Akbar et al., 2021) 21
Figure 2.6 Cement demand and bagasse ash production (Tekleab, 2016)..... 22
Figure 3.1 Filter cake (kaolinite) as landfill at AMASSAF Ethiopia. 27
Figure 3.2. Metakaolin materials preparation from the filter cake. 28
Figure 3.3 Bagasse ash as landfill at Wonji sugar factory, Ethiopia. 29
Figure 3.4 flow chart for preparation of bagasse ash 29
Figure 3.5 (a) Automatic mortar mixer, (b) jolting table, (c) Compacted specimens, ... 32
Figure 3.6 (a) CEN Standard Sand, (b) prisms mold, and (c) De-mold specimens . 33
Figure 3.7 Paste mixer machine 34
Figure 3.8 (a) flexural strength machine and (b) Compressive Strength machine.... 35
Fig.3.9 (a) kerosine in Pycnometer, (b) MK in Pycnometer and (c) settling 36
Figure 3.10 FBT-9 Automatic Specific Area Tester 37
Figure 3.11 Vicat Apparatus for the Determination of Setting Time 38
Figure 3.12 Le-Chatlier Expansion Measurements..... 40
Figure 3.13 (a) Specimen for a durability test, (b) Dry weight and (c) Suspended weight 41
Figure 3.14 (a) Potentiodynamic Measurments and (b) Corrosion cell kit..... 41
Figure 4.1 XRD pattern of metakaolin and filter cake (kaolinite) waste 45
Figure 4.2 XRD pattern of 0% and 10 % MK blended OPC cement paste. 47
Figure 4.3 FT-IR analysis of filter cake-kaolinite and Metakaolin..... 48
Figure 4.4 FI-IR Spectra of control (0%) and 10% MK blended OPC paste..... 49
Figure 4.5 TGA and DTA analysis for filter cake-kaolinite 50
Figure 4.6 TGA and DTA analysis for 0% and 10% MK blended mortar samples. . 51
Figure 4.7 Flexural strength of 0-20% MK-blended OPC mortars..... 52
Figure 4.8 Compressive strength of 0-20% MK-blended OPC mortars 53
Figure 4.9 Setting times at normal consistency of MK- OPC blended pastes. 54
Figure 4.10 Expansion of Control OPC paste (CO) and MK-OPC blended pastes... 55
Figure 4.11 MK blended OPC mortar (a) Water absorption; and (b) Apparent porosity 56
Figure 4.12 SEM result for a) FC before treatment(Kaolinite) and b) FC after treatment (MK) 57
Figure 4.13 SEM image of a) OPC, b) 10% MK blended OPC paste and c) Insitu image 58
Figure 4.14 XRD pattern of BA calcined at different tempratures 62
Figure 4.15 XRD pattern of 0% and 15 % BA blended OPC cement paste 63
Figure 4.16 FT-IR analysis of pretreated Bagasse ash and post-treated Bagasse ash 64
Figure 4.17 FI-IR Spectra of control and 15% BA blended cement paste..... 65

Figure 4.18 TGA and DTA analysis for Bagasse ash sample. 66
Figure 4.19 TGA and DTA analysis for 0% and 15% BA blended mortar samples . 67
Figure 4.20 Flexural strength of BA-Blended OPC mortar 67
Figure 4.21 Compressive Strength of BA-Blended Cement Mortar. 68
Figure 4.22 Setting times at normal consistency of BA- OPC blended pastes. 69
Figure 4.23 Expansion of Control OPC paste (CO) and BA-OPC blended pastes. ... 70
Figure 4.24 BA blended OPC-mortar (a) Water absorption and (b) Apparent porosity 71
Figure 4.25 SEM image of (a) BA at 300℃, (b) BA at 600℃, (c) 15% BA OPC paste and (d) Insitu image 72
Figure 4.26 Phase analysis of MK-BA Blended paste 74
Figure 4.27 DTA/TGA analysis of 5% MK-10% BA Blended cement paste 75
Figure 4.28. Flexural strength of 5% MK, 10% BA, and 5% MK-10% BA 76
Figure 4.29 Compressive strength of 5% MK, 10% BA, and 5% MK-10% BA 76
Figure 4.30 Setting times at normal consistency blended pastes 77
Figure 4.31 Expansion of 5% MK, 10% BA, and MK-BA/OPC Blended Pastes 77
Figure 4.32 Blended OPC-paste; (a) Water absorption; (b) Apparent porosity 79
Figure 4.33 Tafel extrapolation plot of different blended mixed cement paste 80
Figure 4.34 SEM image of 5% MK-10% BA blended composite paste 81

LIST OF ACRONYMS AND SYMBOLS

AAS	Atomic Absorption Spectroscopy
ASCF	Aluminum Sulfate Chemical Factory
ASR	Alkali-Silica Reaction
ASTM	American Society for Testing and Materials
BA	Bagasse Ash
BFS	Blast Furnace Slag
C-A-S-H	Calcium Alumino Silicate Hydrated
C-H	Calcium Hydroxide
C-S-H	Calcium Silicate Hydrated
FC	Filter Cake (waste)
FST	Final Setting Time
GGBFS	Ground Granulated Blast Furnace Slag
GGBFSC	Ground Granulated Blast Furnace Slag Cement
ITZ	Interfacial Transition Zone
IST	Initial Setting Time
MK	Metakaolin (treated filter cake)
PC	Portland Cement
SCBA	Sugar Cane Bagasse Ash
SCC	Self-Compacting Concrete
SCM	Supplementary Cementitious Materials
SEM	Scanning Electron Microscope
SF	Silica-Fume
UCS	Ultimate Compressive Strength
UHPC	Ultra-High-Performance Concrete
XRD	X-Ray Diffraction
℃	Degree centigrade
Θ	Half Diffraction angle

ABSTRACT

In recent years, the transformation of industrial waste into products of commercial interest and utilization of these products plays a crucial role to ensure the circular economy and thereby safeguard the environmental impacts. Filter cakes are the by-product materials of the Aluminate Sulphate chemical factory, Ethiopia. These materials have a similar chemical composition as that of kaolinite and they are simply dumped in a landfill in a factory. Similarly, sugarcane bagasse ash is an abundant by-product of sugar industries, here in Ethiopia, which is disposed of in a landfill. If these by-product materials are collected and pre-treated, they can be used as a partial replacement for cement materials. In this work, the filter cake and the bagasse ash (BA) byproducts were collected from Awash Melkassa and Wonji Sugar factories, respectively. The collected samples were subjected to pretreatments such as size reduction, washing, oven drying, and calcination at a temperature of 600 °C. The pre-treated samples were subjected to characterizations such as chemical composition analysis using XRF, phase purity investigation using XRD, thermal analysis using TGA-DTA, morphological studies using SEM, and functional group determination using FTIR. From the XRF result, the treated filter cake exhibited similar composition as that of metakaolin (MK). Then, the blended mortar/paste was prepared by partial replacement of OPC by MK (0-20 wt%). The result of the XRD of the pre-treated BA showed an amorphous structure. Therefore, a blended mortar/paste was synthesized from partially replaced OPC by amorphous structured BA (0-20 wt%). The mortar/paste samples were subjected to characterizations and mechanical (flexural and compressive) as well as physical property investigations. We obtained better mortar sample properties using 10 % MK partial replacement of OPC cement. While the 15 % BA blended OPC-mortar sample showed a better property compared to neat mortar samples. However, these percentage composite blended mortar do not show better properties. Therefore, experimentally investigating 5% MK and 10% BA results in better performance. The ternary mortar/paste was subjected to characterizations and mechanical, physical, and chemical property investigations. The compressive strength of the neat OPC mortar sample was 44 MPa, 10%MK, and 15% BA, was about 52 MPa, and ternary composite (5%MK-10% BA) about 57 MPa after 28 days of curing time. after 28 days of curing time. The le-Chatelier expansion of the neat paste sample was 0.85, with the addition of MK decreased to 0.4, showing an increment with the addition of BA results of 2.4 mm, while the composite paste resulted in 0.95 mm expansion. The addition of treated waste materials improves the mechanical, physical, and chemical properties of the OPC blended mortar/paste sample.

Keywords: Filter cake; Metakaolin; Bagasse Ash; Amorphous; Pozzolanic; Paste; Mortar

CHAPTER ONE

1. INTRODUCTION

1.1. Background of the Study

In recent years, partially substituting cement with waste materials has garnered a lot of attention due to considerable CO_2 emissions from cement enterprises, the high cost of cement, and the need to improve cement quality (Fairbairn et al., 2010; Worrell et al., 2001). Typically, ashes of rice husk (Papadakis & Tsimas, 2002), bagasse(Deepika et al., 2017; P. Zhang et al., 2020), coffee husk (Deepika et al., 2017), cob corn (Adesanya & Raheem, 2009), fly ash (Tan et al., 2019), and silica fume (Song et al., 2010) were studied as their pozzolanic nature has highly reactive amorphous siliceous and aluminous materials. Currently, industrial waste materials are becoming a serious problem for human beings as well as ecology due to inadequate disposal causes environmental degradation and pollution of soil and water bodies. The recycling of industrial wastes in the productive chain has emerged as an alternative material for minimizing the damage that industrial waste can produce. The Awash Melkassa Aluminum Sulphate in Ethiopia is producing 1,700 tonnes of useful chemicals annually and meantime filter cake(kaolinite) byproducts are disposed of in landfills (Yager, 2010). In the previous study, types of soils mainly clays and waste material from coal mining were examined for the use of alternative cementitious materials. Kaolinite has a higher pozzolanic activity due to the amount and position of OH groups in its structure, as well as a dissimilar breakdown process and loss of crystallinity (Fernandez et al., 2011). Filter cake(Kaolinite) clay impurities, such as Fe_2O_3, TiO_2, and high levels of quartz (SiO_2) (Koutnik et al., 2019), are less of an issue to use as Supplementary cementitious Materials (SCMs) since they do not change pozzolanic activity (de Oliveira et al., 2021).

Furthermore, bagasse ash is a byproduct of sugar plants that is disposed of away at a landfill. Researchers are trying to use these waste materials in meantime to improve the basic properties of cement and reduce CO_2 emissions. At 28 days of curing age, OPC with partial bagasse ash enhanced compressive strength compared to standard concretes (Bahurudeen et al., 2015). Mixed bagasse ash-blended concretes can also improve concrete durability (Lima et al., 2011), and lower the heat of hydration (Chusilp et al., 2009b). However, industrial bagasse ash contains a lot of carbon and unburned organic stuff (Embong et al., 2016). It has a detrimental impact on concrete characteristics and reduces its workability P.D. Trifunovic et al. highlighted how carbon has a detrimental influence on the compressive strength of

bottom ash-blended mortar samples (Trifunovic et al., 2010). As a result, we anticipated that an optimal amount of control-burned bagasse ash replacement would have no adverse effect on the characteristics of Ordinary Portland Cement (OPC). Five (5) percent rice husk ash with an average particle size of 95 μm mixed OPC improved concrete durability and compressive strength from 36.8 MPa to 38.7 MPa after 28 days of curing (Givi et al., 2010). Ash-blended cement has the potential to lower cement manufacturing's energy utilization. Because of its ultra-fine particles, silica fume has also enhanced high-performance concrete, resulting in reduced porosity and the production of calcium silicate hydrate (C–S–H) gel (Elsayed, 2011; Kumar & Dhaka, 2016; Sabir, 1995).

For construction materials particularly mortar and concrete, Cement's usefulness has been rising for decades. This is due to its mechanical qualities and cost-effectiveness, especially when compared to other accessible materials. On the other hand, Cement manufacture, has a significant environmental impact, consuming a vast amount of natural resources and emitting almost a ton of CO_2 into the sky with every ton of Ordinary Portland Cement (OPC) production (Meyer, 2009). It has been estimated that cement production will reach up to four billion tonnes each year by 2030 (Jaishankar et al., 2021). Cement production accounts for more than 5% of all man-made greenhouse gas emissions (Hendriks et al.). Such a negative impact on the environment opens the door for alternative materials that cut CO_2 emissions, reduce uncontrolled natural resource consumption, and recycle industrial and agricultural waste.

Carbon dioxide emission from the cement industry is mostly due to: (a) the composition of fossil fuels in the industrial process since in the rotating kiln materials are required to burn up to 1450 ℃ (Al-Mansour et al., 2019; Gartner, 2004). (b) the major component of cement needs the decomposition of limestone $CaCO_3$ into calcium oxide (CaO) and carbon dioxide (CO_2) (Turner & Collins, 2013). Several types of research are undergoing in the world to overcome these problems through substituting alternative materials. Cement's fresh and hardened characteristics have been successfully improved, for instance, metakaolin (MK) (Lagier & Kurtis, 2007), Fly Ash (FA) and Silica Fume (SF) were used as partial replacements for cement and they reduced the time it took for mass concrete constructions to set while maintaining long-term strength. (Hela et al., 2016; Li, 2004; Ravina & Mehta, 1986). Ground Granulated Blast Furnace Slag (GGBFS) and municipal solid waste ash were partially replaced, resulting in a considerable reduction in CO_2 emissions (Crossin, 2015; Deb et al., 2014) and heat of hydration (Topçu & Ünverdi).

The amorphous nature and amount of pozzolanic oxides in the industrial waste materials are crucial to use as a replacement for cement (Moumin et al., 2020). Among alternative industrial waste materials in Ethiopia, filter cake(kaolinite) waste materials contain the required amount of pozzolanic oxides, simple thermal treatment can change to amorphous state materials, a huge amount of these materials available, and currently, these waste materials are causing a problem to the nearby community. Metakaolin's crystalline structure is broken down by calcination temperatures, which are in general lower than those necessary to generate the liquid phase and produce glassy liquid (B. B. Sabir et al., 2001).

In this paper, we focused on the investigation of the waste products treatment and making them pozzolanic materials. The metakaolin and calcined BA are used as a supplementary cementitious material in mortar/paste preparation. We prepared mortar samples using OPC cement, Metakaolin (0-20%) and BA (0-20%), sand, and water. Heat-treated filter cake (kaolinite) waste materials have higher pozzolanic reactivity and were used for Ordinary Portland Cement (OPC) partial replacement. Calcine BA also have pozzolanic properties and used as partial replacement of OPC. We compared flexural and compressive strengths of MK-blended OPC and BA-blended mortar samples with control mortar samples. Flexural strength & compressive strengths of blended mortars were improved with certain MK and BA replacement OPC cement. By trying the better compressive strength, a composite of 5% Metakaolin and 10% Bagasse ash was also developed as a partial replacement.

1.2. Statement of the Problem

Cement in the construction sector is the primary component of concrete/mortar. Urbanization has accelerated the rate of construction activities therefore there is high demand for cement production. However, the high demand for cement has further led to the excessive exploitation of natural resources as raw materials and the emission of CO_2. Thus, reduction of the extensive exploitation of limited raw materials and carbon dioxide emissions associated with Portland cement production are the foremost challenges faced by the cement industry (Jokar & Mokhtar, 2018). There is also a high interest in improving the properties of OPC cement for various applications especially salty water in marine construction. Moreover, some waste pollutes the environment in our case filter cake and bagasse ash. In this work, the industrial waste products were treated to result in pozzolanic properties and used as a partial replacement for OPC cement. The blended cement mortar samples result in improved mechanical, physical, and chemical properties. Furthermore, it reduces environmental pollution and cost.

1.3. Objectives

1.3.1. General Objective

- The main objective of this thesis work is to investigate the properties of mortar samples using Metakaolin and Bagasse ash as Partial Replacement for Ordinary Portland Cement.

1.3.2 Specific Objectives

The specific objectives of this thesis work are:

- To examine Metakaolin and Bagasse Ash as pozzolanic materials;
- To characterize the chemical composition and morphology of filter cake, MK, BA, and blended mortar
- To analyze the mechanical, and physical properties of metakaolin-Blended, and Bagasse ash blended OPC mortar/paste;
- To investigate the mechanical, physical, and chemical properties of composite (bagasse ash and metakaolin) blended mortar/paste.

1.4. Significance of the Study

This study will have the following overall significance:

- Better properties of treated waste (FC, BA) blended OPC Mortar;
- Reuse of solid waste materials (Filter Cake-Bagasse ash);
- Conservation of natural resources;
- Reduction of CO_2 emissions;
- Potential to create job opportunities for microenterprises to collect and transport industrial solid waste products (Metakaolin and Sugarcane bagasse ash);
- Making green and eco-friendly construction materials and minimizing hazards to the environment.

1.5. Scope of the Study

The scope of this study is to search for industrial waste that has the potential to use as supplementary cementitious materials. After selecting the waste materials, the best process used to make the waste materials pozzolanic materials. The first waste materials were collected from AMCF and treated at 600h/2h. the second waste materials were collected from Wonji Sugar Factories followed by calcination. After producing the pozzolanic

materials the partial replacement is produced with mortar and paste formation, finally, investigate the properties of ternary blended mortar samples for construction materials. In this study, the cost-benefit of using waste materials is not discussed.

CHAPTER TWO

2. LITERATURE REVIEW

2.1 Portland Cement

Portland Cement is the result of the production of clinker through the complex pyro processing presented in Figure 2.1 (P. C. Aïtcin, 2016). Portland cement is a generally used binder material to form the heterogenous mortar or concrete matrix. It's principally made by burning an admixture of limestone and complexion, or other accouterments of analogous bulk composition and sufficient reactivity, eventually to a temperature of about 1450 ˚C. Partial emulsion occurs, and nodes of clinker are produced. The clinker generally has a composition in the region of 67% CaO, 22% SiO_2, 5% Al_2O_3, 3% Fe_2O_3, and 3% other factors, and typically contains four major phases, called alite, belite, aluminate, and ferrite (Bourchy et al., 2020). Several other phases, such as calcium oxide and alkali sulfates, are normally present in minor amounts.

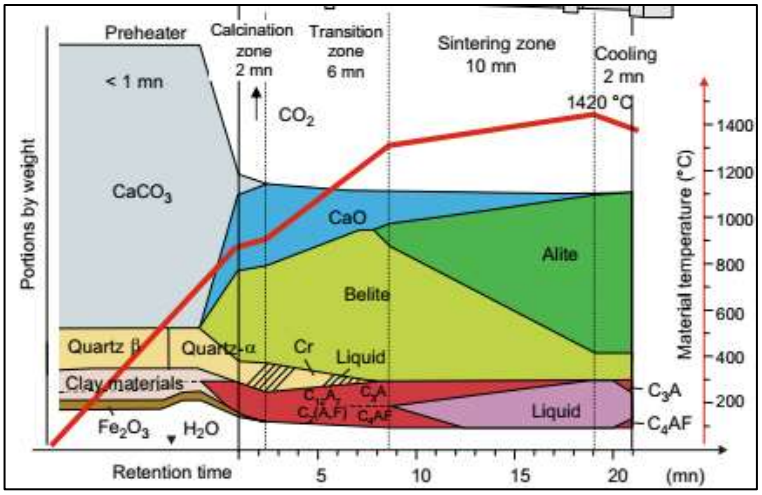

Figure 2.1 Transformation of the raw materials into clinker(P.-C. Aïtcin, 2016).

Alite is the most important element of all normal Portland cement components, of which it constitutes 50-70%. Its tricalcium silicate (Ca_3SiO_5) is modified in composition and demitasse structure by ionic negotiations (Fernández et al., 2018). It reacts fairly snappily with water, and in normal Portland, cement is the most important of the constituent phases for strength development; at periods up to 28 days, it's by far the most important.

Belite constitutes 15-30% of normal Portland cement components. Its dicalcium silicate (Ca_2SiO_4) is modified by ionic negotiations and typically presented wholly or largely as the β polymorph. It reacts sluggishly with water, therefore contributing little to the

strength during the first 28 days, but mainly to the further increase in strength that occurs at latterly periods. At one time, the strengths accessible from pure alite and pure belite are about the same under similar conditions (P.-C. Aïtcin, 2016). Aluminate constitutes 5-10% of the utmost normal Portland cement components. It's tricalcium aluminate ($Ca_3Al_2O_6$), mainly modified in composition and occasionally also in a demitasse. Structure by ionic negotiations. It reacts quickly with water and can beget vastly rapid-fire settings unless a set-controlling agent, generally gypsum, is added (Pintér & Gosselin, 2018). Ferrite makes up 5-15% of normal Portland cement disasters. It's tetra calcium aluminoferrite (Ca_2AlFeO_5), mainly modified in composition by variation in Al/ Fe rate and ionic negotiations. The rate at which it reacts with water appears to be kindly variable, maybe due to differences in composition or other characteristics, but in general is high originally and low or veritably low at latterly periods (Bourchy et al., 2020).

Table 2.1 Composition of the cement clinker (Dunuweera & Rajapakse, 2018)

Chemical Name	Chemical formula	Shorthand Notation	Weight percentage
Tricalcium silicate	$3CaO.SiO_2$	C_3S	55
Dicalcium silicate	$2Ca.SiO_2$	C_2S	20
Tricalcium aluminate	$3CaO.Al_2O_3$	C_3A	10
Tetracalcium aluminoferrite	$4CaO.Al_2O_3.FeO_3$	C_4AF	8
Calcium sulfate dehydrate (gypsum)	$CaSO_4.2H_2O$	CSH_2	5

2.2 Hydration Reaction of Cement

In strictly chemical terms hydration is a reaction of an anhydrous compound with water, yielding a new compound, a hydrate. In cement, chemistry hydration is understood to be the reaction of non-hydrated cement or one of its constituents with water, associated with both chemical and physicomechanical changes in the system, in particular with setting and hardening. Partial hydration of cement may even take place in humid air, whereas, for complete hydration the cement must be mixed with sufficient amounts of water (Panesar, 2019).

Table 2.2 Mechanical and physical (ES 1177-1:2005) (MESERET).

Physical and Mechanical Requirement of Cement Determine under EN 196-3 and EN 196-1. Compressive Strength (N/mm²					**Initial setting Time (min)**	**Expansion (mm)**
Class	Early Strength		Stand strength 28 days			
	3 days	7 days				
32.5 N **32.5 R**	- ≥ 10	>16 -	≥ 32.5	≤ 52.5	>75	≤ 10
42.5 N **42.5 R**	≥ 10 ≥ 20	- -	≥ 42.5	≤62.5	≥ 60	
52.5 N **52.5 R**	≥ 20 ≥ 30	- -	≥ 52.5	-	>45	

As Portland cement is a multi-component system, its hydration is a rather complex process consisting of a series of individual chemical reactions that take place both in parallel and successively. The process gets underway spontaneously upon contact of the binder with water and is associated with the liberation of heat. The hydration of the silicate phases, which make up approximately 75% of ordinary Portland cement, affects the rate of strength development. The progress of hydration and its kinetics are influenced by a variety of factors, especially (P. C. Aïtcin, 2016):

- by the phase composition of the cement and the presence of foreign ions within the crystalline lattices of the individual clinker phases;
- by the fineness of the cement, in particular by its particle size distribution and specific
- surface;
- by the water-cement ratio used;
- by the curing temperature;
- by the presence of chemical admixtures, i.e., chemical substances added in small amounts to modify the hydration rate and properties of the cement paste;
- by the presence of additives, i.e., materials interground with cement in larger amounts, such as granulated blast furnace slag or pulverized fly ash.

The major components of cement that react with water to produce reaction products are tricalcium silicate (C_3S), dicalcium silicate (C_2S),tricalcium aluminate(C_3A), and tetra calcium alumionferite (C_4AF) (Bullard et al., 2011). The important strength-developing hydration reactions are those of C_3S and C_2S. Typical hydration reactions would be presented in equations 2.1 and 2.2:

For C_3S: $2C_3S + 6H$ (water) → $C_3S_2H_3$ (“tobermorite” gel) + 3CH (hydrated lime) ……..……. (2.1)

For C2S: $2C_2S + 4H \rightarrow C_3S2H_3 + CH$……. (2.2)

The formula shown for tobermorite is only approximate, and some texts denote it as $C_3S_2H_4$, in which case both hydration equations above would need additional water (H) to start with. Actually, instead of just tobermorite, a whole family of similar calcium silicate hydrates (C-S-H) may be formed, and C-S-H is the preferred general term for these compounds. It is the C-S-H colloid or gel that is the actual binder in hydrated Portland cement. The ultimate strength of the hardened cement paste will depend not only on the original total content of C_2S and C_3S but also on the completeness of their hydration.

Although the net hydration reactions for both C_3S and C_2S are similar, the reaction for C_3S is relatively fast, and C-S-H from it is responsible for virtually all of the early (e.g., within 3 days of curing) strength development of the cement. Typically, about 60% (by mass) of the C_3S has hydrated to C-S-H within the first 5 days of curing and about 70% has hydrated within about 10 days. Because of the formation of protective hydration shells, the remaining unreacted C_3S particle cores hydrate much more slowly, reaching about 75% hydration after 20 days of curing, about 80% hydration after 28 days (a standard measurement interval), and 85% after 60 days. Beyond 60 days, the rate of C_3S hydration slows dramatically and the incremental hydration and strength contribution is of little practical importance.

In contrast, the hydration of C_2S is relatively slow, with only about 20% hydration after 5 days of curing, about 30% after 10 days, 35% after 20 days, about 40% after 28 days, and only about 55% at 60 days. Its rate of hydration slows further after 60 days. Accordingly, the C-S-H derived from the hydration of C_2S, while making little contribution to the early strength of the concrete, contributes a significant proportion of the strength gain after the first week or so of curing. As shown above, the C_3S and C_2S hydration reactions release free lime. Based on the typical clinker mineral proportions and their hydration reactions, it can be shown that the net free lime released during clinker hydration, overall, is roughly 25%–33% of the original CaO content of the clinker. Free lime in hardened concrete is not particularly desirable because it increases the chemical reactivity of the surface (including along cracks) and can leach out in an unsightly fashion. On the other hand, by maintaining a high pH in the aqueous phase, free lime can help protect steel reinforcing bars (rebar) in

the concrete from corrosion should water and oxygen reach the rebar via cracks. The lime is also available to react with any pozzolans that may have been added to the cement or concrete mix. Alkalis, particularly sodium (Na_2O, or N in shorthand), can combine with C-S-H to form complex hydrates (e.g., C-S-N-H) that are unstable and prone to swelling compared with regular C-S-H.

Alkalis can also react with forms (amorphous, opaline, or very fine-grained crystalline) of silica in some aggregates used in concrete, forming highly hygroscopic alkali-silicate hydrates (e.g., N-S-H), and generally weakening the bond between the aggregates and the cement paste and forming higher volume phases. These and similar reactions, collectively called Alkali-Silicate Reactions (ASR) or alkali-aggregate reactions, can cause cracking of hardened concrete. The cracks not only weaken the concrete but render its interior susceptible to additional alkali or other chemical attacks, and to freeze-thaw damage in cold-weather regions. Approaches to controlling ASR reactions include selecting Portland cement having lower alkali contents (e.g., ASTM C-150 provides for a low-alkali cement designation if the cement has a total alkali content [defined as Na_2O + 0.658 K_2O] content of 0.60% or less), testing of aggregates for reactivity, and the incorporation of pozzolans into the cement paste. Pozzolans contain active silica which sacrificially combines with the alkalis in the paste (thus leaving fewer alkalis available to react with the aggregates), and significantly reduce the hardened concrete ‘s porosity.

The other two clinker minerals, C_3A and C_4AF, have complex hydration reaction paths that are similar to each other, but those of C_3A is more important because they are much more rapid and exothermic. Having C_3A in the cement primarily enhances the initial set and speeds, via the release of heat, and the hydration of C_3S (the presence of C_3A also has benefits to the cement manufacturing process it speeds the overall formation of the clinker). In the absence of significant sulfate, C_3A very rapidly almost instantaneously forms C_3A-hydrates, many of which are unstable and may subsequently convert to other forms. One of the many possible sequential hydration reactions is presented in equation 2.3:

$$2C_3A + 21H \rightarrow C_2AH_8 + C_4AH_{13} \rightarrow 2\ C_3AH_6 + 9H \ldots\ldots (2.3)$$

A minor, but lime-consuming, reaction is present in equation 2.4:

$$C_3A + 12\ H + CH \rightarrow C_4AH_{13} \ldots\ldots (2.4)$$

The hydration of C_3A in the absence of sulfate can be so rapid as to cause the undesirable condition known as a flash set. This is controlled through the addition of sulfate, usually as gypsum and/or anhydrite. Plaster is only rarely used because it hydrates so quickly back to gypsum that its use is rather counterproductive. The use of plaster also increases initial water consumption. A typical hydration reaction of C_3A in the presence of rate-controlling sulfate (here shown as gypsum) would be discussed in equation 2.5:

$$C_3A + 3\,CH_2 + 26\,H \rightarrow C_6A\,3H_{32}\ \text{(ettringite)} \quad \text{(2.5)}$$

Flash set is controlled because ettringite forms a shell around the C3A particles, which slows water diffusion to, and hence the hydration of, the residual C_3A cores. Ettringite is stable only in the presence of excess sulfate. If this condition is not met (i.e., not enough gypsum present, or in the evolving conditions at the ettringite-residual C_3A core interface), then ettringite reacts with C_3A to form a monosulfate phase as equation 2.6:

$$C_6A\,3H_{32} + 2\,C_3A + 4H \rightarrow 3\,C_4A\,H_{12}\ \text{(“monosulfate”)} \quad \text{(2.6)}$$

Alternatively, C3A hydration under low sulfate conditions can be expressed by equation 2.7:

$$C_3A + 10H + CH_2 \rightarrow C_4AH_{12} \quad \text{(2.7)}$$

An important property of the monosulfate phase is that, in the presence of sulfate ions, it can re-form ettringite, such as by the reaction as stated in equation 2.8:

$$C_4A\,H_{12} + 2\,CH_2 + 16H \rightarrow C_6A\,3H_{32} \quad \text{(2.8)}$$

Ettringite has a molar volume of about 735 cubic centimeters (cm^3) per mole and monosolfate about 313 cm^3 per mole. Because of this volume difference, re-formation of ettringite from monosulfate can cause expansion of the concrete. This is not much of an issue while the cement paste has yet to harden, but if ettringite re-forms in hardened concrete, the result can be cracking or spalling of the concrete. This process is known as sulfate attack and is prevalent in regions (commonly desert areas) having sulfate-rich groundwater or it can occur if too much gypsum is present in the cement. Thus, the proportion of gypsum in the cement is important. Where sulfate attack from groundwater is likely, concretes are better made using a sulfate resistant Portland cement, such as Type II, or better yet, Type V; both have low concentrations of C_3A. Type IV cement would also show resistance to sulfate attack but would be less desirable for most applications because its relatively low C3S

content would cause it to develop strength relatively slowly. Alternatively, sulfate resistance is improved by using blended cement, as the addition of pozzolans lowers the overall C3A content of the cement paste and reduces the porosity (hence sulfate entry potential) of the concrete. The ferrite mineral C_4AF does not play a critical role in cement hydration. The chief value of ferrite is in its effects on kiln reactions to form C_3S. The hydration of C_4AF is broadly similar to that of C_3A, although the reactions tend to be slower and much less exothermic. The reaction stoichiometries will vary given the fact that, as noted earlier, C_4AF is merely a mean composition for the ferrite solid solution having end members C_6A_2F and C_6AF_2.

2.3 Supplementary Cementitious Materials

Supplementary cementing materials (SCMs) are used to partially replace the Portland cement component in concrete $SiO_2+Al_2O_3+Fe_2O_3 \geq 70\%$ (Kasaniya et al., 2019). Some examples of SCMs are the following: fly ash, slag cement, silica fume, and metakaolin. Although SCMs vary in origin, physical properties, and chemistry, all of them exhibit pozzolanic and/or cementitious properties (Saillio et al., 2021).

Today SCMs are widely utilized in concrete either in blended cement or added separately within the cement mixer. The use of SCMs such as blast-furnace slag, a byproduct from pig iron production, or fly ash from coal combustion, represents a viable solution to partially substitute PC. The use of such materials, where no additional clinkering process is involved, results in a big reduction in CO_2 emissions per ton of cementitious materials (grinding, mixing, and transport of concrete use very little energy compared to the clinkering process) and is also a means to utilize by-products of industrial manufacturing processes.

Araos Henríquez et al. (2021) reported Ladle furnace slag (LFS) as a partial cement replacement owing to its parallel chemical composition with Portland cement. However, its mineralogical composition needs to be considered due to problems with expansive reactions and lower cementing activity. Galitsky, C. and E. Worrell suggest the existence of considerable potential when compared to other industrialized countries. They examined over 40 energy-efficient technologies and measures and estimated energy savings, carbon dioxide savings, investment costs, and operation and maintenance costs for each of the measures (Galitsky & Worrell, 2008).

The most realistic solution is to use blended cement where cement is partially replaced with more sustainable materials. These alternatives must also develop adequate cementitious properties to maintain the mechanical properties of the cement-based materials, and are

therefore called SCMs. The chemistry of SCMs is commonly characterized by lower calcium content than Portland cement.

In blended cement, there is generally negligible reaction of the SCM on the first day. Nevertheless, the reaction of cement clinker is enhanced by SCM due to its physical presence; this is the so-called filler effect and can be attributed to two main factors. First, when SCM grains substitute clinker grains, there is relatively additional space available for the hydrates of the clinker phases to form in. Secondly, the surfaces of the SCM grains act as places for the heterogeneous precipitation and growth of hydrates. Figure 2.2. presents the relative positions of Portland cement, fly ash, slag cement, silica fume, and metakaolin on a ternary diagram ($CaOSiO_2Al_2O_3$).

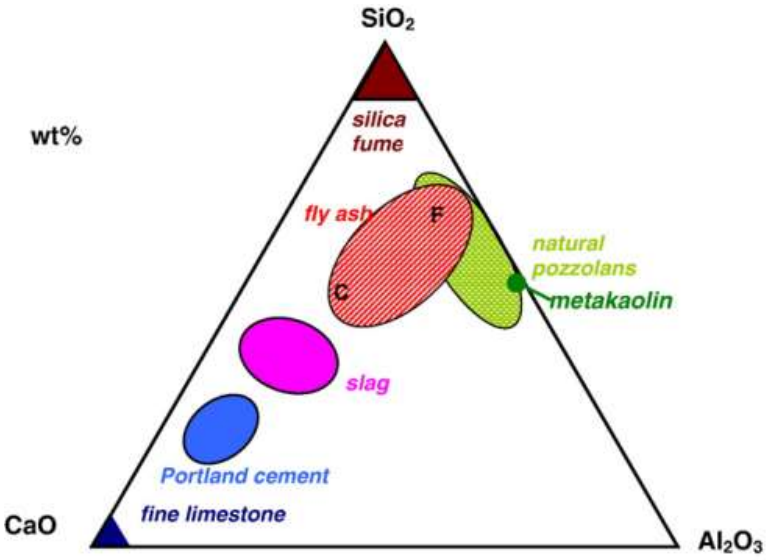

Figure 2.2 Ternary diagram of PC and SCMs (Lothenbach et al., 2011).

The consequence of a natural pozzolan on the compressive strength of concrete varies obviously with the properties of the particular pozzolan and with the characteristics of the concrete mixture in which it is used. The compressive strength development is a function of the chemical interaction between the natural pozzolan and the Portland cement during hydration (G. M. Barger et al., 2001). The goal of manufacturing concrete that gives long-term durability concerning properties like improved sulfate resistance and reduced susceptibility to alkali-silica reactions (ASR) has led to the event of several high-performance materials. While the utilization of fly ashes and ground granulated blast-furnace slags (GGBFS) in concrete is gaining acceptance in various applications, the mineralogical composition of such byproduct materials can't be as easily controlled as a manufactured pozzolan (G. S. Barger et al., 2001). It is well understood that the partial replacement of

hydraulic cement with pozzolans in sufficient proportions leads to the improved long- term strength.

2.3.1 Pozzolanic Properties

Pozzolans are a broad category of siliceous and aluminous minerals that, while having little or no cementitious value in themselves, will react chemically with calcium hydroxide in the presence of water at room temperature to generate cementitious compounds when finely divided. Most supplementary cementing materials have at least some pozzolanic properties. In the pozzolanic reaction the silica (SiO_2) in the pozzolan reacts with calcium hydroxide ($Ca(OH)_2$) and water to form calcium silicate hydrate, the main strength producing component of hydrated cement and concrete.

There are three characteristics of pozzolan that make it reactive. These are:

1. High silica content: Because silica is involved in the reaction with calcium hydroxide, the gel CSH is significant.

2. High degree of amorphousness: Because it has the lowest energy state, silica becomes organized in crystals when it cools from a disordered state like a gas or liquid. When it is rapidly cooled, however, it does not have time to arrange itself before solidifying, resulting in an amorphous structure (glass) or a structure that is halfway between crystalline and amorphous. The silica is metastable and consequently more reactive since this state has higher free energy than the crystalline state.

3. High degree of amorphousness: SSA provides more surface from which the material can react.

In addition, the clinker can be formulated to enhance the reactivity of the pozzolan. Since alkalis activate pozzolans, the alkali content of the clinker can be adjusted for optimal reactivity. Heat can also activate the pozzolanic reaction and, in the case of Class C fly ash, the cementitious reactions as well. The hydration of C_3A generates the most heat of any of the hydration reactions. The hydration of C_3S also generates heat well as calcium hydroxide, one of the reactants in the pozzolanic reaction. In addition, the particle size distribution of the clinker portion of the cement can be adjusted for enhanced reactivity by adjustments to the grinding circuit or simply by finer grinding.

The use of pozzolans to partially replace hydraulic cement in concrete has generally demonstrated beneficial impacts on the strength characteristics of concrete for many years. Kasaniya et al. (2021a) reported a various range of pozzolans including natural pozzolans, ground glasses, and industrial by-products like coal ash (fly ash and bottom ash) and silica fume for their synergistic potential in binary or ternary blends with hydraulic cement in improving resistance to chemical sulfate attack and alkali-silica reaction (ASR). it's generally considered that pozzolans improve most of the sturdiness issues encountered in concrete, including reducing the danger of sulfate attack or ASR (Kasaniya et al., 2021a). The factors affecting the activity of pozzolan are its content of (SiO_2 + Al_2O_3 + Fe_2O_3), its degree of crystallinity, and thus the fineness of its particles. Generally, the pozzolanic activity for various pozzolan is known to depend principally on the content of active SiO_2 and active Al_2O_3 components under the condition of a specific particle (Yu et al., 2015).

2.3.2 Industrial supplementary Materials

2.3.2.1 Fly Ash

Fly ash (FA) is an industrial byproduct of thermal power plants, which has mass storage worldwide (Gollakota et al., 2019). Its use as auxiliary cementing material in concrete is an important way to utilize FA. Furthermore, using FA in concrete can effectively reduce greenhouse gas emissions from cement production (Yao et al., 2015) and modify the properties of concrete (Narmluk & Nawa, 2011). Fly ash is a pozzolanic material. It is a finely-divided amorphous alumino-silicate with varying amounts of calcium, which when mixed with Portland cement and water, will react with the calcium hydroxide released by the hydration of Portland cement to produce various calcium-silicate hydrates (C-S-H) and calcium-aluminate hydrates (Thomas, 2007).

2.3.2.2 Ground Granulated Blast Furnace Slag (GGBFS)

GGBFS may be a by-product that processes both cementitious and pozzolanic properties. the utilization of by-products like furnace slag has been studied for years. Their use comprises both environmental and economic benefits, like conservation of resources, reduced gas emissions, and energy savings. It has been used as a supplementary cementitious for quite 100 years(Shreyas, 2017). The chemical composition of slag varies considerably betting on the composition of raw materials within the iron production process (Saafan et al., 2021). The utilization of furnace slag during the manufacture of cement is assumed to mitigate CO_2 emissions. Generally, the quantity of furnace slag within the slag cement

ranges from 36 try to 95 %. Slag cement is suitable for the assembly of all concrete classes, like large-scale engineering projects (roads, tunnels, bridges).

Slag (as a pozzolanic material) reacts very slowly, and the consumption of calcium hydrate mainly occurs at later ages. Thus, slag with a better pozzolanic activity should be used, and the early performance of the slag incorporated concrete, especially with the next slag content, should be specially monitored. The application of slag in concrete decreases the quantity of cement, which ends up in the reduction of both heat hydration and CO_2 emission(Tang et al., 2017). The employment of slag cement showed good mechanical behavior (compressive strength, modulus of elasticity) at high temperatures, whereas permeability showed a greater loss compared to Ordinary hydraulic cement (Zemri & Bachir Bouiadjra, 2020).

2.3.2.3 Silica Fume

Various types of industrial byproducts are produced. Commercial byproducts have become a lovely alternative to disposal as people have become more mindful of the environment's possible dangers. Silica fume (SF) is one such by-product, which is a by-product of the smelting process in the silicon and ferrosilicon industries. The use of silica fume in the design and development of high-strength, high-performance concrete is extremely effective. (Siddique, 2011). Siddique R. (Siddique, 2011) Industrial byproducts come in a variety of forms. As individuals have become more aware of the potential risks to the environment, commercial byproducts have become a lovely alternative to trash. The silicon and ferrosilicon industries produce silica fume (SF), which is a by-product of the smelting process. It is particularly effective to use silica fume in the design and development of high-strength, high-performance concrete.

Motahari K. et al. wrote a paper that deals with the effect of silica fume as a partial replacement in concrete for cement increasing the sturdiness of ferroconcrete and reducing cement usage. The obtained results indicated a rise in strength and surface electrical resistivity, and a decrease in permeability for both slurry silica fume and granule, compared to the control sample (Motahari Karein et al., 2017). Tripathi D. et al. investigated the effect of Nitric Acid on concrete made using Silica Fume (SF) at the optimum replacement level of Ordinary Portland cement (OPC) with Silica Fume in respect of compressive strength was found i.e., 20%(Tripathi et al., 2020). Zhao, S. and Q. Zhang studied the effect of silica fume in concrete on the mechanical properties and dynamic behaviors of concrete under

impact loading With SF replacing cement, a series of changes have taken place within the organic structure and chemical composition of concrete. SF is especially recommended as another to moderate amounts of cement to get high-performance concrete with better mechanical properties(Zhao & Zhang, 2019).

2.3.2.4 Metakaolin

MK is white, making it particularly attractive in color matching and other architectural applications. Due to the controlled nature of the processing, MK powders are very consistent in appearance and performance. Partial substitution of cement with MK is found to enhance the compressive strength of concrete (Khatib et al., 2018). However, both MK and silica fume contribute to strength development. MK is relatively cheaper than silica fume and may have greater application in high-performance concrete. Caldarone et al.(Caldarone et al., 1994) showed that concrete made with 5%, and 10% MK as partial replacement of CEM 1 had enhanced strength at ages up to 365 days than the control and even 10% higher strength than concrete containing silica fume.

This increase in the compressive strength values was mainly attributed to the pozzolanic effect of the metakaolin in the cement blended pastes, which could be detailed as follows: when water was added to the OPC-MK mixture, free calcium hydroxide (CH) is liberated and its concentration increased as a result of initial hydration of OPC (Ibrahim et al., 2017). The silica and alumina contents in the metakaolin fraction went into the solution quickly and reacted with the calcium hydroxide to form secondary hydration products mainly as calcium silicate hydrate (CSH) together with the formation of calcium aluminates hydrates (C2ASH8, C4AH13, C3AH6) which were precipitated as soon as saturation was approached, according to the following equation 2.9, and 2.10 (Mobili et al., 2016):

$C_3S/C_2S(clinker) + H_2O \rightarrow (C\text{-}S\text{-}H) + Ca(OH)_2$ ……..…….(2.9)

$Ca(OH)_2 + Mk(Al_2O_3.2SiO_2) \rightarrow CSH(2^{ry}\ hydration\ product) + C_2ASH_8, C_4AH_{13}, C_3AH_6$ ……..(2.10)

The strength enhancement is likely to be due to the large surface area of MK which fills the pores, the acceleration of cement hydration due to the large surface area, and the pozzolanic reaction of MK with calcium hydroxide Wild et al.,(Wild et al., 1996). The filler effect is immediate, the acceleration of cement hydration takes place during 502 Waste and Supplementary Cementitious Materials in Concrete in the first 24 hours, and the pozzolanic reaction makes the maximum increase in strength somewhere between 7 and 14 days of age

Wild et al., (Wild et al., 1996). The positive contribution made by MK does not continue beyond 14 days, irrespective of the replacement level. This result was not confirmed by other researchers Ding and Li,(Ding & Li, 2002). Wild et al. (1997) later showed that using MK with a larger specific surface area (15 m^2/g instead of 12 m^2/g) reduces the age at which maximum strength enhancement occurs in MK mortars. The maximum compressive strength occurs at around 7 days for the finer MK as opposed to 14 days. This indicates the influence of fineness on reaction rate. An increase in the surface area has led to faster reaction and higher rate of strength evolution. It should be noted, however, that the change in particle size did not influence the long-term (e.g., 90 days) strength. However, Ding and Li (Ding & Li, 2002) found that both MK and silica fume were effective in increasing strength beyond 14 days.

The purity of kaolin clay varies from 20% to more than 80%. The heating temperature and exposure time play an essential role in the determination of the MK reactivity. Prolonged heating results in recrystallization and formation of mullite ($3Al_2O_3.2SiO_2$) which decreases the material reactivity. The main characteristic of MK is the pozzolanic activity, which is the ability of MK to react, in the presence of water, with calcium hydroxide to form hydrated silicate gel hydrate products possessing cementitious properties (Tippayasam et al., 2014). Portland cement includes 80% calcium silicates: tricalcium and dicalcium silicate (C_3S) and (C_2S), which react with water to produce the following reactions: The final hydrated products consist of about 75% calcium silicate hydrate (C-S-H) and 25% calcium hydroxide (CH) or Portlandite which will react with silicates and aluminate in the pozzolana such as MK to form more hydrated phases.

As an available and high-quality supplementary cementing material (SCMs), the Consumption of Metakaolin (MK) was proposed by many researchers to exchange hydraulic cement to enhance concrete quality and reduce the negative effects of the cement industry on the environment. One of these SCMs is MK which is produced by heating and calcination of kaolin and frequently contains 40–45 % of Al_2O_3 and 50–55 you look after SiO2 (Barbhuiya et al., 2015). Kalpokaitė D. R. et al. administered a look where incinerator residual ash was used in joint with metakaolin as replacement of cement in concrete. it had been found that 10% metakaolin replacement improved the hydration process of cement and consequently, the properties of the concrete (Kalpokaitė-Dičkuvienė et al., 2019). The work of V. Malagavelli et al. focused on the compressive, splitting tensile and flexural concrete infused with metakaolin. it had been observed that 10% metakaolin replacement was above

that obtained within the control sample(Malagavelli et al., 2018). The work of Tawfik , T.A., et al. concluded that the flexural strength of concrete was satisfactory with 10% MK content (Tawfik et al., 2019). Mohd Nasir, N.A., et al. reported metakaolin blended concrete containing 10% treated crumb rubber for its permeation-durability behavior is discovered. The results showed that the reduction in permeation properties and better durability resistance were achieved at a superplasticizer level of 0.75% (Nicoara et al., 2020).

Thus, it will be concluded that the nice workability of the concrete mixture is ready to discontinue pore connectivity and resulted in high permeation and sturdiness resistance of metakaolin blended-rubberized concrete(Mohd Nasir et al., 2021). Abdelmelek N. et al. reported Using different ratios of MK replacements to evaluate the optimum MK dosages at both ambient and after elevated temperatures in three concrete mixes Inclusion of MK has shown beneficial changes in the interfacial transition zone (ITZ) of aggregate with HCP (hardened cement paste), during which ITZ between aggregate and mortar are merged within the bond region (Abdelmelek et al., 2021). The setting time is also affected by the addition of metakaolin as shown in figure 2.4.

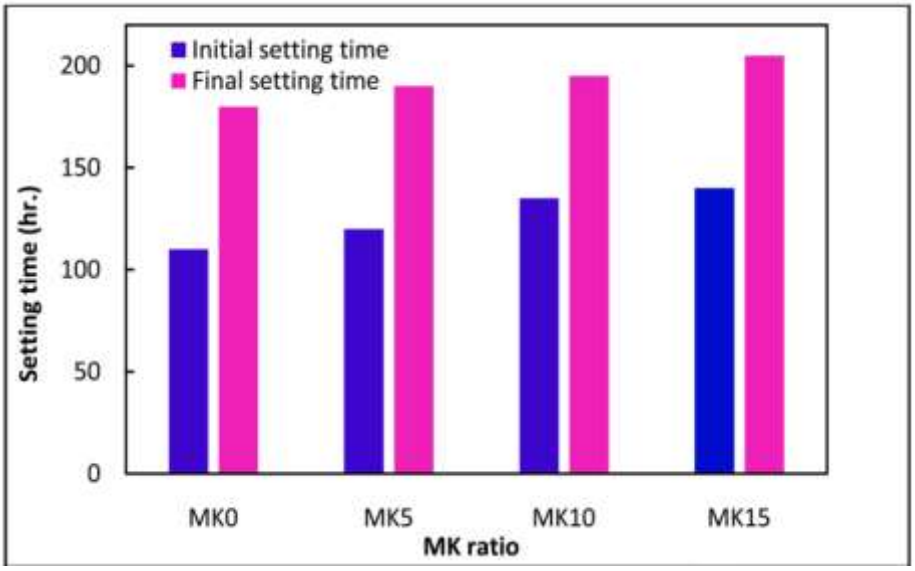

Figure 2.4. Setting times at standard water of consistency (Ibrahim et al., 2017)

2.3.2.5 Sugar Cane Bagasse ash

As described in previous sections pozzolans are siliceous or siliceous and aluminous materials that alone possess little or no cementitious value but which will, in a finely divided form in the presence of moisture, react chemically with calcium hydroxide at ordinary temperature to form compounds possessing cementitious properties. Bagasse ash was also

tested to have such property. It acts as a pozzolanic material when added to cement because of its silica (SiO_2) content which reacts with free lime released during the hydration of the cement and forms additional calcium silicate hydrate (CSH) as a new hydration product (Bahurudeen et al., 2015). This additional CSH improves the mechanical strength of the cement mortar and concrete (Tippayasam et al., 2014).

The silica content of the ash depends on the type of soil and harvesting. It is also found that it depends on the burning temperature of the bagasse. The high temperature helps eliminate impurities in bagasse ash as well (Zareei et al., 2018). In addition to this, it was found that the holding time in the furnace has also some effect on the content of the silica. Research conducted on the burning of sugarcane bagasse at 400, 500, 600, 700, and 800 ℃ for 3, 5, 6, and 8 hours respectively, identified the suitable burning and residence time to be 600 ℃ for 5 hours (Norsuraya et al., 2016). The higher temperatures will give a higher amount of silica content, but the resulting silica is in crystalline form which is not in an active state.

Bagasse is a cellulose fiber remaining after the extraction of the sugar-bearing juice from sugarcane. Bagasse ash is one of the biomass sources and valuable byproducts in sugar milling that often uses bagasse as a primary fuel source to supply all the needs of energy to move the plants (Bahurudeen & Santhanam, 2015). The bagasse ash is about 8-10% of the bagasse and contains unburned matter, silica, and alumina (Praveenkumar & Sankarasubramanian, 2019).

Bagasse ash has been a problem for the environment due to its disposal (Sales & Lima, 2010) Figure 2.5. The most significant pollutant emitted from the boilers is particulate matter, caused by the turbulent movement of combustion gases concerning the burning bagasse and resulting ash (Sales & Lima, 2010). Sometimes some auxiliary fuels typically fuel or natural gas may be used during the startup of the boiler or when the moisture content of the bagasse is too high to support combustion, in such cases the emissions of SO_2 and NOX will increase (Ganesan et al., 2007).

SCBA is a pozzolan that can partially replace clinker in cement production, and its use improves the behavior of the cementitious material (Fairbairn et al., 2010). The main products from the reaction between calcium hydroxide and SCBA are calcium silicate hydrates (C-S-H) gel (Tekleab, 2016). Singh et al. (Bahurudeen et al., 2016) found that in

the presence of SCBA, a large amount of C-S-H was formed in the paste, and the compressive strength increased (Bahurudeen & Santhanam, 2015).

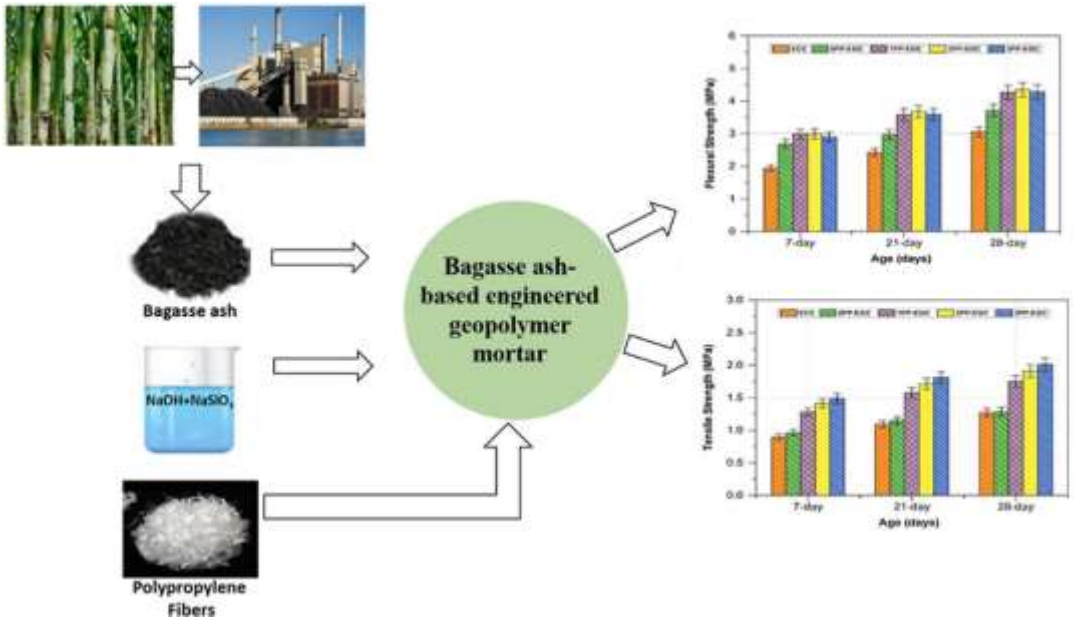

Figure 2.5 Mortar incorporating propylene fibers (Akbar et al., 2021)

2.3.2.5.1 Availability of bagasse ash in Ethiopia

In concern of the abundance of bagasse ash, contemporarily, giant sugar factories are under construction and some already started production with their partial or full production capacity in addition to the existing factories. Among these are: the Kessem project found in Fentallie and Dulecha Woredas of Afar Regional State (expected capacity of 11,000ton of sugar per day), Tendahu found in lower Awash River Basin of Afar regional state around Millie, Doubti, Assaeitta, and Affambo Woredas at a distance of 670 km from Addis Ababa (with completion of phase two of the project production capacity will be of 619,000 ton of sugar per annum) and Omo Kuraz found in South Omo zone (Selamago and Gnanegatom Woredas), Bench - Maji Zone (Surma Maji and Mieinitshasha Woredas) and Keffa zone (Diecha Woreda) of Southern Nations, Nationalities & People Region (when full capacity attained a production of 278,000 tons of sugar per annum will be expected) (Ethiopian Sugar Corporation 2015). The molasses disposed of in the existing factories are mostly utilized for ethanol production. And when all the factories become fully operational, the bagasse ash from all these factories will be expected to be in thousands of tones as shown on the graph in Figure 2.6. As per the information from Ethiopian Sugar Corporation, all of the factories that are operating currently are now using bagasse as a fuel for the boiler. Not only the current factories but the future intended projects will also operate in the same manner as this

method reduces energy consumption. When all the factories start to operate at their full capacity, the respective bagasse ash that will be produced by that time will reach up to two million tons per annum. Bagasse ash of this amount can substantially contribute to both technical and environmental advantages to the cement industry.

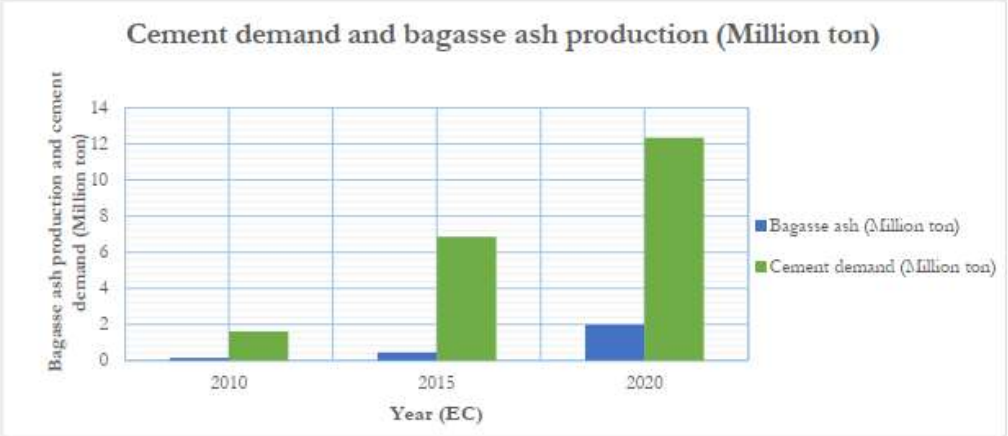

Figure 2.6 Cement demand and bagasse ash production (Tekleab, 2016)

Table 2.3. Annual sugar production capacity and expected BA amount (Tekleab, 2016)

No.	Sugar factories	Tone of cane per day (TCD)	Annual crushing capacity (Ton)	Bagasse (Ton)	Bagasse ash (Ton)
1	Wonji Shoa	12,500	3,000,000	870,000	108,750
2	Metehara	5,000	1,200,000	348,000	43,500
3	Fincha	12,000	2,880,000	835,200	104,400
4	Tendahu	26,000	6,240,000	1,809,600	226,200
5	Beles I	12,000	2,880,000	835,200	104,400
6	Beles II	12,000	2,880,000	835,200	104,400
7	Beles III	12,000	2,880,000	835,200	104,400
8	Kuraz I	12,000	2,880,000	835,200	104,400
9	Kuraz II	12,000	2,880,000	835,200	104,400
10	Kuraz III	12,000	2,880,000	835,200	104,400
11	Kuraz IV	24,000	5,760,000	1,670,400	208,800
12	Kuraz V	24,000	5,760,000	1,670,400	208,800
13	Kesem	11,000	2,640,000	765,600	95,700
14	Arjo dedesa	8,000	1,920,000	556,800	69,600
15	Wolkayte	24,000	5,760,000	1,670,400	208,800
		218,500	**52,440,000**	**15,207,600**	**1,900,950**

The annual production capacity data was taken from the Ethiopian Sugar Corporation; communication department. As per the combined information taken from the corporation's technical office and chemical laboratory technicians in the Wonji sugar factory, the bagasse that will be extracted from the cane accounts for 28-30% of the total cane production. And the bagasse ash that will be obtained from the bagasse was estimated to be 11-14% of the bagasse produced. The above calculation in the table was done using the average percentage of the range and an annual operational period of 240 days.

From table 2.3, it can be seen that around 2 million tons of bagasse ash per year will be disposed of from the sugar industry when the intended sugar factories will start to operate at their full production capacity (Akbar et al., 2021). This amount can significantly support and strengthen the cement industry if there will be a system and mechanism that makes the proper utilization of this material into practice.

2.4 Blended or Composite Cement

Blended cement with more than one blending material is called composite cement.

Advantages of producing blended cement are: -

1) Conservation of thermal (Subedi et al., 2019)
2) Increase in productivity (G. C. Cordeiro, R. D. Toledo Filho, L. M. Tavares, et al., 2009)
   - Redaction of production cost (Tippayasam et al., 2014)
     - Improved clinker factor
     - Saving on thermic & electrical energy
     - Increased cement output
   - Reliable basis for the decision regarding the selection of grinding system (Singh et al., 2000)
3) Lower investment risk & cost-saving (Subedi et al., 2019)
4) Pressure to decrease CO and heat emission (Subedi et al., 2019)
5) Pressure to dispose of industrial by-products (Singh et al., 2000)
6) Opportunity to produce differentiated or tailored products(Priya & Ragupathy, 2016)
7) Improvement of cement properties and quality & or production of special cement for a specific application (Chusilp et al., 2009a)

The disadvantage of Composite Cement is: -

1) Reduced reactivity, i.e., slower setting & lower early strength compared to pure Portland cement.

Blended cement can be used instead of special or pure Portland cement where the following concrete characteristics are required:

- Improved workability(Dineshkumar & Balamurugan, 2021)
- Lower heat development of bulk concrete(Galitsky & Worrell, 2008)
- High to very high final strength (Ibrahim et al., 2018)
- Increased water tightness(Bergold et al., 2013)
- Improved resistance to sulfate & other chemical attacks (Malagavelli et al., 2018)
- Lower sensitivity for alkali-aggregate reaction(Araos Henríquez et al., 2021)
- Reduced tendency to unsoundness due to free lime & MgO (Abdelmelek et al., 2021).

Table 2.4 Summary of Literature Review

No.	Pozzolanic Materials	Replacement ratio	Improved properties	Reference
1	Bagasse ash	(0, 10, 15 ,20, and 25) wt%	Durability and strength	(Zareei et al., 2018)
2	Metakaolin	(0 ,5 ,10 ,15 ,20, and 25) wt%	Compressive strength	(Dinakar, 2011)
3	Bagasse ash	0%,5%,10%,15%,20%, and 25%	Reduction of CO_2	(Fairbairn et al., 2010)
4	Metakaolin	0%,5%,10%,15%,20%, and 25%	Reduction of Pollution Hazard	(Ibrahim et al., 2017)
5	Blast furnace Slag	0%,5%,10%,15%,20%, and 25%	Earth block strength	(Sekhar & Nayak, 2018)
6	Blast furnace Slag	0%,5%,10%,15%,20%, and 25%	Heat of hydration	(Bourchy et al., 2020)
7	Silica fume	0%,5%,10%,15%,20%, and 25%	Alkaline resistance	(Tripathi et al., 2020)
8	Bagasse ash	(0, 5, 10, 15 ,20, and 25) wt%	Durability and mechanical properties	(Chindaprasirt et al., 2019)
9	Metakaolin and silica fume	(5, 10, and, 15) wt%	Mechanical performance and durability	(Nadeem et al., 2013)
10	Coal fly ash	0%,5%,10%,15%,20%, and 25%	Resistance to sulphate attack	(Yao et al., 2015)
11	Kaolin	0%,2.5%,5%,7.5%, and 10%	Mechanical and chemical properties	(Tippayasam et al., 2014)

12	Silica fume	0%, 10%, 20%, 30%, 40% and 50%	Mechanical properties	(Zhao & Zhang, 2019)
13	Metakaolin	0%,5%,10%, and15%	Pore structure and hydration	(Jiang et al., 2015)
14	Metakaolin	(0,10, 20, 30 and 40) wt%	Mechanical properies, and durability	(Varma et al., 2019)
15	Bagasse ash	(0, 5, 10, 15, 20) wt%	High Strength	(Dineshkumar & Balamurugan, 2021)

2.5 Research Gap

The partial replacement of MK with a range of 0-15 wt% was presented and only the mechanical property test was conducted there is no physical and chemical property test in the previous studies (Qian & Li, 2001). From a lot of literature, Metakaolin is processed from the Kaolin clay, not from the industrial waste. The calcined clay got the maximum strength at 5% metakaolin partially replaced. The partial replacement of bagasse ash results in maximum compressive strength at 10 wt% replacement (Rukzon & Chindaprasirt, 2012). The highest (40%) replacement ratio of bagasse ash and metakaolin results in decreasing compressive strength (de A. Mello et al., 2020). This is the indication of much decrease in C3Sresult lower mechanical properties (B. B. Sabir et al., 2001).

In this paper, we focused on the investigation of heat-treated filter cake byproduct material (metakaolin) and Bagasse ash as a supplementary cementitious material in mortar in single effect and combined effect. We prepared mortar samples using OPC cement, heat-treated filter cake-kaolinite (Metakaolin (0-20%MK)), sand, and water. Heat-treated filter cake kaolinite waste materials have higher pozzolanic reactivity and were used for Ordinary Portland Cement (OPC) partial replacement. The second one is the recalcine Bagasse ash (0-20%) partial replacement of OPC. We compared flexural and compressive strengths of MK-blended OPC mortar samples with control mortar samples and bagasse ash blended OPC mortar with control mortar samples. Flexural strength & compressive strengths of blended mortars were improved with certain MK and BA replacement OPC cement. Finally, the improved properties of MK and BA composite will be developed.

CHAPTER THREE

3. MATERIALS AND METHODS

This chapter describes the raw materials used in the experiments, characterization devices, and how to conduct a study as well as the procedures for the experiment.

3.1 Materials and Chemicals

The basic material used in this study are Ordinary Portland Cement (OPC) 42.5R, Bagasse ash (BA), filter cake (F.C), and CEN standard sand. Sodium chloride. The following basic apparatus and instruments are used for cement physical and mechanical properties analysis such as drying oven, digital balance, muffle furnace, the crucible, sieve machine, stopwatch, small brushes, Le-Chatelier ring, sample mixer, ruler, Vicat apparatus, prism molds, jolting apparatus, humidity cabinet, and water bath.

3.2 Measuring and Characterization Techniques

Flexural and Compressive strength testing machine (universal testing machine) used for measuring the flexural and compressive strength of mortar samples. Vicat apparatus and Le Chatelier apparatus were used for the determination of setting time, and Soundness (ES 1176-3:2005) respectively. An automatic Blaine fineness machine is also used for fines test measurements. X-ray powder Diffraction (XRD-700, Shimadzu, South Korea) using copper Kα radiation (λ Cu ka = 1.5418 Å) was used to determine phase purity. We also used Fourier Transform Infrared Spectroscopy (FTIR-400 series, JASCO), to identify functional groups, and the thermal stability of the sample was investigated in a temperature range from 23 ℃ to 1000 ℃ using the TGA-DTA curve (DTG-60H), Shimadzu, South Korea), and the chemical composition is evaluated by X-Ray Fluorescence (XRF) DY1507 Epsilon3. The morphology of the sample was examined using a Scanning Electron Microscope (SEM) (COXIEM-30, Shimadzu, South Korea). Shimadzu-3600 plus UV visible spectrophotometer was used for evaluating the Cl ion penetration. The electrochemical property was measured using Biologic. The flexural strength, compressive strength, fineness, setting time, density, Soundness, and chemical composition analysis was performed in the Habesha Cement Factory quality control and assurance laboratory.

3.3 Experimental Procedures

3.3.1 Collection and Pre-treatment of Metakaolin (MK)

Currently, industrial waste materials are becoming a serious problem for human beings as well as ecology due to inadequate disposal causes environmental degradation and contamination of soil and water sources. The reuse of industrial wastes in the productive chain has emerged as an alternative material for minimizing the damage that industrial waste can generate. The Awash Melkasa Aluminum Sulphate in Ethiopia is producing 1,700 tonnes of useful chemicals annually and meantime filter cake-kaolinite byproducts are disposed of in landfills (Yager, 2010). Byproduct residue material obtained during the production of aluminum sulfate chemicals in Awash Melkassa Aluminum Sulphate PLC, Ethiopia as shown in Figure 3.1, and leave as a landfill.

Figure 3.1 Filter cake (kaolinite) as landfill at AMASSAF Ethiopia.

In this work, the filter cake by-product from Awash Melkasa Aluminum Sulfate and Sulfuric Acid Production Factory was collected. Then the collected filter cake -kaolinite ground using mortar and pestle to reduce its size followed by a sieve using 45μm. The sieved powder is transferred to a crucible and then heat-treated at 600 °C for 2 h in a muffle furnace, followed by quenching using cold water and oven drying for 24h. The process of converting kaolinite to metakaolin adopted from with some modification (B. Sabir et al., 2001). The as-collected and calcined filter cake was subjected to characterizations. The procedure for producing Metakaolin is presented in figure 3.2.

Figure 3.2. Metakaolin materials preparation from the filter cake.

3.3.2 Collection and Pre-treatment of Bagasse Ash

The raw sugar cane bagasse ash will be collected from Wonji Sugar producing factories, in Ethiopia. The bagasse ash is the result of the extraction of Sugar and after used for boiler. After extraction, the bagasse ash was disposed of at a landfill as shown in figure 3.3. Distilled water will be used to remove different impurities, especially salt, and soil compounds, and oven-dried at 100 ℃/24h. The dried bagasse ash was calcined to remove carbon and extract more amount of silica (Gupta et al., 2002). Experimental findings suggested that BA obtained from uncontrolled burning (raw BA) is not suitable for concrete application due to its high carbon content. However, post-processing of raw BA yields a material with adequate pozzolanic performance for concrete applications, which is comparable to BA produced under controlled burning conditions (Subedi et al., 2019). To obtain low carbon content and most amorphous quartz the waste Bagasse ash calcine from 500 to 700 ℃ was followed by XRD characterization (Rashad, 2013). The production process is shown in figure 3.4 for bagasse ash disposed of after use for power generation.

Figure 3.3 Bagasse ash as landfill at Wonji sugar factory, Ethiopia.

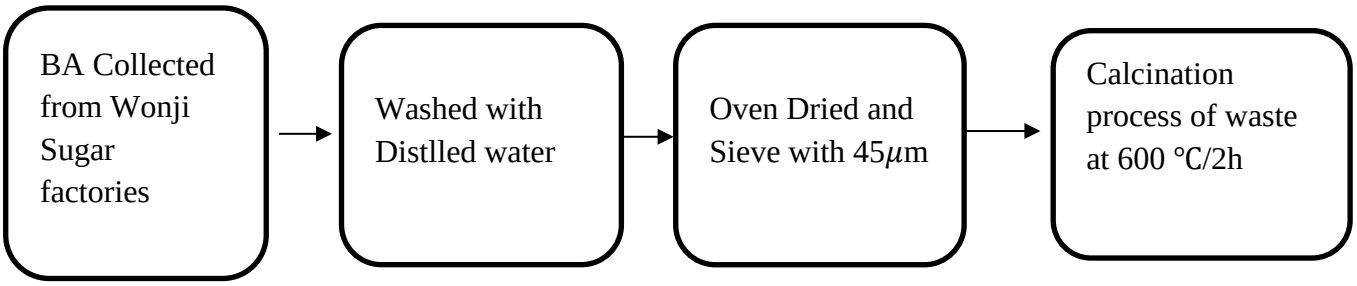

Figure 3.4 flow chart for preparation of bagasse ash

3.3.3 Preparation of Metakaolin (MK)-Blended OPC Mortar Samples

The byproduct materials were heat-treated at a temperature of 600 ℃/2 h and then quenched in cooled water rapidly. The samples were ground and sieved them using mesh sizes of 45 µm. MK blended OPC-mortar samples with sizes of 4 × 4 × 16 cm prisms were prepared using Metakaolin, Ordinary Portland Cement (OPC), standard sand, and water as shown in Table 3.1. Water to binders (OPC+ Mk (0%, 5%, and 10%)) ratio was 0.5. However, as metakaolin content increased (above 10%), the workability of mixing proportion MK blended mortars decreased a lot. Thus, extra water (15 mL) was added while MK 15% and 20% were added to cement for blended mortar preparation. The ingredients of mortar were thoroughly mixed in an automatic mortar mixer machine till uniform consistency was achieved. Before casting, machine oil was smeared on the inner surfaces of the cast iron mold. Fresh mortar mixtures were poured into the mold as quickly as possible; the mortar mixture was scooped into each mold (to half the depth) in a single layer. The assembled mold was placed on a vibrating machine and well secured in place; a suitable hopper was used to facilitate filling. The mold was vibrated on a jolting machine for 120 sec. The fabricated samples were de-molded after 24 h and then cured in the standard curing condition (at a temperature of 20 ± 3 ℃ and relative humidity of 95%) until the prescribed

period. The samples measured the flexural and compressive strengths at the curing age of 3, 7, and 28 days.

Table 3.1 Mixing proportion of MK-Blended OPC mortars, Cement: Sand = 1: 3.

Mix proportion	% OPC	%MK	OPC (gm)	MK (gm)	Sand (gm)	Water (mL)
C	100	0	450	0	1350	225
MK5	95	5	427.5	22.5	1350	225
MK10	90	10	405	45	1350	225
MK15	85	15	382.5	67.5	1350	240
MK20	80	20	360	90	1350	240

3.3.4 Preparation of Bagasse Ash (BA)-Blended OPC Mortar Samples

The mortar is prepared by replacing BA with 0%, 5%, 10%, 15%, and 20% by weight. The total mixing program is present in table 3.2. Mechanical mixing and compacted in a mold using a standard jolting apparatus. The specimens in the mold are stored in a moist atmosphere for 24 hr and then the de-molded specimens are stored underwater until strength testing. At the required age, the specimens are taken from their wet storage and broken in flexure into two halves, and each half is tested for strength in compression.

Table 3.2 Mixing proportion of BA-Blended OPC mortars, Cement: Sand = 1: 3.

Mix proportion	% OPC	%BA	OPC (gm)	BA (gm)	Sand (gm)	Water (mL)
C	100	0	450	0	1350	225
BA5	95	5	427.5	22.5	1350	225
BA10	90	10	405	45	1350	225
BA15	85	15	382.5	67.5	1350	240
BA20	80	20	360	90	1350	240

3.3.5 Preparation of MK-BA Blended OPC Mortar Samples

The optimum ratio was selected using trials done in Adama science and technology in the civil engineering department. The measured compressive strength showed the best result in 5% MK and 10% BA. The formation of composite is to obtain the best combination in terms of mechanical and physical properties. The attractive characteristics of BA are its abundancy and amorphous nature after calcination at a specific temperature relatively lower than GGBFSC. However, this BA has a drawback of relatively high alkali oxide which harm

the long-term strength of cement mortar. This alkali oxide found in BA may result in corrosion in the reinforced mortar/concrete. To minimize this challenge making a composite of BA and so, to achieve better performance metakaolin will be used. This is due to MK having a lower alkaline oxide resulting in no adverse effect in alkaline silica reaction.

Table 3.3 Mixing proportion of MK-BA Blended OPC mortars.

Mix proportion	**% OPC**	**%MK**	**%BA**	**OPC (gm)**	**MK (gm)**	**BA (gm)**	**Sand (gm)**	**Water (mL)**
Composite	85	5	10	382.5	22.5	45	1350	240

3.3.6 Preparation Procedures of the Mortar for all Specimens

Three test specimens were Prepared in a batch of three samples under the conditioning of specimens in the mixing room, testing room curing chamber & curing water tank of desired temperature & humidity. The Procedures are as follows first weigh the amount of cement as described in tables 3.1, 3.2, and 3.3 for MK blended mortar, BA blended mortar and composite. For instance, for 5%MK Blended mortar OPC = 427.5g, MK = 22.5g and 255 ml of water. Then placed the dry paddle and bowling in the mixing position followed by pouring the water into the bowl. Before adding the powder to the container, it was mixed well in a dry state to obtain uniform mixing and dispersity of MK. Placed the well-mixed powder into a bowl and placed the standard sand into its container as shown in figure 3.5(a). After this start the mixer immediately which is automatically programmed. The automatic mixer proceeds as follows: -

- The mixer immediately Starts at a low speed & after 30sec standard sand drop automatically within 30sec
- Mix slowly for 30sec period at a slow speed followed by mixing to the high speed & continue the mixing for an additional 30sec
- Then after it stops for 1min 30sec during the first 15sec remove utilizing a rubber scraper all the mortar adhering to the wall & bottom part of the bowl & place in the middle of the bowl. Finally, Continue the mixing at a high speed of 60sec.

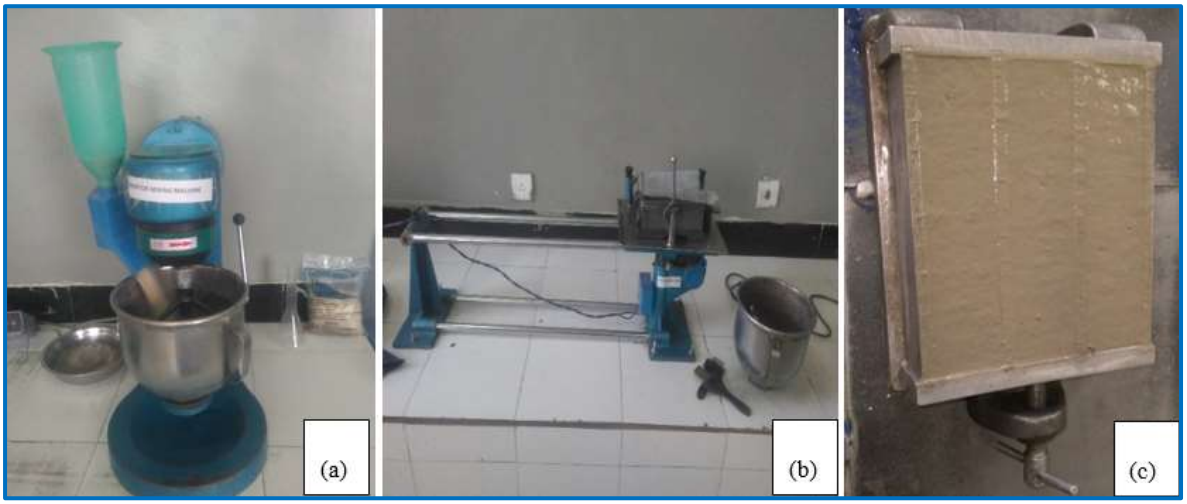

Figure 3.5 (a) Automatic mortar mixer, (b) jolting table, (c) Compacted specimens,

3.3.6.1 Preparation of the Test Specimen

- Mold the specimens immediately after the preparation of the mortar on 40mm x 40mm x 160mm prisms as shown in figure (3.6b) that are previously lightly oiled & cleaned.
- With the mold & hopper firmly clamped to the jolting table as shown in figure 3.5b, introduce using a suitable scope, in one or more increments, the first of two layers of mortar (each about 300g) into each of the mold compartments, directly from the mixing bowl.
- Spread the layer uniformly using the lager spreader held vertically with its shoulders in contact with the top of the hopper and drawn forwards and backward once along with each mold compartment.
- Compact the first mortar layer using 60 jolts
- Introduce the second layer of mortar level with the smaller spreader & compact the layer with a further 60 jolts.
- Lift the mold gently from the jolting table & remove the hopper.
- Immediately strike off the excess mortar with the metal straight edge held almost vertically & moved slowly with a transverse sawing motion once in one direction
- Smooth the surface of the specimens using the same straight-edged held almost flat
- Label or mark the molds to identify the specimens and their position relative to the jolting table.

- The fabricated samples were de-molded after 24 h and then cured in the standard curing condition (at a temperature of 20 ± 3 ℃ and relative humidity of 95%) until the prescribed period figure 3.6(c).
- Submerge the marked specimen immediately either horizontally or vertically in water at (20±1) ^{O}C and kept in a suitable container.
- The samples measured the flexural and compressive strengths at the curing age of 3, 7, and 28 days.

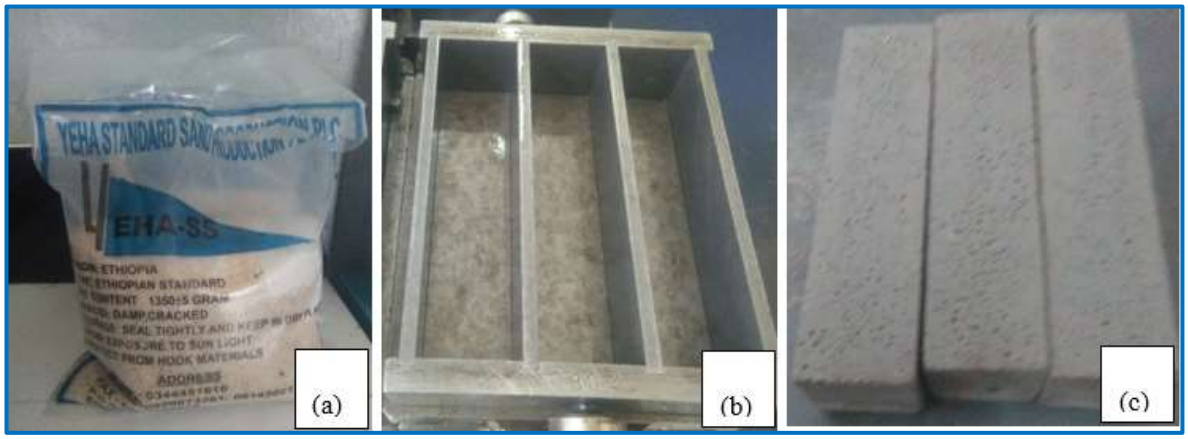

Figure 3.6 (a) CEN Standard Sand, (b) prisms mold, and (c) De-mold specimens

3.3.7 Blended Cement Pastes Preparation

A 500g of cement sample was weighed and 25% water content of the mass of dry cement was added as a start as given in ES 1176-3:2005 as shown in the figure 3.7. The mixture was mixed for 3.0 minutes by using a trowel to give a paste and was immediately transferred into the mold lying on the steel plate. The top of the mold was smoothened off as quickly as possible with the aid of the trowel. The mold and paste were placed under the plunger in the Vicat apparatus and the plunger lowered gently to contact the surface of the paste. This material was released quickly and allowed to sink into the paste. The scale reading of the Vicat apparatus was noted after 1 minute and recorded. If the plunger penetrates to a point 5 to 7 mm above the bottom of the mold, the water-cement ratio is taken as the consistency, if not, a new water-cement ratio is taken and the procedure is repeated.

Figure 3.7 Paste mixer machine

3.4 Mechanical, Physical, and Chemical Property Test

3.4.1 Determination of the Flexural and Compressive Strength

Determining the compressive and flexural strengths of cement mortar is the primary requirement for its structural use.

3.4.1.1 Flexural Strength Test

Use the center-point loading method to determine the flexural strength of the machine (figure 3.8a). Test the half prisms obtained in the flexural test in compression on the de-molded side faces over an area of 40mm x 40mm. Record the flexural strength value & carry the compressive strength test on the two halves of the prism. Determination of Flexural Strength Test Places the prism in the flexural testing machine with one side face on the supporting rollers and with its longitudinal axis normal to the supports. Apply the load vertically utilizing the loading roller to the opposite side of the prism & increase it smoothly at the rate of (50±10N/mm^2 until fracture. Keep the prism damp until tested in compression.

3.4.1.2 Compressive Strength Test

Test the prism halves in compression on the side faces by using a compressive strength machine (figure 3.8b). Center the prism halves laterally to the platens of the machine & longitudinally so that the end face of the prism overhangs the platens. Increase the load smoothly at the rate of (2400±200) N/S over the entire load application until the fracture. Make adjustments for the decrease of the loading rate near the fracture load, and the compressive strength (Rc) in N/mm^2 calculate using equation 3.1.

$$R_c = \frac{F_c}{A} \quad (3.1)$$

Where, F_c is the maximum load at fracture in Newton (N), A is the area of the platens or auxiliary plates in mm^2 will be 40mm x 40mm =1600mm^2

Figure 3.8 (a) flexural strength machine and (b) Compressive Strength machine

3.4.2 Chemical analysis with X-ray fluorescence spectroscopy (XRF)

An XRF spectrometer was used to investigate the characteristic spectra of elements present in the solid sample. For quantification analysis, the intensity of the characteristic line of the element analyzed was measured. The powdered cement sample was calcined at 850°C for 4 hours to remove all organic compounds and water contained in the sample. The calcined sample was converted into a solid solution by fusion with lithium tetraborate ($Li_2B_4O_7$). The prepared solid solution and standard were placed in sample holders and placed in the sample compartment of the DY1507 Epsilon3 XRF spectrometer. The intensity of a characteristic line of the element to be determined was measured. The concentration of the element in the sample was calculated from the intensity measured.

3.4.3 Determination of density of samples

Pycnometer was used to determine the density of cement, MK, and BA. To measure the density of samples we follow the following procedure according to ASTM D 854 (Helsel et al., 2016). a clean & dry pycnometer was taken and filled with alcohol (CH_3CH_2OH density at 20 °C = 0.79g/cm^3 up to the mark) and read as initial volume. a known mass of cement, MK, and BA and carefully transfer and shake properly and read as a final volume after settling the powder as shown in the figure 3.9. Using equation 3.2 it is possible to obtain the volume change. From the known mass transferred to Pycnometer density of sample obtained using equation 3.3.

$$Change\ in\ volume = \ final\ volume - \ initial\ volume \ldots\ldots\ldots\ldots\ldots (3.2)$$

$$\rho = \frac{Mass}{Change\ in\ volume} \ldots\ldots\ldots\ldots\ldots\ldots\ldots\ldots\ldots\ldots\ldots (3.3)$$

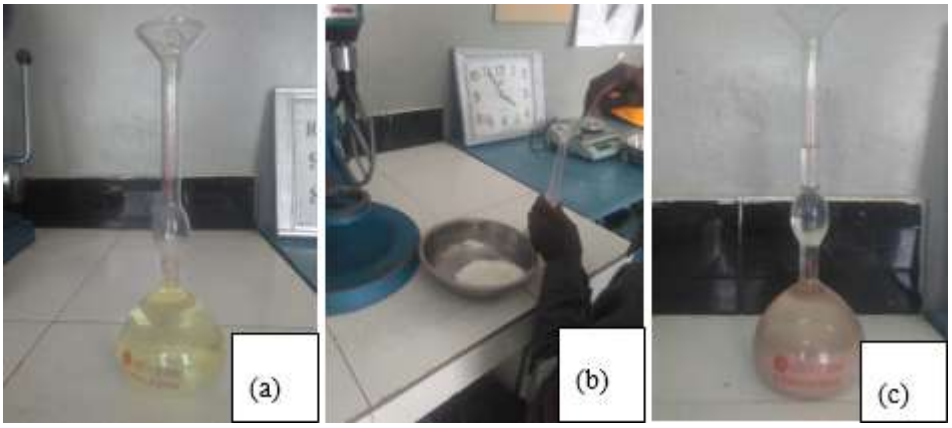

Fig.3.9 (a) kerosine in Pycnometer, (b) MK in Pycnometer and (c) settling

3.4.4 Determination of Fineness of the samples

Approximately 95% of cement particles are smaller than 45µm, with the average particle around 15 µm. The overall particle size distribution of cement is called fineness. The fineness of cement affects heat released and the rate of hydration. Greater cement fineness (Smaller particle size) increases the rate at which cement hydrates and thus accelerates strength development. Cement fineness is one of the physical properties of cement that mainly affect the hydration reaction of cement. Therefore, controlling the cement fineness is mandatory for cement manufacturers.

The fineness of cement is measured as a specific surface by observing the time taken for a fixed quantity of air to flow through a compacted cement bed specified. Under standardized conditions, the specific surface of cement is proportional to $\sqrt{t}$ where t is the time for a given quantity of air to flow through the compacted cement bed. The number and size range of individual pores in the specified bed is determined by the cement particle size distribution which also determines the time for the specified airflow as given in ES 1176-6:2005 [32]. For the Blain method: A mass of 2.66 g of cement sample was weighed and placed into the blain sample holder of PC- The controlled Automatic Blaine apparatus. Adjust the level of the oil at the correct position, set the stopwatch, and take the time taken in seconds from the initial level to the final level of the oil travels repeated three times and we take the average. The specific surface area was calculated with the following formula (3.4):

$$Specific\ surface\ area\ = k\sqrt{tav} \ldots\ldots\ldots\ldots\ldots\ldots\ldots\ldots (3.4)$$

Where: k = constant [cm^2/g.s] (2.1426 cm^2/g.s), and tav = average time in second.

Figure 3.10 FBT-9 Automatic Specific Area Tester

The tested result for metakaolin is lower than reported by (Poon et al., 2006) they got 12,680 cm^2/g. Which indicates the over finesse of metakaolin. The finesse of bagasse is nearly similar 4716 cm^2/g to as reported (Bahurudeen & Santhanam, 2015). As the finesse of supplementary materials increases it grows the rate of reaction hydration is due to high surface area. The replacement of cement with BA would decrease the contents of C_3A and C_3S, leading to a reduction in hydration heat (Bahurudeen et al., 2015). Therefore, BA can be used in concrete with low hydration heat requirements, such as mass concrete work.

3.4.5 Setting Time Determination

The primary factors that affect normal Setting time are free lime and the forms of calcium sulfate. The secondary factors are fineness and C_3A content. The initial setting time is the time elapsed between the hydration of cement and the paste starts losing its plasticity. As stated in ES 1176-3:2005, the determination of the initial setting time requires Vicat apparatus (figure 3.11), Stop clock, Needle (1mm square cross-section), and a non-porous plate. The quantity of water to be taken is 0.85 % of the standard consistency of cement paste. The experimental procedure remains the same for the determination of consistency. The initial setting time is regarded as the time recorded from the instant of water added to the cement to the needle fails to pierce the paste for about 5mm measured from the bottom

of a mold. The final setting time is regarded as the time elapsed from the water added to the cement, to the complete loss of its plasticity. The determination of the final setting time requires Vicat apparatus, Stop clock, 1 mm square cross-section needle with annular attachment. The experimental procedure remains the same for the determination of the initial setting time. It's the time required from the hydration of cement to the needle that fails to make an impression on the cement surface.

Figure 3.11 Vicat Apparatus for the Determination of Setting Time

A sample of cement paste of standard consistency was prepared and the time of first mixing the water with cement was noted down. A slight excess of paste was immediately transferred into the mold in one layer by using a hand trowel. The top of the mold was smoothened and leveled. The mold was placed under the initial set needle of the cross-sectional area of 1mm and the needle was covered gently onto the surface of the paste and was quickly released by allowing it to sink to the bottom. These tasks were repeated several times at regular intervals of 10 minutes in different positions of the mold until the paste has stiffened sufficiently for the needle not to penetrate deeper than 5mm above the bottom of the mold.

3.4.6 Expansion Test

The main purpose of the soundness test is to assess the possible risk of late expansion due to hydration of uncombined CaO and /or MgO. The standard specifications ES1177-1 and EN197-1 allow the Le chatlier expansion a maximum value of 10 mm. The determination of the soundness of the cement by the Le-chatelier method is to find the extent

of free uncombined lime present in the cement. Lime causes a large change in volume after the setting of concrete known as unsoundness. It is important to determine the soundness as it leads to crack, distortion and disintegration. The requirements are a Le-chatelier mold, a glass plate of 50mm square, a water bath is used. The Le-chatelier mold conforms to IS 5514-1996. The glass plate over which the mold was placed, keeping the edge of the mold gently together and cement paste was filled. Cover the mold with a glass plate over which a small weight was placed. The whole assembly was kept submerged in water for 24 hours at a temperature of 27±2 °C. The distance between the indicator points is measured as the initial distance and again submerged in a boiling water bath for about 3 hours and allowed to cool. Measure the distance between the indicator points. The difference between these two measurements represents the expansion of cement.

Carry out the test simultaneously on two specimens from the same batch of cement paste. Prepare a cement paste of standard consistency. Place a lightly oiled Le-chatelier mold on the lightly oiled base- plate & fill it immediately without undue compaction or vibration using only the hands & a straight-edged implement if desired, to level to the top surface. During filling, prevent the split in the mold from accidentally opening e.g., by gentle pressure with the fingers or by tying or by use of a suitable rubber band. Cover the mold with the lightly oiled cover plate. Add the additional mass if necessary and then immediately place the complete apparatus in the humidity cabinet or water bath. Maintain it for (24± 0.5) h at (24± 1)℃ and not less than 98% relative humidity. Measure the distance (A) between the indicator points to the nearest 0.5mm. Then heat the mold gradually to boiling temp. for 3h± 5min. Measure the distance (B) between the indicator points to the nearest 0.5mm at end of boiling. Allow the mold to cool to (20±2)℃. Measure the distance (c) between the indicator points to the nearest 0.5mm.

- For each specimen, record the measurements A and C and calculate the difference C-A.
- Calculate the mean of the two values C-A to the nearest 0.5mm.

Figure 3.12 Le-Chatlier Expansion Measurements

3.4.7 Durability Test

According to ASTM C64213 water absorption, and apparent porosity a test was performed for metakaolin, bagasse ash, and composite metakaolin and bagasse ash blended mortars to taste the durability of the samples.

- The mass of each specimen was first determined after the specimens were dried in an oven at a temperature of 100 ^{o}C for 24 h and the specimens were allowed to cool in dry air to determine the (A), in grams.
- After this, the specimens were immersed in water for 3 and 7 days. The specimens were again surface-dried and the mass assigned as (B).
- The specimens were boiled for 5 h in water and allowed to cool for 12 h. after this, the specimens were suspended by a wire and the apparent mass in water was determined as shown in figure 3.13b. This apparent mass was assigned as (D)

- The surface moisture of the specimens was then removed with a towel and the mass of the specimen was determined. The soaked, boiled, surface-dried mass was designated as (C). Finally, tests were conducted for 3, and 7 days,
- To calculate water absorption, and apparent porosity, Equation 3.5 and 3.6 are used as described below (Standard, 2015)

$$\text{Water absorption} = \frac{B - A \times 100}{A} \ldots\ldots\ldots\ldots\ldots\ldots\ldots\ldots\ldots\ldots (3.5)$$

$$\text{Apparent porosity} = \frac{C-A}{C-D} \times 100 \ldots\ldots\ldots\ldots\ldots\ldots\ldots\ldots\ldots\ldots (3.6)$$

Where A= Dry weight, B = Wet weight, C = Soaked weight and D = Suspended weight

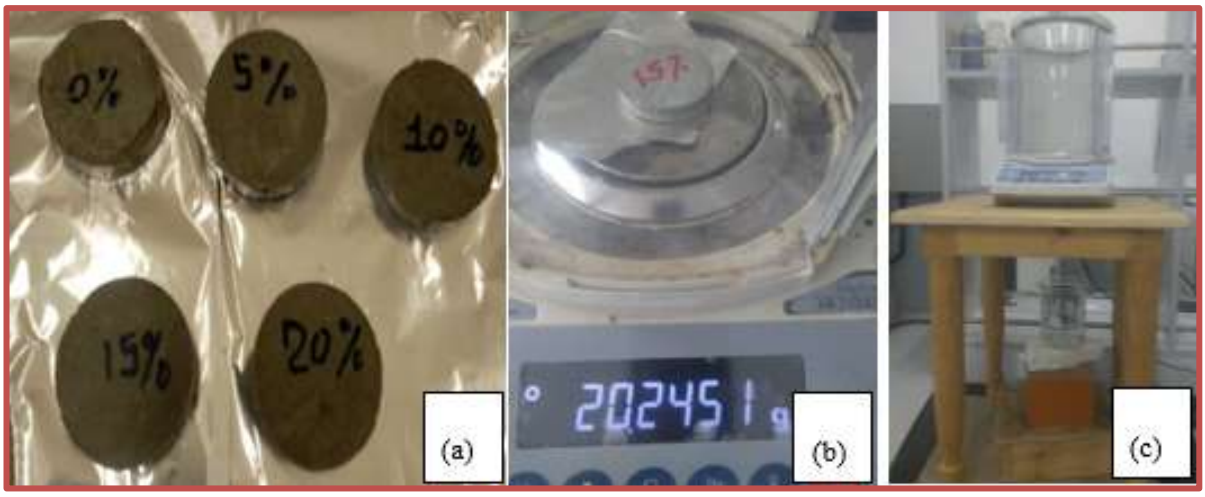

Figure 3.13 (a) Specimen for a durability test, (b) Dry weight and (c) Suspended weight

3.4.8 Electrochemical Corrosion Measurements

The Potentiodynamic polarization curve shows the relationship between potential and logs current density which is also referred to as corrosion rate. The blended and control test specimen was cured with 3.5% NaCl solution at room temperature. The test helps to know how much chloride ions penetrate construction materials and result in deterioration. This test is carried out within a frequency of 100 kHz to10 MHz, accelerated with AC over a potential 10 mV amplitude to Tafel Plot of each specimen after 28 days of curing (Nivin M. Ahmed et al., 2021). The electrolyte was 3.5% sodium chloride solution maintained at a temperature of 25°C. This test is important to know the effect of saltwater environment construction for instance Wonji. In the experiment, we use three electrodes these are reference electrode, a counter electrode, and the working electrode.

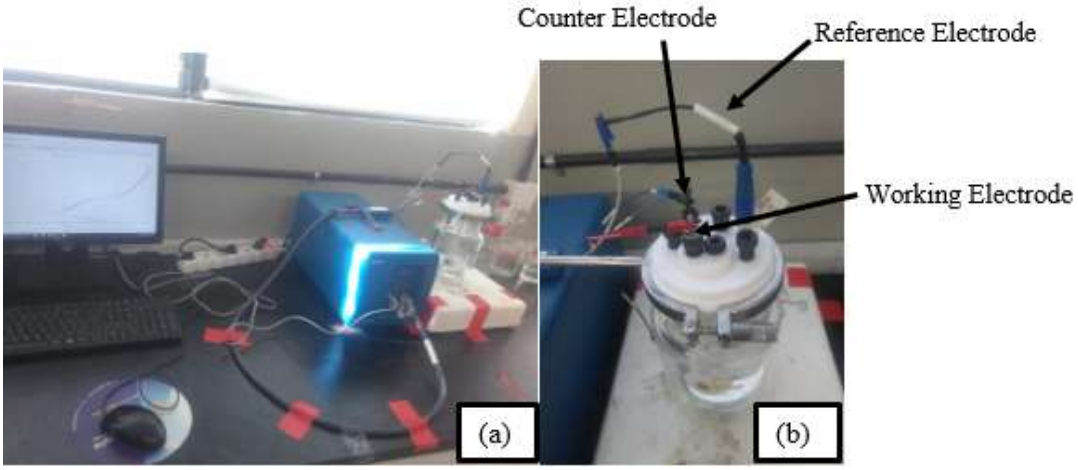

Figure 3.14 (a) Potentiodynamic Measurments and (b) Corrosion cell kit

Table 3.4 Summary of Experimental Program Used in this Thesis work

No.	**Tests**	**Number of samples**	**The test method used**
1.	Metakaolin Powder Preparation	1	The heat treatment followed by Quenching
2.	Bagasse Ash Preparation	1	Calcination
3.	Chemical Analysis of Filter cake, MK, BA, and OPC	4	XRF, DY1507 Epsilon3
4.	Density of MK and BA		ASTM D 854
5.	The fineness of MK, BA, and OPC	3	ES 1176-6:2005 /FBT-9
6.	Flexural and Compressive Strength of Mortar Sample	81	ES 1176-1:2005
7.	XRD Characterization	10	Shimadzu, XRD 7000,
8.	FT-IR Characterization	8	FT/IR-6600typeA
9.	TGA-DTA Characterization	8	Shimadzu, DTG-60H
10.	Setting Time and Soundness of Cement Paste	18	ASTM standard C191-82, and ASTM C151respectively
11.	Durability Test	18	ASTM C20-00 (2015)
12.	SEM Characterization	9	SEM, Shimadzu, COXIEM-30
13.	Electrochemical Properties	4	Biologic

CHAPTER FOUR

4 RESULTS AND DISCUSSION

4.1 Characterization of MK and MK Blended OPC Mortar/paste

4.1.1 Mineralogical compositions of Metakaolin (MK)

The mineralogical compositions of the pre-treated byproduct material (filter cake-Kaolinite) which was collected from the AMAS chemical factory, post-treated byproduct material (Metakaolin), and Habesha OPC cement are present in Table 4.1. We used XRF measurement to reveal the major and minor oxide composition of the powder, the loss of ignition (LOI) percent, to check its pozzolanic oxide contents (SiO_2 + Al_2O_3 + Fe_2O_3), and alkaline oxides.

Table 4.1 Chemical composition of filter cake-kaolinite, MK, and Habesha OPC

Chemical compositions	**Filter cake**	**Metakaolin**	**OPC**
SiO_2	65.44	69.2	19.74
Al_2O_3	16.57	18.7	4.98
Fe_2O_3	0.48	0.72	3.31
CaO	< 0.01	0.51	64.48
MgO	< 0.01	0.3	2.63
Na_2O	< 0.01	< 0.01	-
K_2O	1.6	1.6	-
MnO	< 0.01	< 0.01	-
P_2O_5	0.19	0.2	-
TiO_2	< 0.01	< 0.01	-
H_2O	1.22	< 0.01	-
LOI	14.73	7.56	0.69
SiO_2+Al_2O_3+Fe_2O_3	82.49	85.62	28.03
Blaine fineness (cm^2/g)	-	12,430	3,394
Specific gravity (g/ml)	-	2.07	2.23
Color	Off white	Off white to white	Grey

The amount of pozzolanic oxides (SiO_2 + Al_2O_3 + Fe_2O_3) in Metakaolin material is 88.62% which satisfies the content of pozzolanic oxides (70%) required by ASTM C-618 (Testing & Materials, 2012). Thus, the result testified to the pozzolanic nature of the prepared Metakaolin materials, thus it is possible to take the treated material as cement partial replacement. Moreover, the loss on ignition (LOI) of the MK is 7.56%, which is less than 10%. Thus, the pozzolanic activity would increase with Metakaolin's partial replacement of OPC cement as stated in a previous study (Ramezanianpour & Jovein, 2012). Chemical analysis results indicated the MK has a three-time higher silica content (69.2%) than OPC (19.74%). Moreover, it has a low alkali content (Na_2O + K_2O = 1.61%), implying a lower potential for the alkali reaction.

4.1.2 XRD Analysis of Filter Cake-Kaolinite, MK blended paste

To verify the conversion of filter cake-kaolinite to amorphous metakaolin (after heat-treatment at 600 ℃/2h), X-ray diffraction of both samples was measured as shown in Figure 4.1. Three different phases, i.e. kaolinite, illite, and quartz were observed in the filter cake. The presence of kaolinite in filter cake was confirmed by the characteristics reflections at 2θ: 12.4 (001) and 24.9 (002) by reference code (ICDD 01-083-0971). There are also minor peaks at 2θ (19.83, 20.3, 56.79, 59.9, and 72.3) with their hkl value correspondence to (020), (-110) (1-51) (-134), and (-135) respectively. The anatase phase was also observed at 25.28^o with hkl values of (101) (ICDD 00-021-1272). The presence of anatase in filter cake-kaolinite is widespread owing to the geological location where the clay is mined, and it is regarded as an impurity in the finished product. Many investigations have found impurities such as Fe, Ti, and Al minerals in these clays (Schwanke et al., 2022; Segura et al., 2017). One of the main minerals of clay illite was also observed at 23.05, 29.8, and 47.4 in 2θ with correspondence hkl at (222), (082), and (444) respectively. Thus, the XRD measurement result revealed that the pre-treated byproduct (filter cake-kaolinite) has several peaks which is an indication of crystal phases in the materials. However, post-treated materials (metakaolin) have shown a broad hump around 20° (figure 4.1) which confirmed post-heat-treatment at 600 ℃/2h and then rapidly quenching processes converted crystalline materials to an amorphous state as stated in a previous study (Souri et al., 2015). The calcination step proved to be efficient, and the complete destruction of the kaolinite structure by the de-hydroxylation reaction was observed. Consequently, an amorphous material was characterized by an elevation of the diffractogram background as prior reported (Pinheiro et al., 2020; Rimaz et al., 2022). In this work, we produced amorphous silica by calcining at

600 ℃/2h followed by water quenching. A similar result was also reported as metakaolin has high free energy and pozzolanic properties as the most reactive clay (Dinakar, 2011). Metakaolin with lesser amounts of quartz and illite is highly reactive and is suitable for its applications like the formation of binding materials (Khan et al., 2017). In our study, XRD results of the filter cake-kaolinite and metakaolin closely resemble as stated in previous studies (Dinakar et al., 2013)**.**

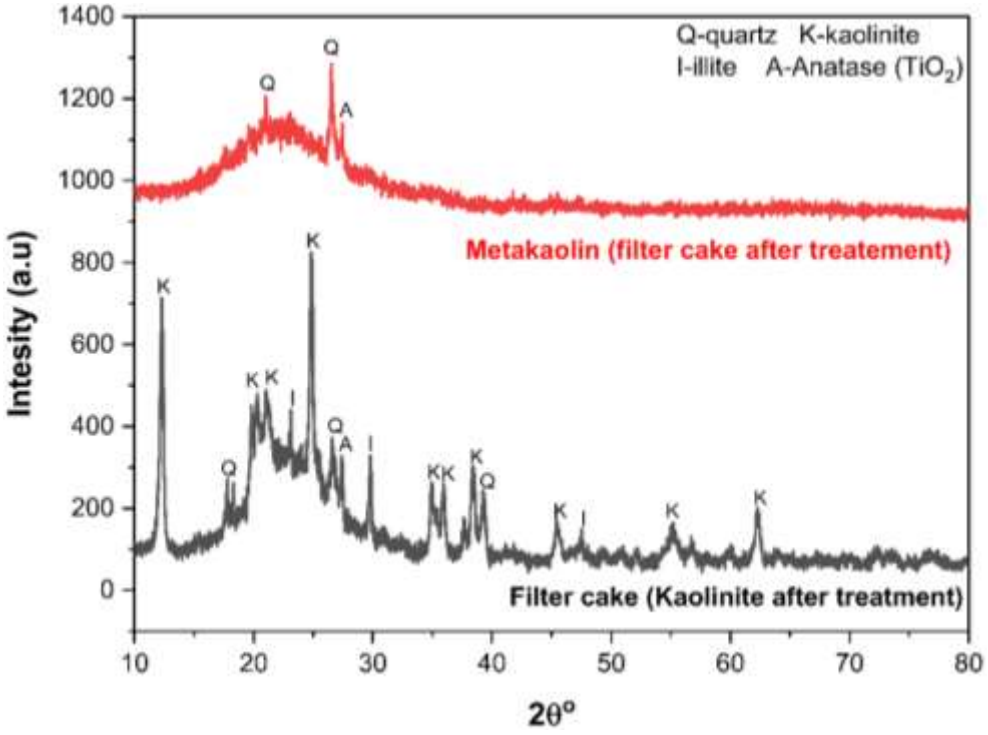

Figure 4.1 XRD pattern of metakaolin and filter cake (kaolinite) waste

The X-ray diffraction for the hardened cement pastes (after 28 days of curing) without and with the addition of 10% MK has shown that the formation of phases such as CSH, CH, CASH, unreacted SiO_2, and free CaO in both sample materials. Tricalcium aluminates (C3A) phase was not detected due to the fast rate of hydration as shown in figure 4.2. This mineral phase was transformed into the mono-sulfate hydrate ($C_3A{\cdot}CaSO_4{\cdot}12H_2O$ =CASH) during the early stages of hydration. These peaks seemed to be overlapped with the peaks of anhydrate silicate and hydrated calcium silicate phases. The calcium hydroxide (CH/Portlandite) peaks were strongly distinguished at the 2θ angles: 18.08°, 32.6°, 34.36°, 41.3°, 47.2°, 50.9°, and 56.4° with their correspondence hkl (001) (400) (011) (012) (023) (110) and (003) respectively by reference code 00-044-1481. In addition, the calcium silicate hydrates, CSH (I) and (II) appeared in both samples as the main hydration products, Figure 4.2 On the other hand, it was known that the main hydration products of hardened 10%MK

blended OPC-paste were nearly amorphous, besides the calcium silicate hydrates (CSH), calcium hydroxide (CH/Portlandite), and calcium aluminosilicate hydrates (CASH). However, it could be remarked that the intensity of calcium hydroxide (CH/portlandite) peaks of MK10% blended OPC-paste was lower than in the case of neat OPC paste as shown in peaks position at 2θ angles (18.08°, 32.6°, 34.36°, 47.2°, 50.9°, and 56.4°) due to its consumption after the reaction with metakaolin. When metakaolin is used as a partial replacement, it reacts with calcium hydroxide ($Ca(OH)_2$), which is one of the by-products of the hydration reaction of cement, and results in additional Calcium Silicate Hydrate (CSH) that results in increased strength (Cyr et al., 2014). The peak intensity of the hydration products of calcium silicate hydrates (CSH), for instance, peaks at 23.1°, 27.57°, 29.44°, and 39.48°. MK also contains alumina, which on reaction produces additional alumina containing phases some of which are crystalline. These include calcium aluminates silicate hydrates (CASH) (Astutiningsih et al.). Calcium aluminates silicate hydrates (CASH) of MK10 blended OPC paste was higher (at peaks of 29.5°) than conventional OPC paste (Figure 4.2). XRD pattern revealed that CSH gel formed in both samples by referring code 01-086-0402, i.e., CSH peaks appears at 2θ angles: 27.57°, 29.44°, 32.19°, 32.54°, 38.75°, and 39.48° which is correspondence to hkl (310), (-221), (003), (-222), (-223) and (-131) respectively. We also confirmed that unreacted Quartz existed in both samples by referring code (01-085-0335) which was identified at 2θ angles 20.9°, 26.74°, 46.01°, 50.1° with hkl values (100), (011) (201), (11-2) respectively as stated in a previously reported article (Ibrahim et al., 2017).

The silica and alumina contents in the metakaolin fraction went into the solution and reacted with the calcium hydroxide to form secondary hydration products mainly as calcium silicate hydrate (CSH) equation 4.1 together with the formation of calcium aluminates hydrates_(C_2ASH_8, C_4AH_{13}, C_3AH_6) which were precipitated as soon as saturation was approached, as shown in equation 4.2.

C_3S/C_2S(clinker) + H_2O → Calcium Silicate Hydrate (CSH) + Calcium Hydroxide (CH)……. (4.1)

$Ca(OH)_2$ + $MK(Al_2O_3.2SiO_2)$→ CSH (2ry hydration product) + C_2ASH_8,C_4AH_{13},C_3AH_6…….. (4.2)

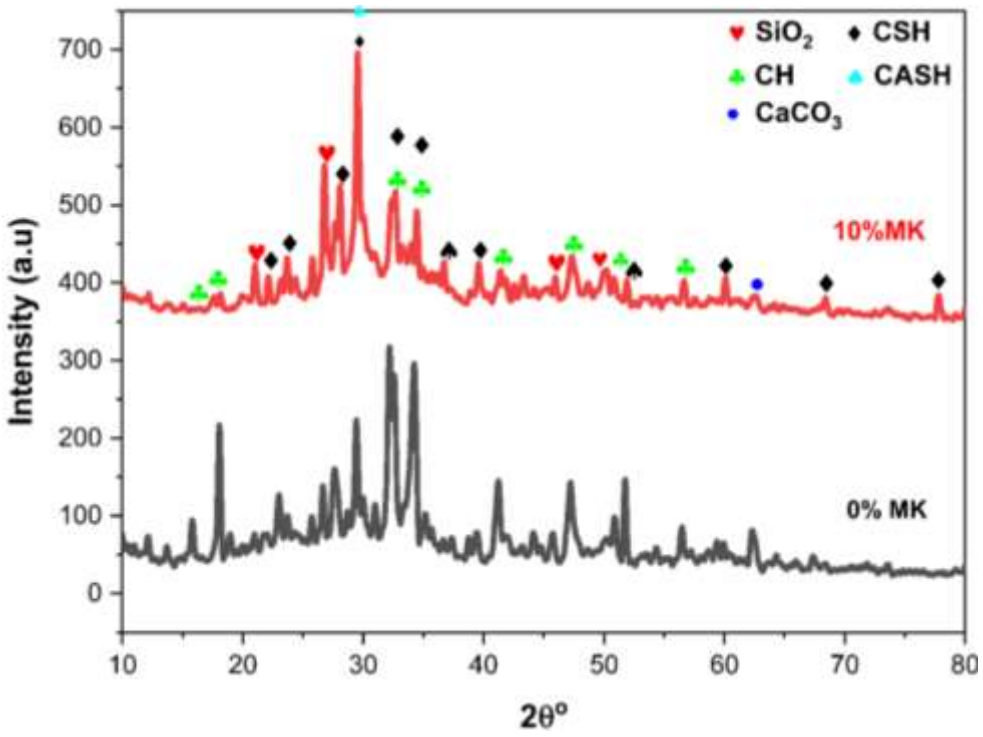

Figure 4.2 XRD pattern of 0% and 10 % MK blended OPC cement paste.

4.1.3 FTIR Analysis of Filter Cake (Kaolinite), MK, -blended paste

Figure 4.3 illustrates FTIR spectra of pretreated filter cake-kaolinite and post-treated Metakaolin. Pretreated filter cake-kaolinite show notable broad stretching at 3435 cm^{-1} this is mostly due to H-O-H stretching with a compound class of absorbed water (Kumar & Lingfa, 2020). The peak at 1641 the bending vibrational bonding of absorbed water. The presence of three key vibrational modes in FT-IR spectra of post-treated by-product (Metakaolin), 1089 cm^{-1} of Si-O-Si asymmetric stretching, 799 cm^{-1} of Al-O-Si, and 461 cm^{-1} of Si-O bending, indicated the formation of Metakaolin after calcining waste product filter cake at 600 ℃/2h (Gao et al., 2020b; Wang et al., 2005).

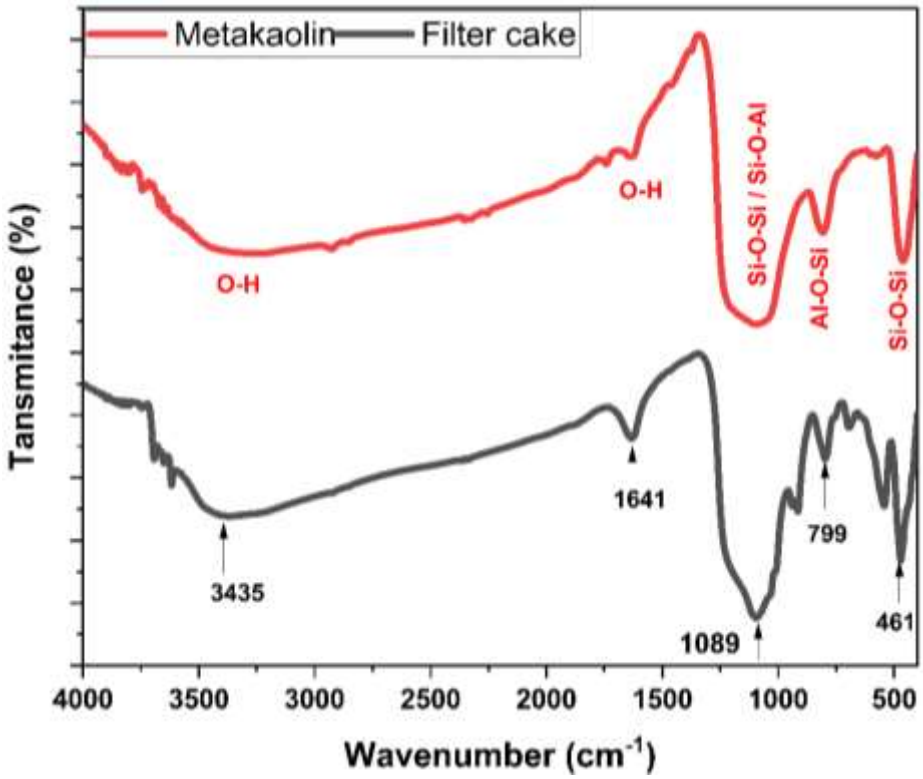

Figure 4.3 FT-IR analysis of filter cake-kaolinite and Metakaolin.

Figure 4.4 shows the infrared spectrum of the paste sample with 0% and 10% metakaolin contents. The samples show both a broad band at 3435 cm^{-1} and a narrow band at 1641 cm^{-1}, which are assigned to stretching and bending vibrations of OH and H-O-H from water hydroxyl groups, respectively (Panda et al., 2018; Wen et al., 2020). The peak at 1415 cm^{-1} observed in 0% MK and 10%MK samples correspond to the O-C-O bond, which may be due to the adsorption of CO_2 from the air (Chen et al., 2017). Compared with 0% MK the 10% MK shows a new absorption peak at 455 cm^{-1} representing the in-plane bending vibration of the Si-O bond (Gao et al., 2020a).

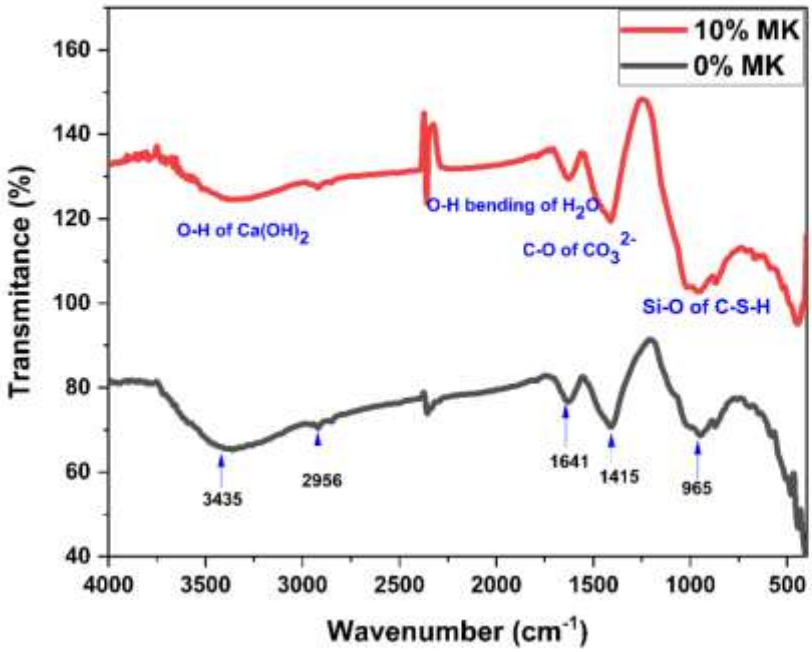

Figure 4.4 FI-IR Spectra of control (0%) and 10% MK blended OPC paste

4.1.4 Thermal Analysis of filter cake-kaolinite and mortar samples

There was a phase transformation of waste filter cake-kaolinite material to mullite & cristobalite crystalline at a temperature above 1000 ℃ which is not preferred to replace OPC-cement. Thus, we heat treated waste filter cake-kaolinite samples up to 1000 ℃ with a heating rate of 10 ℃/min. From the DTA/TGA measurement, an endothermic peak was observed at nearly 82 ℃, which is attributed to loss of absorbed water (2.3%) as shown in figure 4.5. The endothermic peak at 274.2 ℃ exhibits the decomposition of organic volatile components. Maximum mass loss from waste filter cake-kaolinite material was occurring at temperature 508.5 ℃, i.e., the large mass loss (4.9%) in this temperature range represents the de-hydroxylation of waste filter cake-kaolinite to metakaolin. Filter cake-kaolinite transforms to non-crystalline metakaolin ($Al_2Si_2O_7$) after calcination at 450– 600 ℃ losing the chemically bound water molecules.

The formed metakaolin ($Al_2O_3{\cdot}2SiO_2$) material has increased pozzolanic reactivity. Dehydroxylation continued up to 850 ℃ (Wang et al., 2011). The DTA curve of kaolin showed a broad characteristic melting exothermic of approximately 940 ℃. This is due to the recrystallization (0.42%) and transformation of dehydrated substances to mullite,

cristobalite, and quartz characteristic for metakaolin dissociation and formation of spinel (Aragaw & Kuraz). Total mass loss of filter cake-kaolinite sample up to 1000 ℃ is 8.04%.

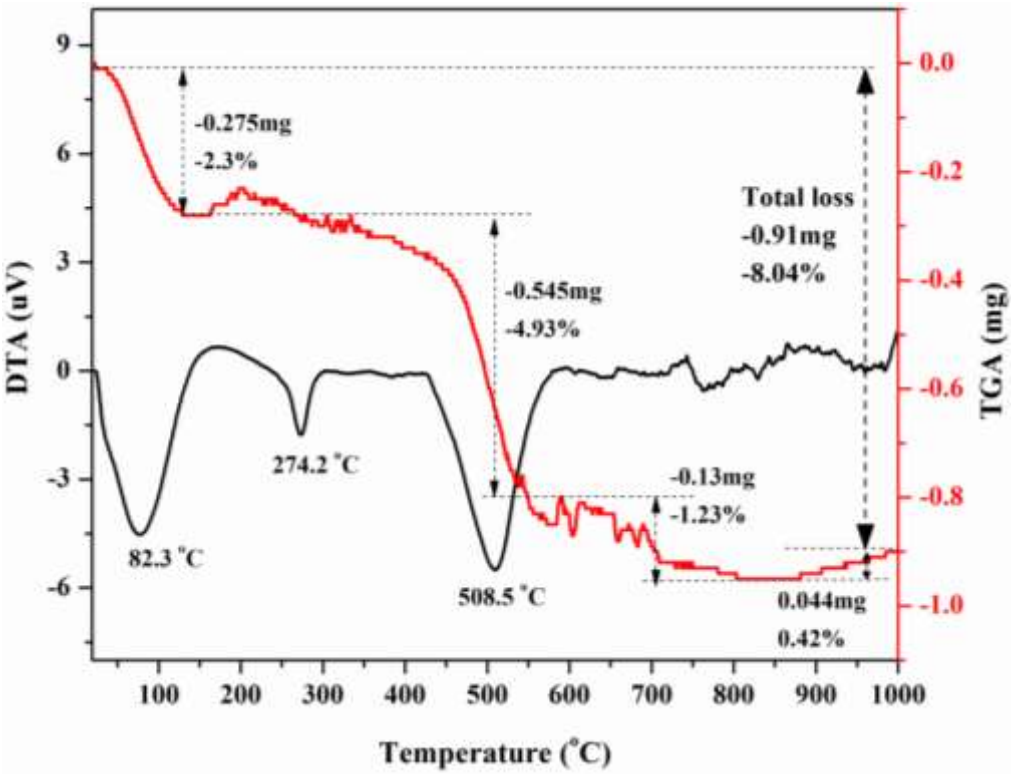

Figure 4.5 TGA and DTA analysis for filter cake-kaolinite

We also used DTA/TGA analysis to evaluate the thermal stability of hardened mortars with the addition of Metakaolin (10% MK) and without MK respectively (Figure 4.6). As the temperature increased, the weight of both samples increased due to water loss, the breakdown of components, and the escape of volatile particles from mortars. The endothermic peak at 83.4 ℃ is caused by moisture loss from the samples. An endothermic peak at 447.5 ℃ is also related to loss of water combined with calcium hydroxide as explained in a previous study (Qian et al., 2019). The endothermic peak at 703.8 ℃ is caused by the decomposition of $CaCO_3$ to lime (CaO) and carbon dioxide (CO_2) (Zhao & Khoshnazar, 2020).

In figure 4.6, the first endothermic peak located below 100 ℃ is mainly due to the removal of free water and the decomposition of the amorphous part of calcium silicate hydrates (CSH). The endotherm located at about 447 ℃ represents the dehydration of calcium hydroxide ($Ca(OH)_2$) (Abdullah & El-Sokkary, 2022). The last endothermic peak located at 703.8 ℃ is due to the decomposition of $CaCO_3$ (Li et al., 2022). The weight loss of the samples above 600 ℃ is most likely due to the decomposition of $CaCO_3$ to free CaO

and CO_2 (g), causing volatile matters to escape (Nadeem et al., 2013; Nežerka et al., 2014). According to our TGA investigation, the total weight of the 10% MK-contained mortar sample (-10.4 percent) is lower than that of the 0% MK mortar sample (11.4 percent). This is due to the dehydration of the interlayer calcium silicate hydrates (CSH), calcium aluminate hydrates (CAH), and calcium sulphoaluminate hydrates (CSAH). The lower weight loss showed the excessive formation of larger amounts of CSH due to the addition of MK as it is explained in the previous studies (Ibrahim et al., 2018; B. Sabir et al., 2001). It is further supported by the results of XRD on 0% and 10% MK samples.

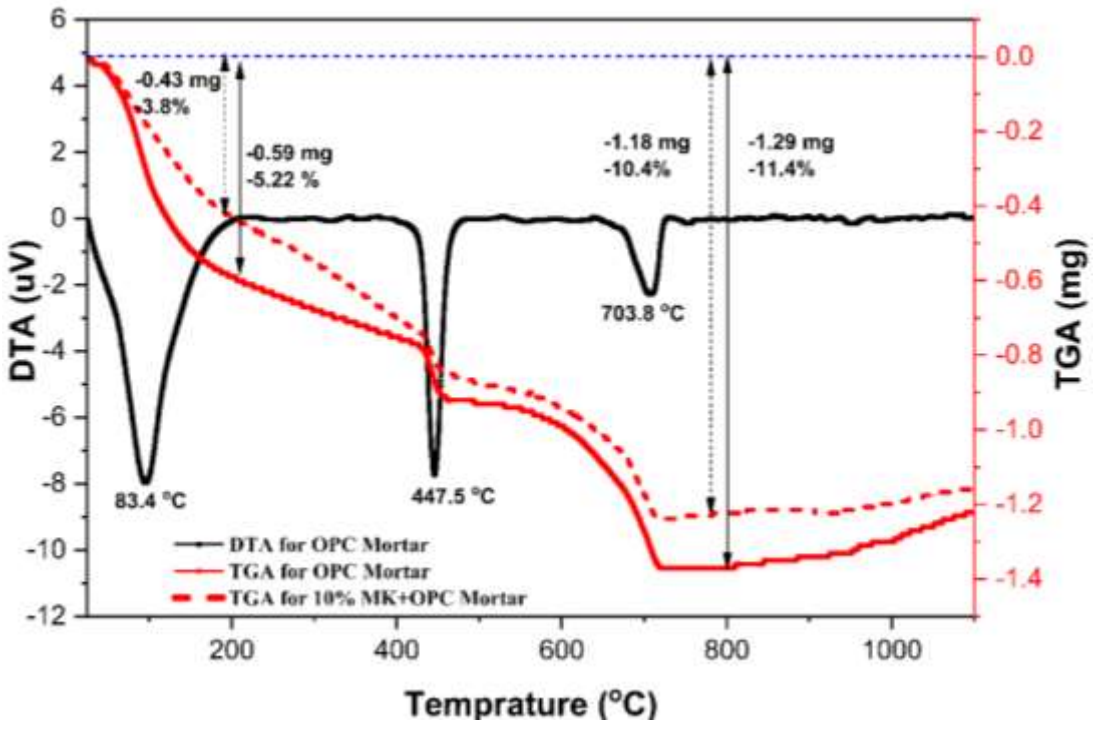

Figure 4.6 TGA and DTA analysis for 0% and 10% MK blended mortar samples.

4.1.5 Flexural and compressive strength of MK-Blended OPC-mortar

Flexural strength of OPC-mortar samples decreased with the addition of Metakaoline at 3 days curing ages. At 7 and 28 days of curing, the flexural strength of OPC-mortar samples increased up to 10% MK replacement (Figure 4.7). This is most likely related to the reduction of CaO and large formation of CSH with MK addition. For instance, the flexural strength of OPC-mortar is 8.9 MPa and 10% MK with OPC-mortar is 9.6 MPa. The presence of metakaolin may enhance the dissolution of cementitious phases and/or provide additional, well-dispersed sites for nucleation of hydration products. However, the flexural strength of

MK blended OPC-mortar samples decreased with 15% and 20% MK replacement which is most likely related to a decrease in C_3S (alite) content in mortar, and MK may also form aggregate due to the large surface area of MK (12,430cm^2/g) compared to the surface area of cement (3,394 cm^2/g) (Bahurudeen & Santhanam, 2015).

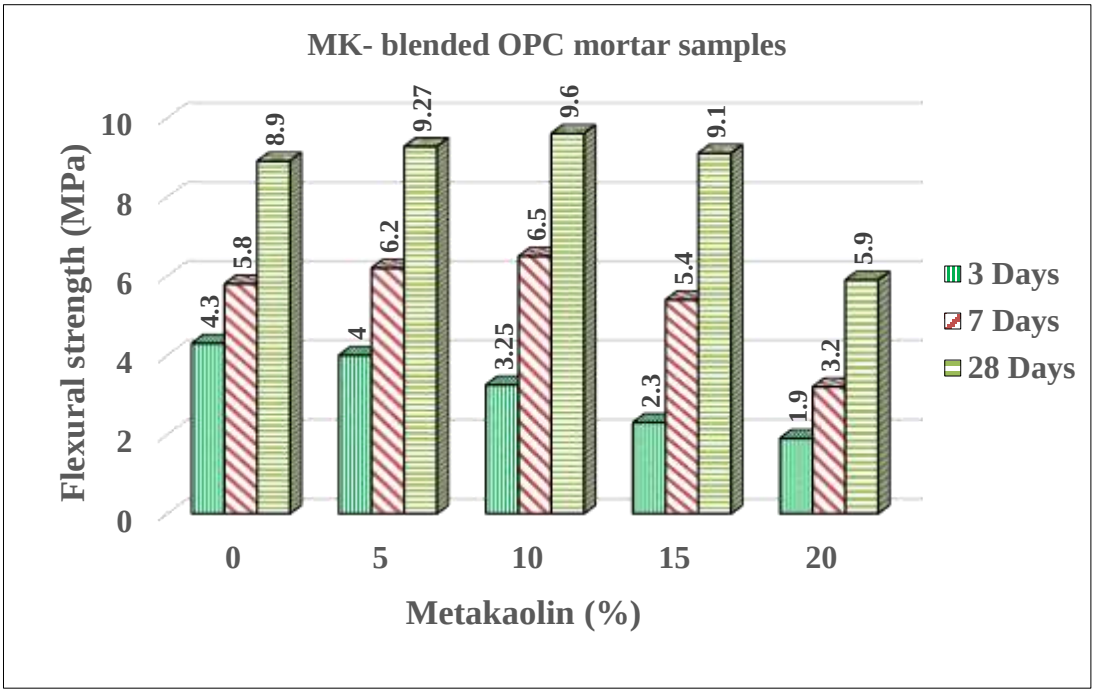

Figure 4.7 Flexural strength of 0-20% MK-blended OPC mortars.

Similarly, the Compressive strength of OPC mortar samples decreased with the addition of Metakaolin at 3 days of curing ages as shown in Figure 4.8. This is owing to the reduction of the $3CaO{\cdot}SiO_2$ (C3S) alite phase amount in a mortar with MK replacement which is responsible for early age strength. The heat of the hydration rate most probably decreased with MK, as explained in a previous study (Jiang et al., 2015). A higher compressive strength of mortar was obtained at 10% MK replacement OPC, compared to neat mortar at 7 days and 28 days curing ages. Pores among the cement and sand in mortars were probably filled with fine MK, which caused an increase in the MK-blended mortar's strength at 7 and 28 early ages. Moreover, the formation of additional Calcium Silicate Hydrated (C–S–H) gel is a result of the reaction of the active silica of MK and the $Ca(OH)_2$ from cement hydration. However, the compressive strength of MK blended OPC-mortar samples decreased with 15% and 20% MK replacement for all curing ages due to decreased alite phase-$3CaO{\bullet}SiO_2$ content (responsible for giving early-age strength) in mortar. This might also decrease the formation of Calcium Silicate Hydrated (C–S–H) gel. It was also expected that the Aluminite

phase, $3CaO•Al_2O_3$, decreased with more MK content replacement. Moreover, we added an extra 15 ml of water as 15% and 20% MK-blended mortar preparation time to increase the mixtures' workability. High water content most likely created pores inside the dried mortar bricks and it might also cause to decrease compressive strength of mortar bricks. In our investigation, the highest compressive strength was obtained at 10% MK blended OPC mortars as compared to conventional OPC mortars for all curing ages.

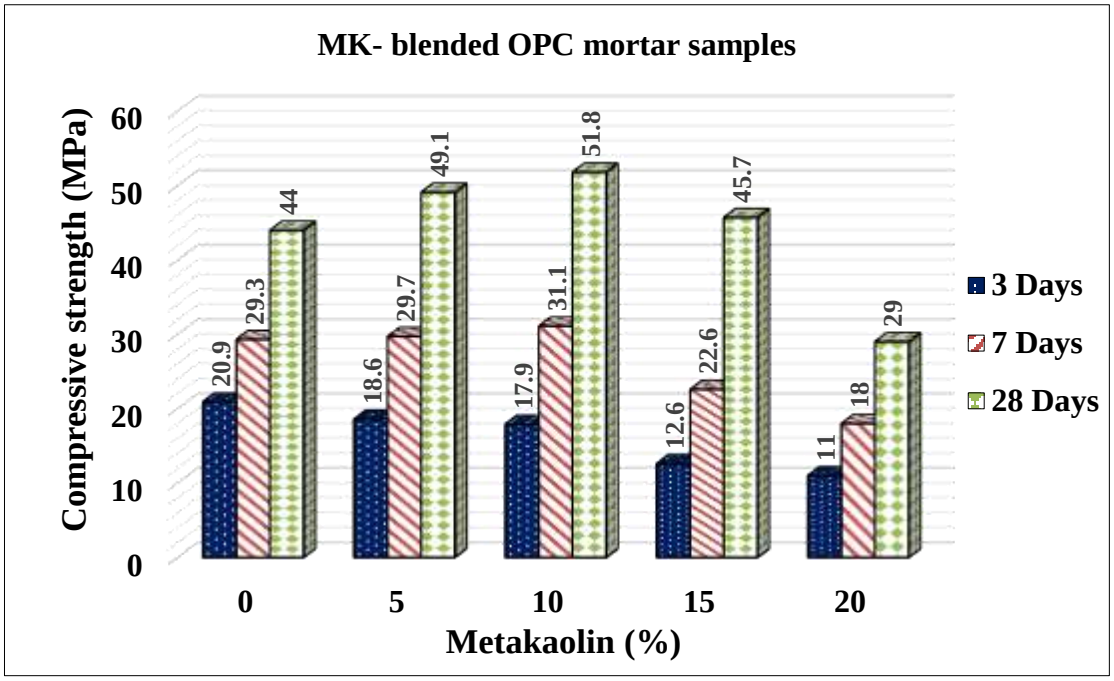

Figure 4.8 Compressive strength of 0-20% MK-blended OPC mortars

4.1.6 Setting time and Expansion of Mk-Blended OPC-pastes

The importance of setting time in concrete construction practices is attributed to the need of scheduling the different phases of construction operations, such as transporting, concrete placing, consolidating, and finishing. The time of formwork de shuttering is also dependent on concrete setting time. We checked the setting time and soundness of the MK-Blended OPC-Mortar Sample at normal consistency. Water required for normal consistency increased with increasing in MK amount. For instance, the consistency values for 0 and 20% MK replacement were 0.28 and 0.48%, respectively. As the metakaolin was hygroscopic and the specific surface area of metakaolin was 12,430 cm^2/g which is three times higher than cement it needed more water for proper consistency. The incorporation of MK has an impact

on the setting of cement paste and mortar (Khatib et al., 2018) indicating that the setting time for paste increases with the substitution of cement by 10% of MK.

The standard specifications ASTM standard C191-82 limit the initial setting time to a minimum of 45 minutes and the final setting time to a maximum of 600 minutes (ASTM, 2004). All our samples satisfied these requirements (Figure 4.9). The setting time of the MK-OPC blended pastes was longer than that of conventional OPC cement paste due to the lower amount of C3A used during MK-OPC blended pastes. As MK was partially replaced the amount of tricalcium aluminate found in OPC indirectly decrease which is an important component in releasing high heat of energy. The decrease in C3A results in a long time take to lose its plasticity. The setting time is controlled by the content of phases like Aluminite (C3A) and Alite (C3S) which are decreased in MK-OPC blended pastes. The increase in the setting time is compared to the conventional cement paste but the result did not exceed the ASTM standard.

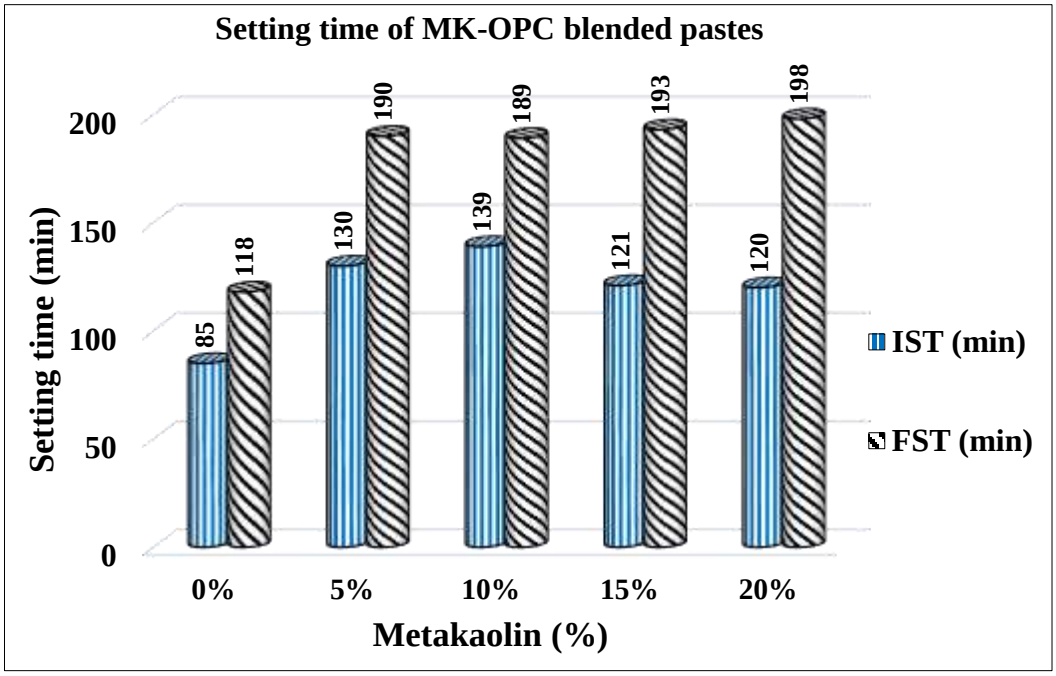

Figure 4.9 Setting times at normal consistency of MK- OPC blended pastes.

Expansion (soundness) of dried cement paste might occur due to hydration of uncombined free CaO and /or MgO inside the cement. We checked the soundness of the MK-OPC blended pastes using Le- Chatelier apparatus conforming to IS: 5514-1969. Figure 4.10 clearly shows that as the amount of MK increased, the expansion of dried pastes reduced marginally. Lower expansion of MK-OPC blended pastes might be related to lesser content of MgO and CaO in metakaolin as observed in our XRF data table 2 and results in the lesser

formation of $Mg(OH)_2$ and $Ca(OH)_2$. According to the ASTM C151 (Kabir et al., 2020), the upper limit of Le-Chatelier expansion is 10 mm; however, as shown in figure 4.10, Le-Chatelier expansion did not exceed the limitations with the addition of metakaolin.

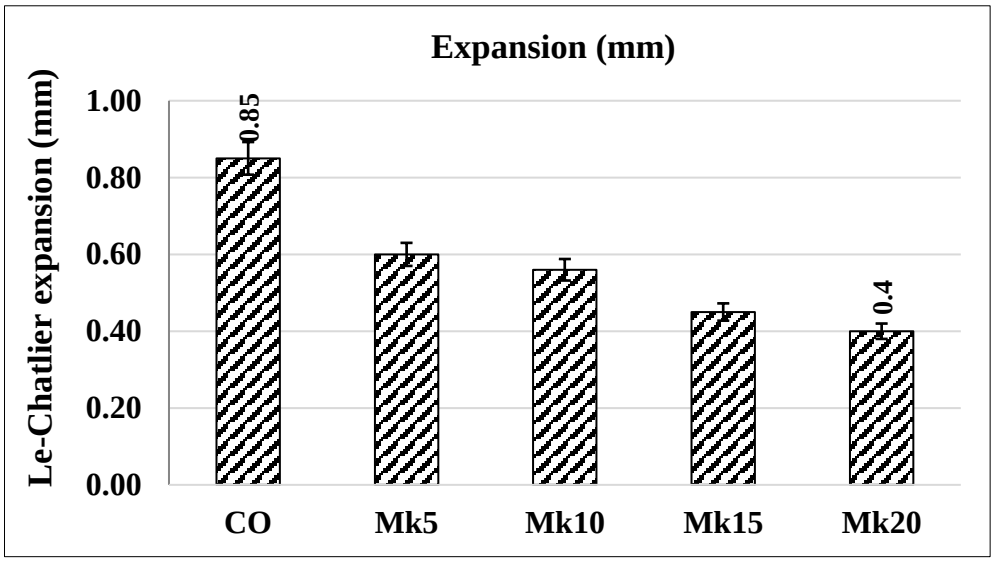

Figure 4.10 Expansion of Control OPC paste (CO) and MK-OPC blended pastes

4.1.7 Water absorption and apparent porosity of MK-Blended OPC Mortar

Water absorption of mortars increased from 17.88% to 30.49% with increasing MK contents from 0 to 20% MK in mortars at 3 days of curing age (figure 4.11a), due to a higher specific surface area of MK (12,430 cm^2/g), compared to the surface area of cement (3,394 cm^2/g) (Bahurudeen & Santhanam, 2015). Similarly, water absorption increased from 13.9% to 26.55% with increasing MK contents from 0 to 20% MK in mortars at 7 days curing age. MK-blended OPC mortars have higher water absorption at a curing age of 3 days compared to the 7 days for OPC mortars. This may be attributed to 7 days of curing being favorable for important compound formation compared to 3 days of curing. Pores spaces in the blocks decreased with increasing curing age. Apparent porosity of MK-blended mortars shows initially decreasing from 26.3% to 19.11% with the increment of MK from 0 to 10% MK replacement. This is owing to the finer particle size of MK acting as filling voids as shown in figure 4.11b. Then apparent porosity increased above 10% MK replacement. This is most probably due to finer particle size increased as a result of agglomeration increases. Moreover, as we explained before, extra water was added for 15 & 20 % MK blended OPC mortars during sample preparation, which might result in more pore formation in dried

mortars. Apparent porosity is expressed as a percentage of the volume of the internal open pores in the specimen to its exterior volume.

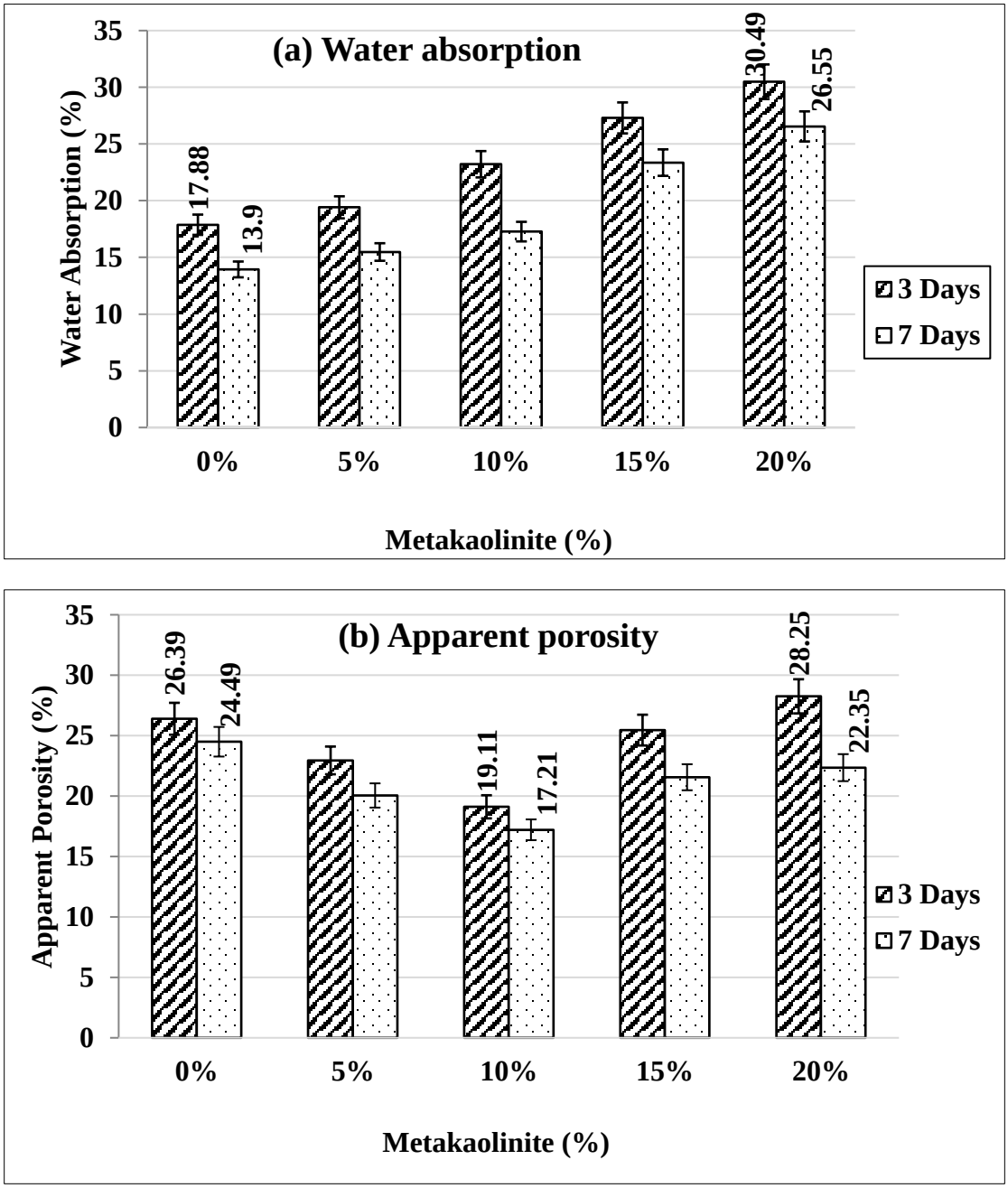

Figure 4.11 MK blended OPC mortar (a) Water absorption; and (b) Apparent porosity

4.1.8 Microstructure characterization of MK and MK-blended mortar

SEM images of filter cake-kaolinite and MK are shown that particles with different morphology. Metakaolin has porous microstructures (figure 4.12b) compared to filter cake (kaolinite) (figure 4.12a). it is most probably due to the removal of H_2O and other

components from the filter cake at a higher temperature of 600 ℃. Additionally, the fast-cooled quenching results in an amorphous structure which is in agreement with XRD results.

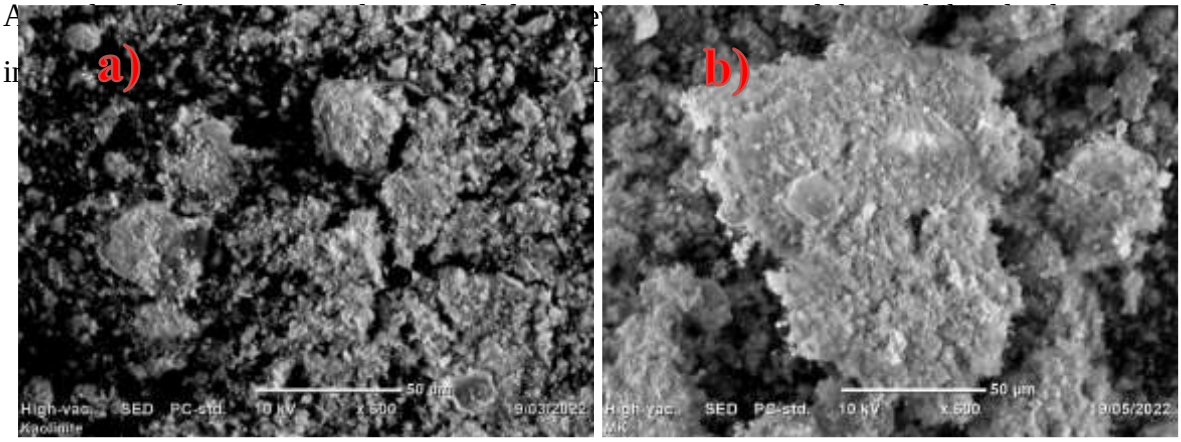

Figure 4.12 SEM result for a) FC before treatment(Kaolinite) and b) FC after treatment (MK)

SEM images of 0% and 10% MK blended OPC paste are shown particles of different morphology. 0% MK blended mortar has crystalized and not well-dispersed microstructure (figure 4.13a) compared to 10% MK blended mortar (figure 4.13b). It is probably due to the pozzolanic activity of MK and the formation of C-S-H gel. This is in agreement with XRD results. In a previous study, the C-S-H gels are amorphous or poorly crystalline (Soler, 2007). we can conclude that 10% MK paste has a well-distributed amorphous morphology compared to 0% MK mortar. It is also expected that a large amount of CSH gel formed in the case of 10% MK-blended mortar as compared to conventional mortar.

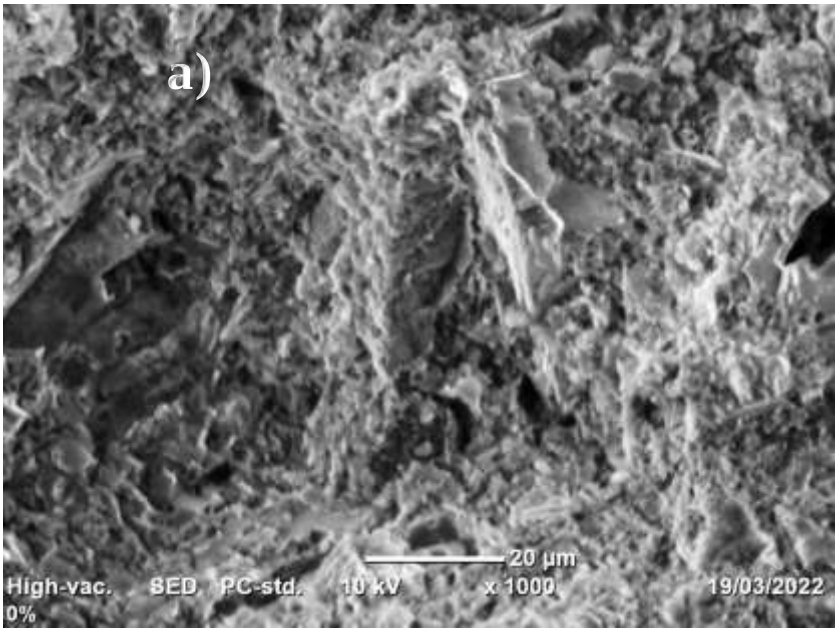

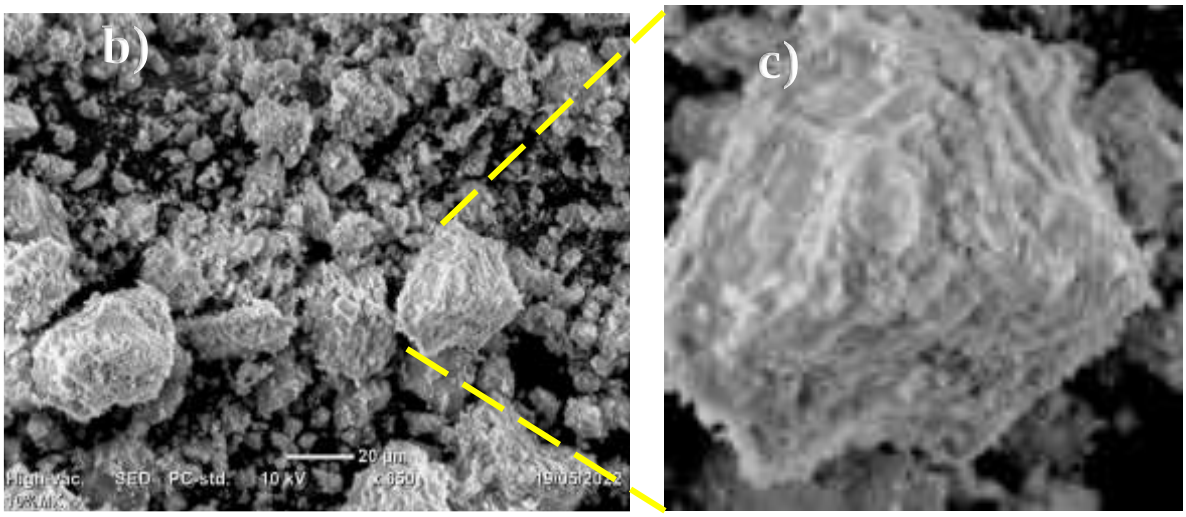

Figure 4.13 SEM image of a) OPC, b) 10% MK blended OPC paste and c) Insitu image

4.2 Characterization of BA and BA Blended OPC Mortar/paste

4.2.1 Mineralogical Compositions of Bagasse Ash (BA)

Table 4.2 displays mineralogical compositions of BA collected from the sugar industry. We used an XRF to reveal the major and minor oxide composition of the bagasse ash, as well as the loss on ignition (LOI) percent to check its pozzolan oxide contents (SiO_2 + Al_2O_3 + Fe_2O_3), alkaline oxides, and loss on ignition. It is essential to distinguish the chemical properties of BA and its reaction with OPC when both materials are combined (Norsuraya et al., 2016). According to ASTM C618 (Kasaniya et al., 2021b) if the total sum of SiO_2 + Al_2O_3 + Fe_2O_3 is above 70 % of the total mass, then the matter can be considered as a pozzolanic material. As per Table 4.2, the sum of SiO_2 + Al_2O_3 + Fe_2O_3 for BA amount to 80.02 %, which is greater than 70% revealed that the bagasse ash can be assigned as class N pozzolan, as per ASTM C618 classification. implies that BA can eventually be used as a pozzolana and could contribute to the strength development process in concrete. These results were in agreement with the reporting from (Seyoum et al., 2021). The sum of pozzolan oxides of OPC is 31.6%, but bagasse ash has 80.02%, as shown in Table 4.2 Thus, the result testified to the pozzolanic nature of BA as per ASTM C-618 specifications and taken as pozzolan materials for cement replacement. Moreover, loss on ignition (LOI) of BA is 4.75% which is less than 10%. Thus, the pozzolanic activity would upsurge with partial BA replacement cement as stated in a previous study (Chusilp et al., 2009a). Chemical analysis data has also indicated BA has a three-times higher silica content (65.06%) than OPC (22.82%). However, bagasse ash has a high alkali content (Na_2O + K_2O = 8.66%), implying a high potential for the alkali-silica reaction, which might have an adverse effect.

The loss on ignition (LOI) value was found to be 10.48% which is slightly higher than that specified by the same standard, which is 10%.

The physical properties are as important as the chemical properties and significantly impact the concrete's hardened properties. The specific gravity of BA was noted to be lower than OPC, which suggested that the BA concrete density will be lower compared to normal concrete (Fapohunda et al., 2017). This could imply that increase in BA content will decrease the density of the concrete. It was also observed that the color of BA was changed from black to in a range of light brown to white after the samples were further burned in a muffle furnace at 600 ^{0}C for 2 h. This could conclude that the carbon content in the BA has decreased. Katare and Madurwar (Katare & Madurwar, 2017) stated that the color of the BA depends on the completeness of the combustion process and the structural transformation of silica in the ash.

Table 4.2 Chemical composition of Sugarcane Bagasse Ash (BA)

Chemical compositions of BA	**Oxide percentage (%)**
SiO_2	65.06
Al_2O_3	10.88
Fe_2O_3	4.08
CaO	1.14
MgO	1.3
Na_2O	2.06
MnO	0.1
P_2O_5	0.79
TiO_2	0.24
H_2O	0.66
LOI	4.75
SiO_2+Al_2O_3+Fe_2O_3	80.02
Blaine fineness (cm^2/g)	4,716
Specific gravity (g/ml)	2.12
Color	Light brown to white

4.2.2 XRD Analysis of Calcined Bagasse ash

High BA pozzolanic activity could be obtained by controlling calcination temperature and duration, whereby most silica is kept in a noncrystalline form (G. Cordeiro et al., 2009).

Different boiler/furnace systems usually run on different combustion temperatures ranging from 550 to 1000 ℃ (Arif et al., 2016; Bahurudeen & Santhanam, 2015). In the case of 50% bagasse humidity, the flame temperature of the burning bagasse may vary from 850 to 920 ◦C and if the bagasse humidity is less than 35%, the flame temperature may reach 1000 ºC (Sales & Lima, 2010). A high combustion temperature within the boiler can result in silica crystallization, which eventually leads to poor BA pozzolanic activity (G. C. Cordeiro, R. D. Toledo Filho, L. M. Tavares, et al., 2009). Incomplete combustion would result in high carbon content in BA. Calcining bagasse under low temperature (600 ◦C) for a short time (1 h) would generate char-like ash, which contains cristobalite SiO_2 and graphite (carbon). Prolonged heating is necessary for the complete combustion of sugar cane bagasse into white ash(Embong et al., 2016). The BA pozzolanic activity recalcined at 800 ◦C is stronger than that of the raw BA. The sample calcined at 700 ◦C had the highest pozzolanic activity. The gradual transformation from amorphous silica to cristobalite above 700 ◦C is clearly shown in Figure 4.14, resulting in a pozzolanic activity reduction. The increasing burning temperature and burning period gradually transformed the ash from char to white ash, yet with slight change to the amorphousness degree. The amorphous phases in sugarcane bagasse consist primarily of a disordered Si-O structure which is the product of solidification or condensation from a fused material (Embong et al., 2016). It is better to use BA as a supplementary materials recalcined at 600 ℃. Due it have amorphous silica and less crstabolite phase.since as increse tempreture the crystabolite phase existance increse this is clearly shown in fig below(Priya & Ragupathy, 2016)

High BA pozzolanic activity could be obtained by controlling calcination temperature and duration, whereby most silica is kept in a noncrystalline form (G. Cordeiro et al., 2009). Different boiler/furnace systems usually run on different combustion temperatures ranging from 550 to 1000 ◦C (Arif et al., 2016; Bahurudeen & Santhanam, 2015). The increasing burning temperature and burning period gradually transformed the ash from char to white ash, yet with a slight change to the amorphousness degree. Incomplete combustion would result in high carbon content in BA. Calcining bagasse under low temperature (600 ◦C) for a short time (1 h) would generate char-like ash, which contains cristobalite SiO_2 and graphite (carbon). Prolonged heating is necessary for the complete combustion of sugar cane bagasse into white ash (Embong et al., 2016). The amorphous phases in sugarcane bagasse consist primarily of a disordered Si-O structure which is the product of solidification or condensation from a fused material (Embong et al., 2016). It is better to use BA as a

supplementary material recalcined at 600℃. Due it has amorphous silica and less crstabolite phase. since as increase temperature the crystabolite phase existence increase, this is clearly shown in figure 4.14. The sample calcined at 600 ◦C had the highest pozzolanic activity (Priya & Ragupathy, 2016). The gradual transformation from amorphous silica to cristobalite above 600 ◦C is clearly shown in Figure 4.14**,** resulting in a pozzolanic activity reduction.

BA burned at 300, 500, 600, and 700 °c as characterized by the X-ray diffractometer. The XRD result for BA calcine at 300°c shows crystalline silica and carbon. This is mainly due to incomplete combustion results in high carbon content. Peaks found at 2θ= (43.99°, 61.89°, and 77.39°) with their correspondence hkl (102), (108), and (110) respectively indicate the presence of carbon by reference code (00-026-1077). Also, XRD results show crystalline quartz at 2θ=(27°) with their hkl (011) reference code (01-086-1564). At 500℃ calcine temperature the carbon amount decreased and the formation of crystalline quartz was observed at 2θ (26.7°) with hkl (011) with reference code 01-085-1054. Also, a minor peak associated with carbon was observed at 2θ (39.54°, 42.53°, 50.26°, 51.02°, 54.95°, 60.04°, and 68.30°) with their hkl (102),(200), (11-2), (003), (022), (21-1), and (203) by referring code 00-026-1077, which is the indication of no complete combustion takes place. The cristobalite peak appears at 28.06° with hkl (001) by reference codes (01-081-0067). At 600 ℃ calcination temperature) quartz peaks exist at 2θ =20.8°, 26.61°, 36.52°, 50.11°, 59.93°, and 68.11° with correspondence hkl (100), (011), (110), (112), (121), and (203) by referring to code (01-078-1252). A small cristobalite peak appears at 2θ= 27.46° with hkl (111). At 600 °c calcination temperature a wider hump between 15° and 30° at 2θ which is the indication of the occurrence of the amorphous silica and also quartz. A similar observation was also explained in previous studies (Bahurudeen et al., 2015; Nasir & Al-Kutti, 2018). This amorphous character contributed to the pozzolanic activity of the material to be added to OPC. Katare, V.D et al., stated that the optimal temprature for producing pozzolanic bagasse ash is 600 °c (Katare & Madurwar, 2017). At this firing temperature of bagasse, it has mainly amorphous silica, which is more reactive and has a high pozzolanic activity index (Bahurudeen et al., 2015; Katare & Madurwar, 2017). modification of silica assists in the development of C-S-H, as stated in the previous study (Baltakys et al., 2007). At 700 °c the calcination temperature from XRD results from the transformation of amorphous silica to crystabolite at 700 °c calcination temperature is clearly shown. Which is resulting in a pozzolanic activity reduction (Mohomane et al., 2017). With reference code 01-083-2466

quartz peaks appear at 2θ=26.73° with hkl values (101). The major peak in this crystalline peak is crystabolite appears at 2θ=28.06° with hkl (101) by reference code 01-079-1913.

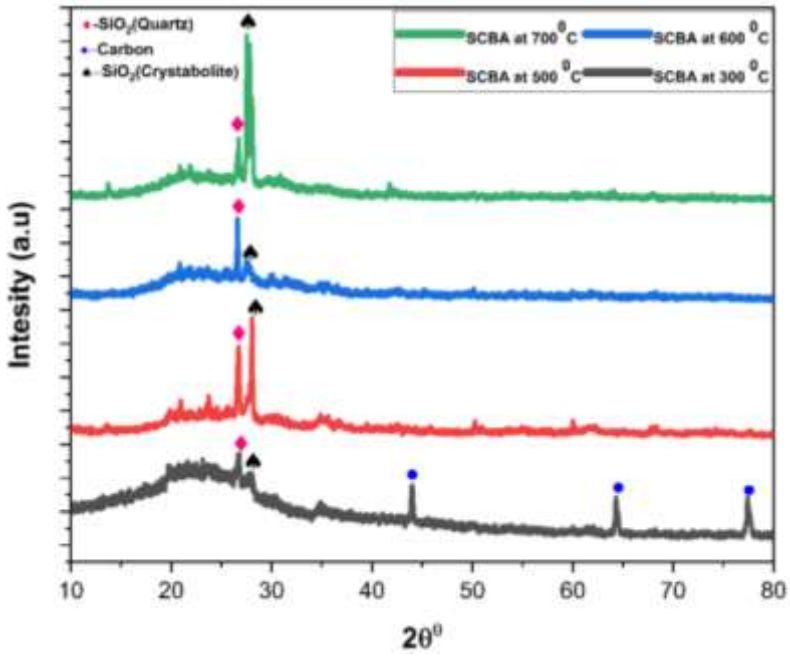

Figure 4.14 XRD pattern of BA calcined at different tempratures

4.2.3 Phase Analysis of Hardened 0% and 15% BA Blended Mortar.

From XRD measurement, we also confirmed the formation of calcium silicate hydrate (C-S-H) in both mortar samples with BA-blended and without BA-blended mortar. However, BA-blended mortar revealed the higher intensity of C-S-H peaks at 2θ and diffracted angles 27.6°, 28.04°, 29.54°, and 39.5° with their correspondence hkl values (040), (004), (211), and (226) by reference code 01-085-1378. The more intense C-S-H peaks were observed with 15% BA compared to the mortar without BA as shown in figure 4.15. This is Due to a high proportion of reactive amorphous silica of BA reacted with $Ca(OH)_2$ from cement hydration, which is crucial to forming C-S-H that assist to increase the strength of samples. In figure 4.15 at 2θ between 25° and 30°, it is known that CH/Portlandite peak intensity decreased for BA-blended mortar. The diffracted angle at 2θ =18.08°, 32.6°, 34.36°, 41.3°, 47.2°, 50.9°, and 56.4° with their correspondence hkl (001) (400) (011) (012) (023) (110) and (003) with reference code 00-044-1481. Similarly, a previous study also used XRD to detect and analyze the C-S-H (Bergold et al., 2013; Nasir & Al-Kutti, 2018). C-S-H is a nanoscale material, which is mainly responsible for the compressive strength of

cement. The calcium aluminate silicate hydrates peak appears at 60° and the calcium carbonate peak appears at 62.5° with correspondence hkl (-225), and (531) respectively.

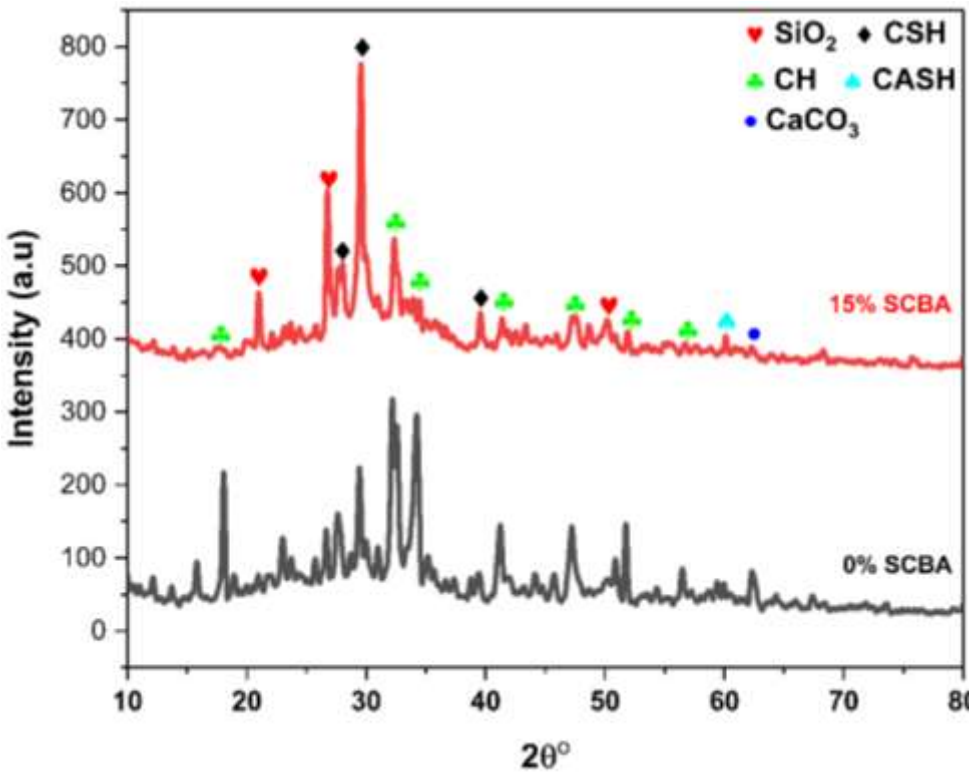

Figure 4.15 XRD pattern of 0% and 15 % BA blended OPC cement paste

4.2.4 FTIR Analysis of BA (300℃), BA (600℃), and BA-Blended paste

Figure 4.16 showed broadband at 3435 cm^{-1} indicating the presence of hydroxyl group, O-H in cellulose, hemicellulose, and pectin (Ahmad et al., 2018). The broadband at 3435 cm^{-1} is due to symmetric and asymmetric vibration of (O–H) water bounded in ash particles implies the hygroscopic nature of BA. Broad absorption bands are due to O–H stretching vibrations, with the broad asymmetric band at around 3435 cm^{-1} due to hydrogen-bonded molecular water molecules. The absorption at 2,880 cm^{-1} arises from C–H stretching. Also, absorbance at 1,730 cm^{-1} stretching of unconjugated C=O groups present in polysaccharides and xylan (Raslan et al., 2018). The wavelength band of 1100 cm^{-1} shows that quartz in form of SiO_4 in asymmetric vibration which is tetrahedral shape. The lowest bending mode of Si–O is noted at a band of 500 cm^{-1}. Two different stretching groups are identified in the BA sample, one is a strong band between 500 cm^{-1} and 1100 cm^{-1} and the other one is the broadband at 3400 cm^{-1}. The strong band indicates the presence of symmetric stretching vibration of silicon bonds. Sharp absorption peaks below 1400 cm^{-1} are recognized as

relating to the stretching and bending of Si–O bonds (Sun et al., 2004). The SiO_4 symmetric stretching vibration at 820 cm^{-1} and 620 cm^{-1} were observed clearly (Jagadesh et al., 2015).

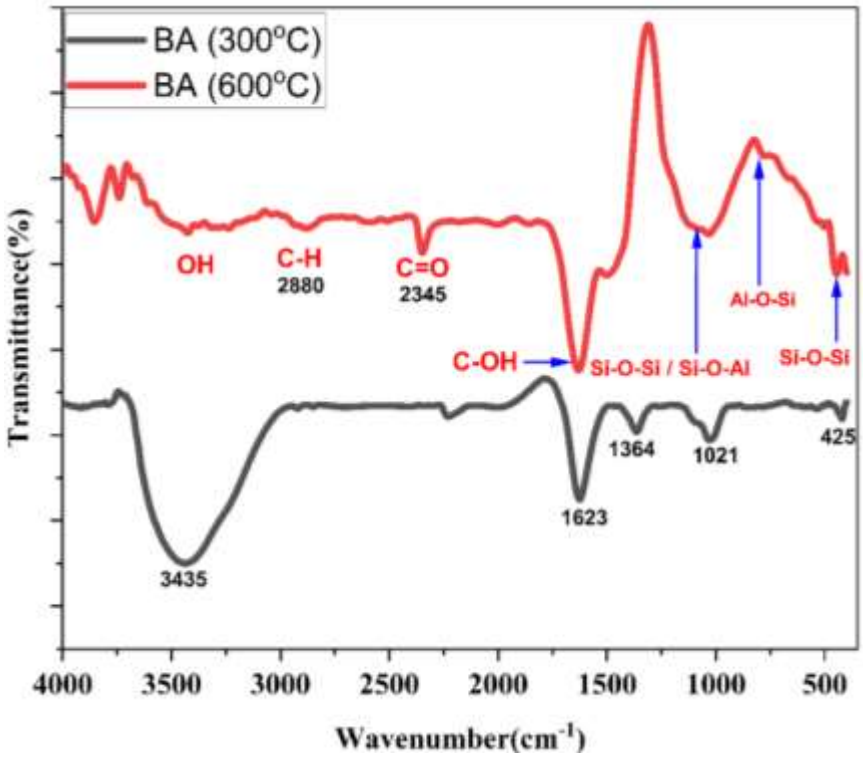

Figure 4.16 FT-IR analysis of pretreated Bagasse ash and post-treated Bagasse ash

Figure 4.17 compares the FTIR analysis results of the 28-day cured paste samples of the control and 15% BA. A more broad peak appears at 3435 cm^{-1} due to O-H stretching of $Ca(OH)_2$ in neat OPC than in 15% BA, indicating a greater degree of CH formation (Ou et al., 2011). Comparing the bands of the two samples from silicate at 930–1020 cm^{-1}, it is clear that amorphous silica accelerates the formation of CSH, as the band is quite reinforced in 15% BA compared to 0% BA. As illustrated in figure 4.17, the peaks between 850 and 1100 cm^{-1} are attributed to the vibrations of Si–O bonds in the C–S–H phase (Yu et al., 1999). Compared to the control samples, the relative intensity of the (Si–O–Si) band is higher in paste samples with the addition of 15% BA. The shift in the Si–O band toward a high wavenumber is due to the polymerization of silica. A slight shift (965 cm^{-1}) is observed in the binary mix sample containing 20% BA. The shift in the spectra of these binary (15%BA) mixes indicated the formation of a large amount of high-density C–S–H gels. The formation of more C–S–H gels might be the possible reason for the development of the high compressive strength of these mixes. Additionally, the calcite formed due to carbonation is linked to the peaks at 1415 cm^{-1}. The degree of hydration is a fundamental parameter for cementitious materials because the evolution of mechanical properties greatly depends on it.

The FTIR analysis thus helps confirm the formation of more hydrated products (CH and CSH) in mixes (Jo et al., 2017). For 15% BA blended mortar the most significant absorption bands of silica appear at 1101, 796, and 467 cm^{-1} which are attributed to the asymmetric stretching vibration of Si–O–Si, symmetric stretching vibration of Si–O–Si, and bending vibration of O–Si–O respectively (Baltakys et al., 2007). The carbonate absorption band that appears around 1429 cm^{-1} is attributed to the asymmetric stretching vibration of carbonate (CO_3^{2-}).

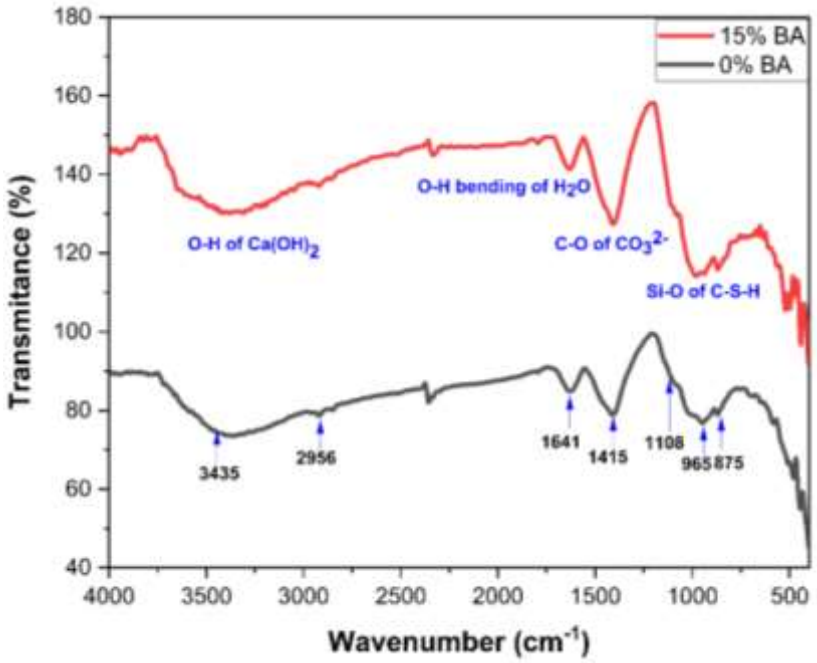

Figure 4.17 FI-IR Spectra of control and 15% BA blended cement paste

4.2.5 Thermal Analysis of BA and BA-Blended mortar samples

We used DTA–TGA to measure the thermal stability of bagasse at different temperatures, as illustrated in Figure 4.18. From the DTA measurement, a small endothermic peak was observed at nearly 77 ℃, which is attributed to water evaporation (4.6%). During the combustion process, a strong exothermic peak was detected at 468.1 ℃. This is due to the oxidation of the volatile product (Seyoum et al., 2021), and represents carbon removal from bagasse ash stated in previous studies; i.e., at nearly 600 ℃ for prolonged heating, carbon can be removed from BA (Embong et al., 2016; Katare & Madurwar, 2017). TGA analysis has shown the mass loss between 350 to 500 ℃ is more than 80%, which is caused by the decomposition of organic matter and the combustion of unburned carbon. Furthermore, mainly associated with the thermal decomposition of hemicellulose with much less cellulose and lignin (Maliger et al., 2011).

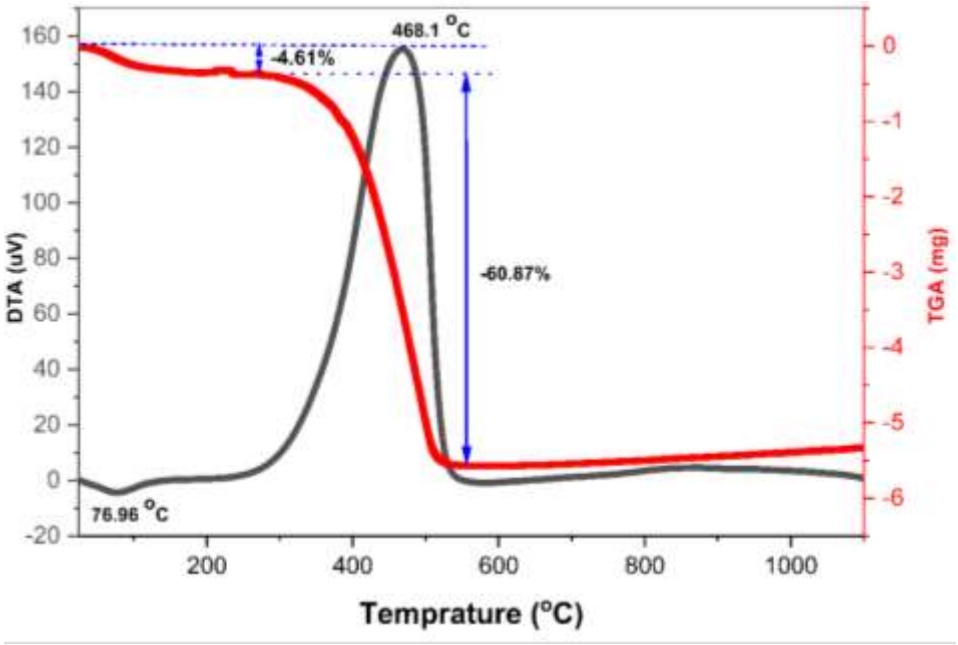

Figure 4.18 TGA and DTA analysis for Bagasse ash sample.

The thermal analysis encompasses many classical techniques such as differential thermal analysis (DTA) and TGA. DTA locates the ranges corresponding to thermal decompositions of different phases in paste, while TGA simultaneously measures the weight loss due to the decompositions. The calcium silicate hydrate (C-S-H) endothermal peak can be identified at a temperature range of 70~100 ℃, calcium hydroxide (CH) in the range of 430~550 ° C, and calcium carbonate ($CaCO_3$) at 700~800 ℃ as shown in figure 4.19. The calcium silicate hydrate (C-S-H) decomposition for neat OPC paste is -9.4% and for 15% BA blended paste is 4.8% this reduction is due to a high and strong formation of C-S-H. The large water loss from portlandite (CH) is also another reason for high weight loss in 0% BA blended paste. The endothermic peak at 447.5 ℃ is due to decomposition of calcium hydroxide which show -3.1% weight loss in the case of 15% BA blended cement Paste. The neat OPC Paste loss weight of 4.3% at 447.5 ℃ represents the dehydration of calcium hydroxide ($Ca(OH)_2$). The major weight loss also occurs at the endothermic peak of 708.8 ℃ this is due to carbonation of $CaCO_3$. The weight loss of mixes containing BA decreases with dosages of BA and is lower than that of the control mix (BA0) at the age of 28 days. 15% BA showed less loss in C-S-H and CH compared to 0%BA.

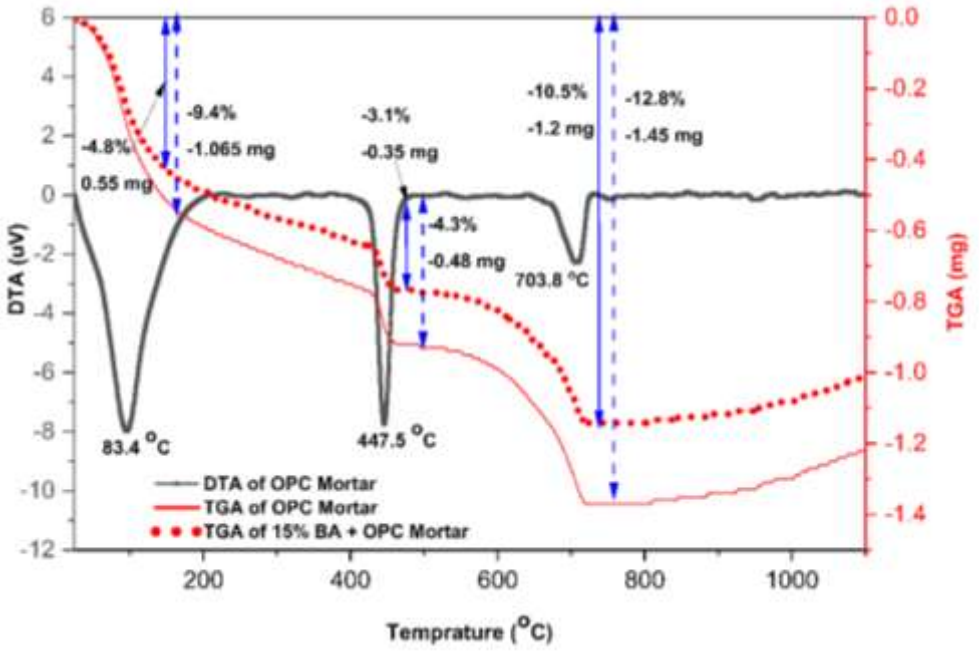

Figure 4.19 TGA and DTA analysis for 0% and 15% BA blended mortar samples

4.2.6 Flexural and Compressive Strength of BA-Blended OPC-Mortar

Figure 4.20 shows the flexural strength of the BA blended mortar sample. The highest increase in the flexural strength was observed with 15% of BA blended mortar. In 28 day curing period the 15% BA increased by 5.6% from the conventional mortar sample.

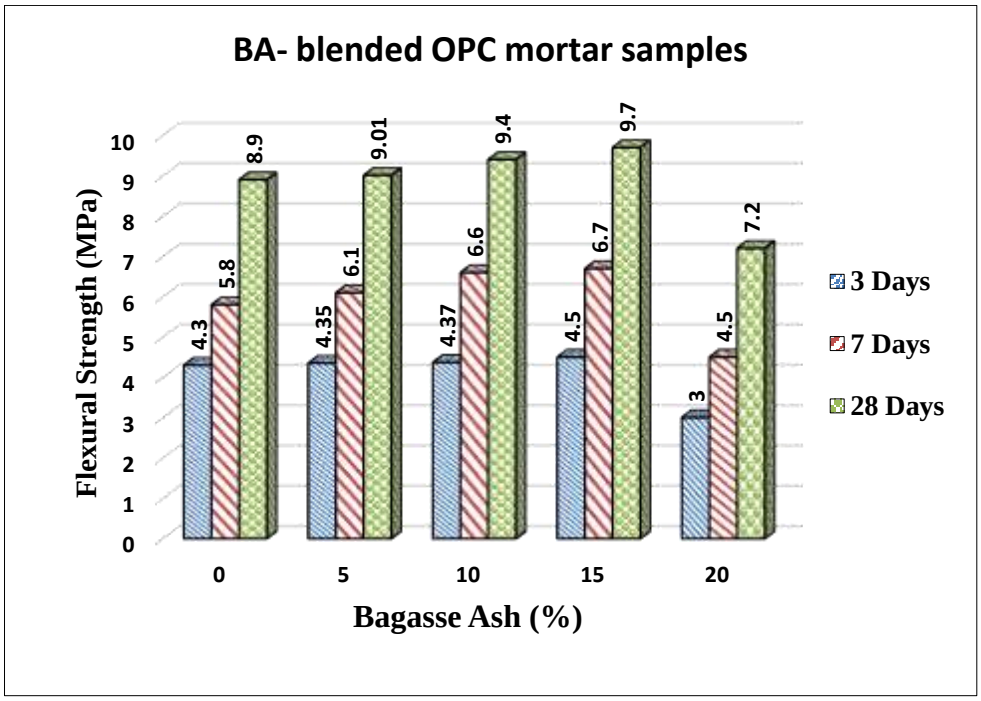

Figure 4.20 Flexural strength of BA-Blended OPC mortar

Portlandite, Ca $(OH)_2$, is a primary product in cement hydration, on which, portlandite has inferior mechanical properties because of its layered microstructure and crystal brittleness (Zheng et al., 2020). Variations of compressive strength of BA blended mixes containing 5–20 wt% of replacement of cement by bagasse ash at different 3, 7, and 28 days are shown in Fig. 4.21. An increase in the compressive strength may be due to the reaction of bagasse ash with calcium hydroxide and the formation of CSH gel (Ganesan et al., 2007). The calcium silicate hydrate is the component that gains strength due to the binding effect. Up to 15% replacement of cement with bagasse ash shows increased compressive strength. The addition of bagasse ash beyond 15% has no significant reaction with calcium hydroxide. Excess bagasse ash does not react or act as a binder in BA-Blended mortar (Praveenkumar & Sankarasubramanian, 2019); hence, it reduces strength at 28 days of curing. The factor responsible for the strength of the partial replacement of cement with ground bagasse ash is the pozzolanic reaction as shown in equations 4.3 and 4.4. Furthermore, can be highly activated due to a larger surface area and small particles of bagasse ash can fill the voids or air spaces in a mix.

$$\text{Quartz } (SiO_2) + Ca(OH)_2 + XH_2O \longrightarrow CaO.SiO_2.XH_2O \quad \ldots\ldots\ldots\ldots\ldots\ldots\ldots (4.3)$$

$$S + CH \longrightarrow C\text{-}S\text{-}H \ldots\ldots\ldots\ldots\ldots\ldots\ldots\ldots\ldots\ldots\ldots\ldots\ldots\ldots\ldots\ldots\ldots\ldots\ldots.. (4.4)$$

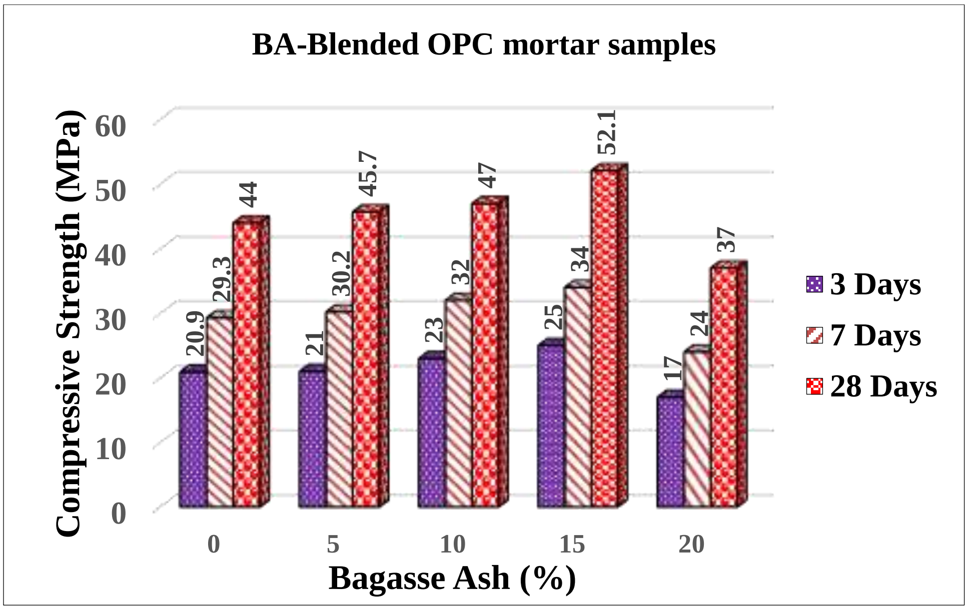

Figure 4.21 Compressive Strength of BA-Blended Cement Mortar.

4.2.7 Setting time and Expansion of BA-Blended OPC-pastes

The setting times of cement pastes at normal consistency, containing increasing amounts of BA are shown in figure 4.22. There was an increase in both the initial and final setting times. The increase in the set times may be due to the reduction in cement content and increases in water as BA content increases. Increases in setting times have previously been reported using BA (Arif et al., 2016; Singh et al., 2000). However, all setting times were within the limits outlined in ASTM standard C191-82 (ASTM, 2004), where the initial setting time should be ≥45 min and the final setting time should be less than 10h as shown in figure 4.22. As the partial replacement percentage increase the percentage of C3A decrease and a lower rate of hydration which results in a long setting time (delayed). The final setting time is decreasing with a higher proportion of replacement as mentioned (Dineshkumar & Balamurugan, 2021). The result is also confirmed in previous studies (Tech, 2019).

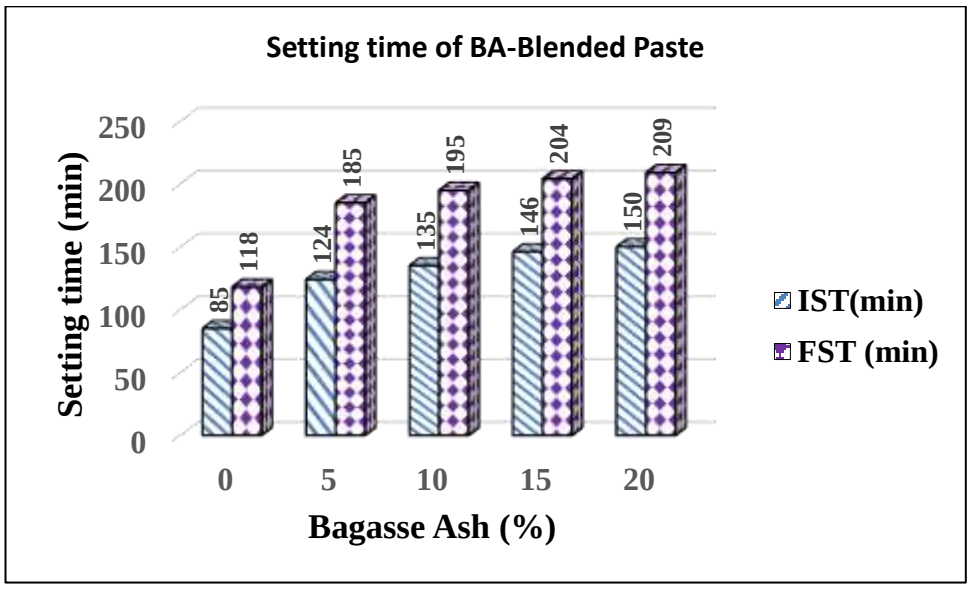

Figure 4.22 Setting times at normal consistency of BA- OPC blended pastes.

Le-Chatelier's expansion test was used to detect the change in volume caused by free lime and magnesium hydroxide. As bagasse ash consists of 8.95% of calcium oxide, reaction with water is responsible for the production of $Ca(OH)_2$. This causes the unsoundness of the bagasse ash content mix. The results in figure 4.23 show that the control mix has 0.8 mm expansion, while the 20% bagasse ash content mix has 2.4 mm expansion. Hence, the increase in expansion does not make an adverse effect since the results are within permissible limits of 10mm specified according to ASTM C151 (Kabir et al., 2020).

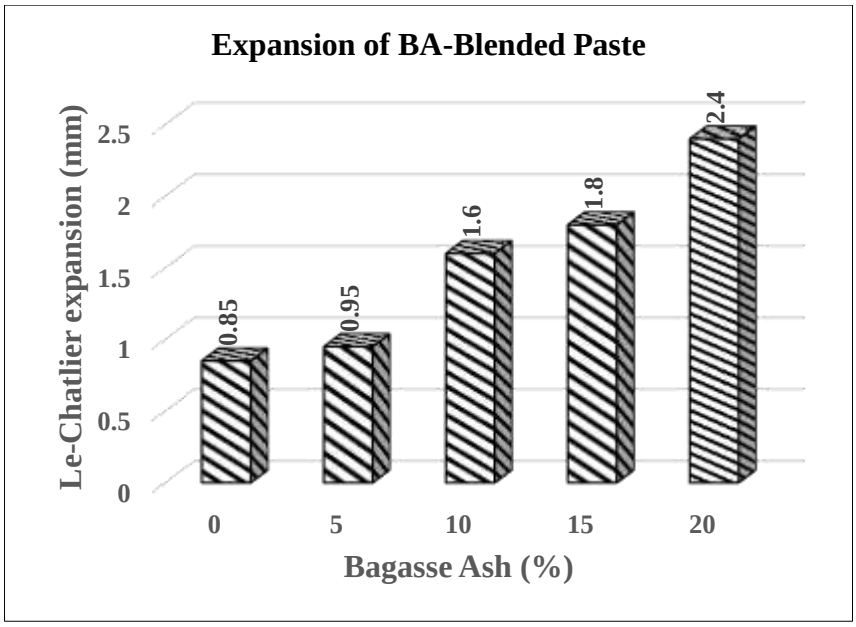

Figure 4.23 Expansion of Control OPC paste (CO) and BA-OPC blended pastes.

4.2.8 Water Absorption and Apparent Porosity of BA-Blended OPC Mortar

The results of the water absorption of mortar are demonstrated in Figure 4.24. It showed an increasing trend of water absorption with the addition of BA in the mix. Moreover, it was observed that with increasing time, the water absorption rate decreased. It was observed that the water absorption increased with an increasing amount of BA materials and decreased with an increasing curing period. This could be explained by the fact that BA has a high absorption value due to the presence of pores in BA (Rukzon & Chindaprasirt, 2012). Similar results were obtained from (Chindaprasirt et al., 2019; Le et al., 2018; Zareei et al., 2018), which ascribed the high absorption rate due to the increased number of voids in the samples thus producing a more porous specimen.

It can be seen that at 3 and 7 days of curing the percentage of water absorption increases with BA content. Because BA is finer than OPC and also it is hygroscopic. Because BA has a higher specific surface area (4,716 cm^2/g) than cement (3,394 cm^2/g), water absorption in mortars rose from 17.88 percent to 22.6 percent as BA content increased from 0 to 20% BA in mortars at 3 days of curing age (figure 4.24 a) (Bahurudeen & Santhanam, 2015). Similarly, water absorption increased from 13.9% to 20% with increasing BA contents from 0 to 20% BA in mortars at 7 days curing age. BA-blended OPC mortars have higher water absorption at a curing age of 3 days compared to the 7 days for OPC mortars. This is due to the gradual closing of pores. Obviously, with prolonged curing, the addition

of BA leads to the reduction of permeable voids. Pores spaces in the blocks decreased with increasing curing age (Ganesan et al., 2007). Apparent porosity of BA-blended mortars shows decreasing from 26.3% to 20% with the increment of BA from 0 to 15% BA replacement. This is due to BA's smaller particle size filling spaces, as seen in Figure 4.24 b. Then apparent porosity increased above 15% MK replacement. This is most probably due to finer particle size increased as a result of agglomeration increases. The volume of the internal open pores in the specimen is indicated as a percentage of the specimen's outer volume.

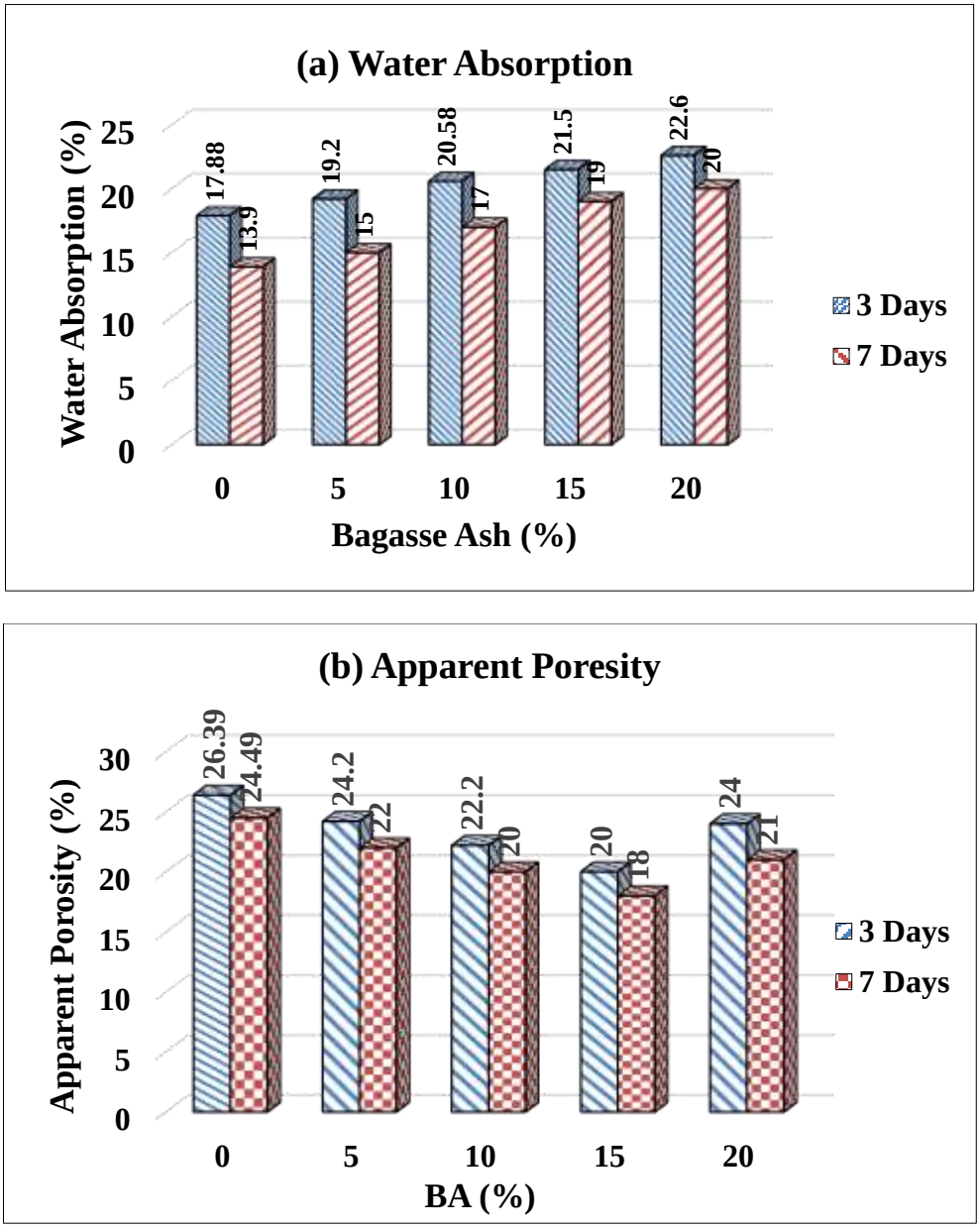

Figure 4.24 BA blended OPC-mortar (a) Water absorption and (b) Apparent porosity

4.2.9 Microstructure Characterization of BA and BA-Blended Mortar

SEM images of BA at 300 ℃ and BA at 600 ℃ are shown particles with different sizes & morphology. BA (600 ℃) has porous structures (figure 25(b)) compared to BA (300 ℃) (figure 25(a)). It is mainly due to the removal of carbon from the BA calcine at 600℃ while we burned at higher temperatures, 600 ^{o}C/2hrs. A similar explanation was also done in previous papers, and they exhibited a decrement of carbon content with an increment of calcination temperature (G. C. Cordeiro, R. D. Toledo Filho, & E. M. R. Fairbairn, 2009). The morphology of 15%BA blended paste (figure 4.25c) shows a densified structure with no significant porosity. In the SEM result of 15% BA, we could not observe crystalline structure. This is the indication of a very less amount of portlandite in the BA blended paste sample. The result confirms the consumption of $Ca(OH)_2$ and results in the formation of CSH gel.

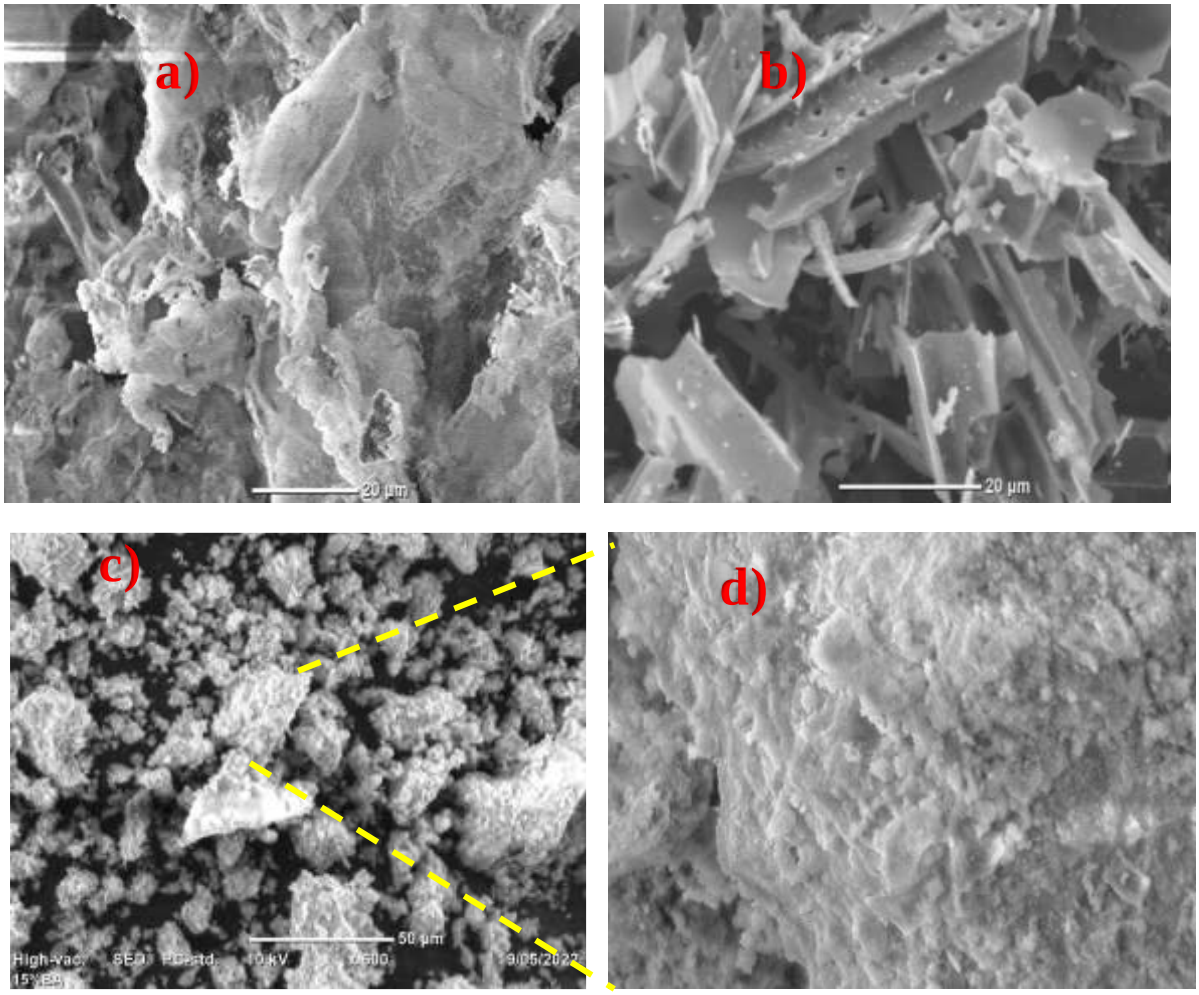

Figure 4.25 SEM image of (a) BA at 300℃, (b) BA at 600℃, (c) 15% BA OPC paste and (d) Insitu image

4.3 Characterization of Composites MK/BA/OPC blended Mortar/paste

The composite is selected from the trial test of compressive strength done in the civil engineering department by fixing the total amount of replacement by 15%. This is due to the essential compound tricalcium silicate not being reduced which is found in the OPC. The maximum replacement is also shown from the partial replacement of BA. Form different literature the mechanical properties increase at a certain point and show a decrease meant above a certain level. So, in our case from a single replacement, we can understand that above 15% replacement the mechanical properties decrease. The trial composition of mechanical properties results in the appendix. From the trials, 5 %MK and 10% BA partial replacement result in better compressive strength. We further characterize and investigate the better proportion.

4.3.1 XRD Analysis of Composite MK-BA /OPC Paste

The objective of producing composite materials is to use both possibilities in the properties of materials. From metakaolin, we have a high amount of reactive silica which implies that a high state of free energy can react with oxide most probably with $Ca(OH)_2$ forming of vital compound C-S-H. moreover, the specific surface area takes attraction to metakaolin since the finer particle size makes filling voids and creates densified structure resulting in mechanical strength. Finally, the absence of alkalis in metakaolin chemical composition indicates lower potential in alkaline silica reaction. Results are resistant to corrosion and provide chemical stability. The fundamental properties of bagasse ash are its amorphous nature and the thermal stability that make it attractive. Additionally, the abundance of bagasse ash in large quantities helps to form composite and partially replace with OPC. From these Unique properties, we can make a composite that can have a better performance than the trial sample.

Phase analysis of hardened 5% MK-10% BA blend produced after 28 days of hydration. The addition of very reactive pozzolanic materials produces a large amount of C-S-H as shown in figure 4.26. This is the indication of the total consumption of Ca $(OH)_2$ results in the secondary formation of C-S-H. For the neat OPC, the calcium hydroxide (CH) peaks were strongly distinguished at the 2θ angles: 18.08, 32.6, 34.36, 41.3, 47.2, 50.9, and 56.4 with their correspondence hkl (001) (400) (011) (012) (023) (110) and (003) respectively were consumed in the case of composite consumption. In addition, the calcium

silicate hydrates, CSH (I) and (II) appeared in MK-BA addition samples as the main hydration products by reference code 01-086-0402. The important gel formed at 2θ 22.9, 27.7, 29.3, 32.5, 34.3, 37.3, 41.1, 43.9 with their correspondence hkl (-112) (021) (-221) (-222) (221) (211) (-404), and (221) respectively. Figure 4.26 On the other hand, it was known that the main hydration products of hardened 10%MK blended OPC paste were nearly amorphous, besides the calcium silicate hydrates (CSH).

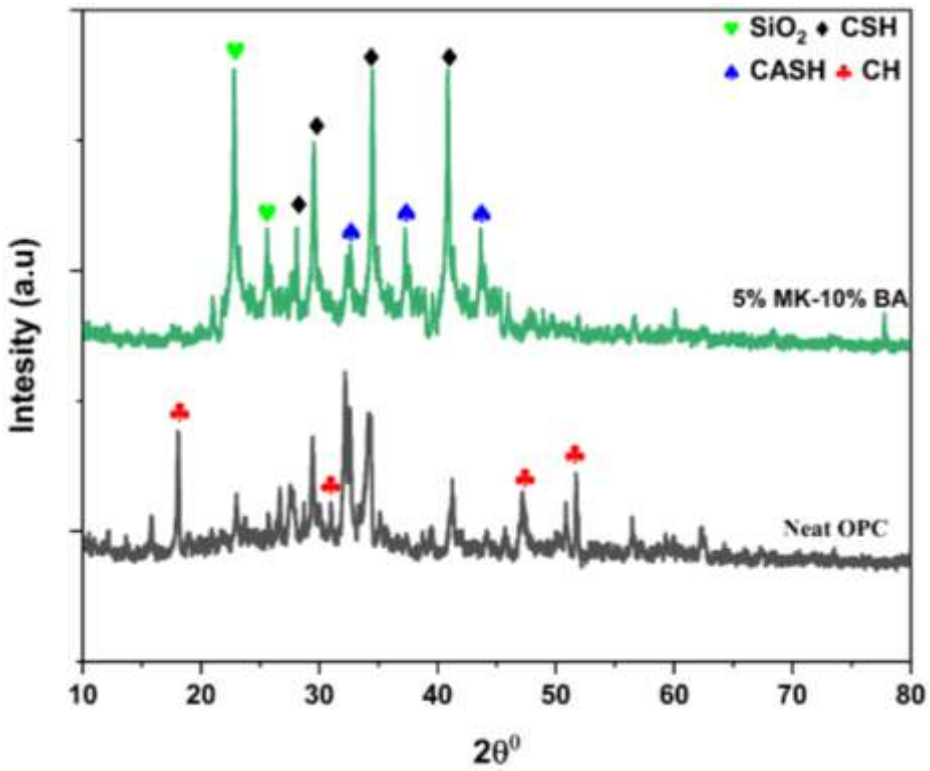

Figure 4.26 Phase analysis of MK-BA Blended paste

4.3.2 Thermal Analysis of MK-BA Blended Mortar

In figure 4.27, the first endothermic peak located below 100 ℃ is mainly due to the removal of free water and the decomposition of the amorphous part of calcium silicate hydrates (CSH). The endotherm located at about 447 ℃ represents the dehydration of calcium hydroxide ($Ca(OH)_2$) (Abdullah & El-Sokkary, 2022). The last endothermic peak located at 703.8 ℃ is due to the decomposition of $CaCO_3$ (Li et al., 2022). The weight loss of the samples above 600 ℃ is most likely due to the decomposition of $CaCO_3$ to free CaO and CO_2 (g), causing volatile matters to escape (Nadeem et al., 2013; Nežerka et al., 2014). According to our TGA investigation, the total weight loss of the MK-BA contained mortar sample (-9.23 percent) is lower than that of the 0% MK mortar sample (13.8 percent). This is due to the dehydration of the interlayer calcium silicate hydrates (CSH), and calcium aluminate hydrates (CAH).The larger weight loss showed the excessive formation of larger

amounts of CH due to there is no addition of MK or BA unreacted CH left as it is explained in the previous studies (Ibrahim et al., 2018; B. Sabir et al., 2001). The total weight loss for MK-BA blended composite show lower than single blended mortar.

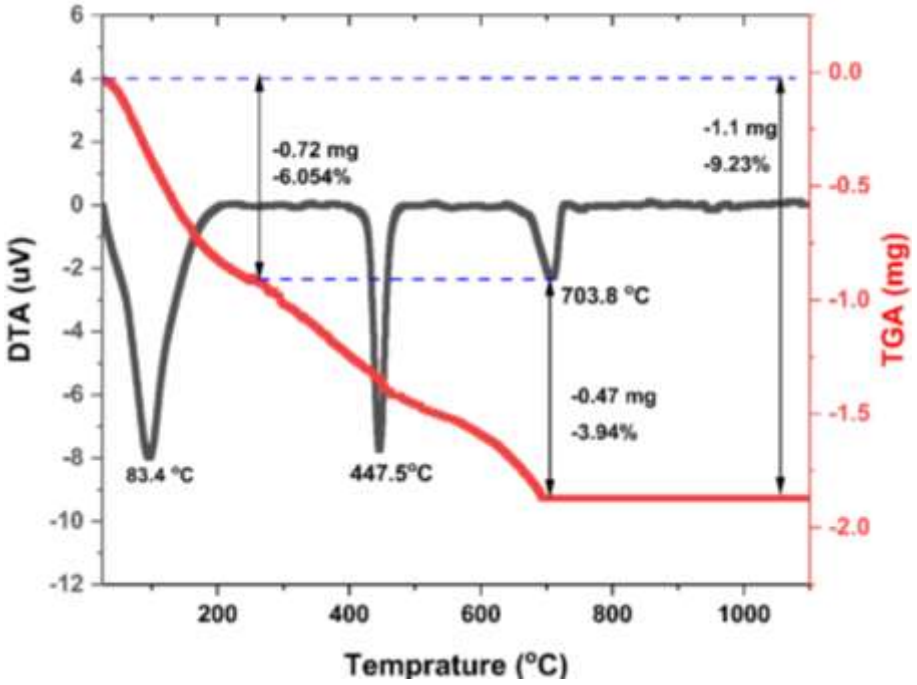

Figure 4.27 DTA/TGA analysis of 5% MK-10% BA Blended cement paste

4.3.3 Flexural and Compressive Strength of MK-BA OPC-Mortar

Figure 4.28 explain the flexural strength of composite blended mortar. The flexural strength of MK and BA blended composite OPC cement mortar show an increase in all ages of curing. This is due to the very reactive pozzolanic activity of MK-BA. One of the required properties of pozzolanic material is reactive silica which results in CSH gel formation.(Larissa et al., 2020) explain the higher potential of CSH formation.

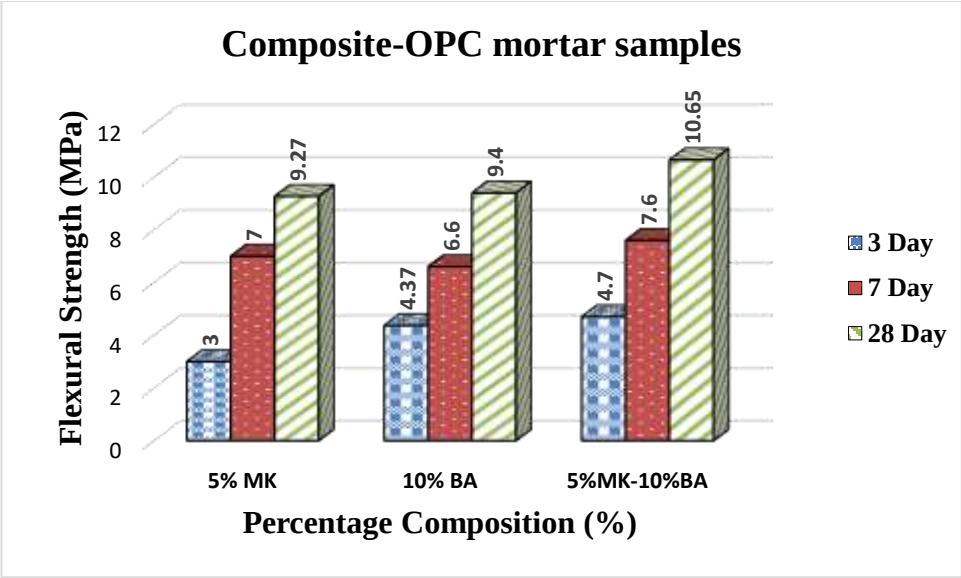

Figure 4.28. Flexural strength of 5% MK, 10% BA, and 5% MK-10% BA

MK–BA OPC demonstrated 49% higher compressive strength than that of control concrete at 28 days (Kumar & Revathi, 2020; Tippayasam et al., 2014). The higher the compressive strength indicates the total consumption of $(CaOH)_2$ and the large formation of Calcium Silicate Hydrates.

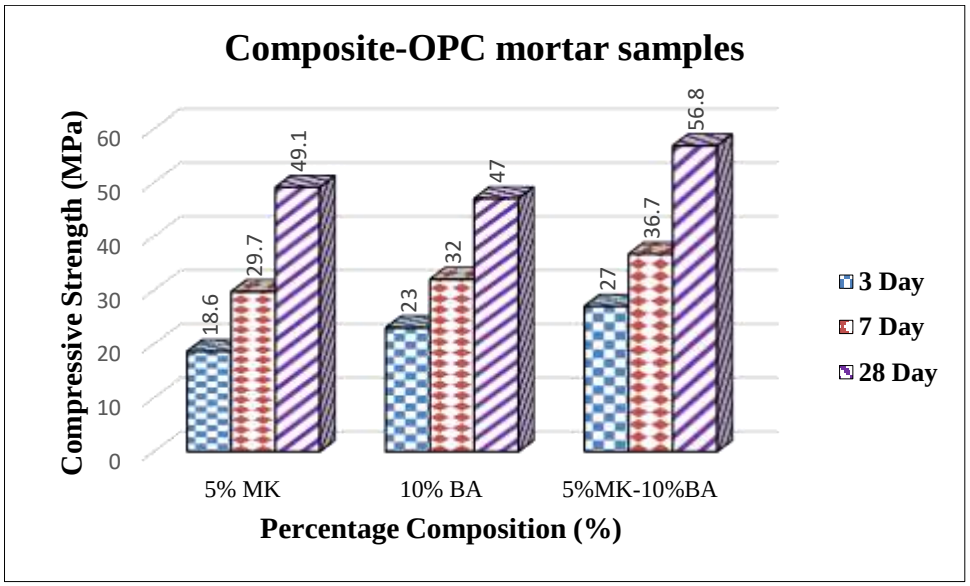

Figure 4.29 Compressive strength of 5% MK, 10% BA, and 5% MK-10% BA

4.3.4 Setting Time and Expansion of MK-BA Blended OPC-Pastes

The setting time of paste is mainly dependent on the amount of tricalcium aluminate. 15% replacement means decreasing the amount of C3A in OPC cement result a delay in conversion of plasticity to solid-state. The initial and final setting times obey the ASTM

standard which is the initial setting time is above 60 min and the final setting time below 600 min. Figure 4.30 show the setting time for the composite formation initial setting time is 142 min and final setting time is 205 min.

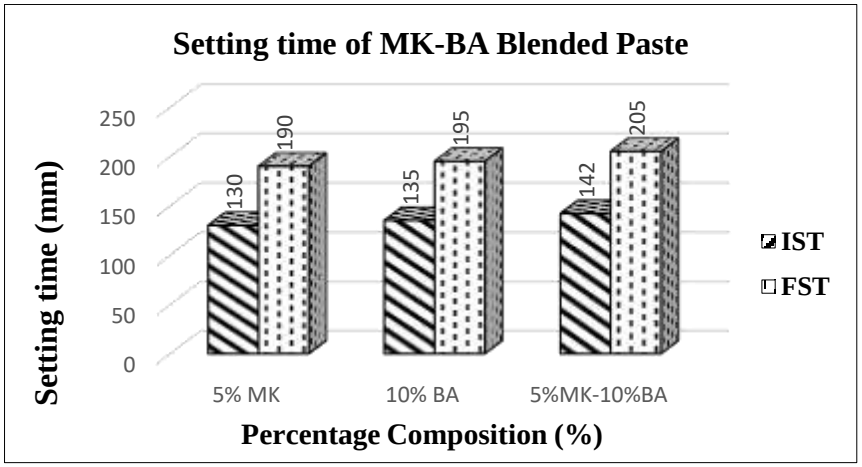

Figure 4.30 Setting times at normal consistency blended pastes

Free lime in hardened concrete is not particularly desirable because it increases the chemical reactivity of the surface (including along cracks) and can leach out in an unsightly fashion. The le-chatiler expansion for the composite blended cement show average of the two. This is due to the amount of free lime decrease in composite blended cement and the probability of forming free $Mg(OH)_2$ decrease due to lower concentration in MK. Another view of decreasing free lime is the indication for the formation of secondary CSH. Figure 4.31 show the reduced expansion with the addition of 5% MK and 10% BA.

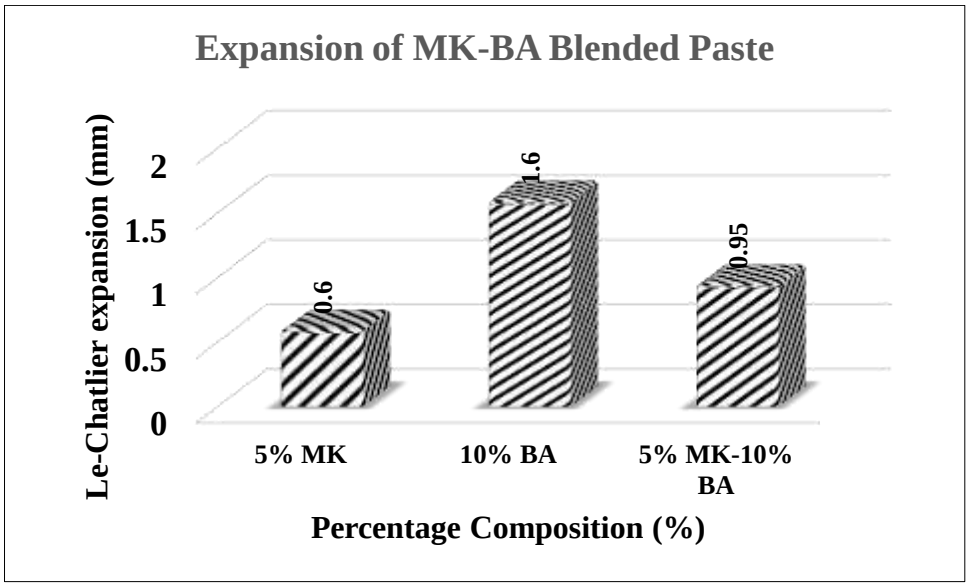

Figure 4.31 Expansion of 5% MK, 10% BA, and MK-BA/OPC Blended Pastes

4.3.5 Water Absorption and Apparent Porosity of MK-BA Blended

It is one of the important properties which influences the strength and durability of the mortar. The mortar with higher water absorption indicates the existence of a porous microstructure (Revathi, 2021). A low percentage of water absorption is a reliable reason for the higher compressive strength of composite mortar. From the test results, it is observed that as the day prolongs the percentage of water absorption is comparatively less because of the fineness and also the density of the composite mortar (figure 4.32 a). Also, it is very well known that in the study, water absorption was much lower, which indicates a high degree of densification (Saravanakumar & Revathi, 2017). Apparent porosity of the composite materials decreases which is the indication of largely pores filled by the finer particle size and pozzolanic activity of Silica helps to form calcium silicate hydrates (CSH).

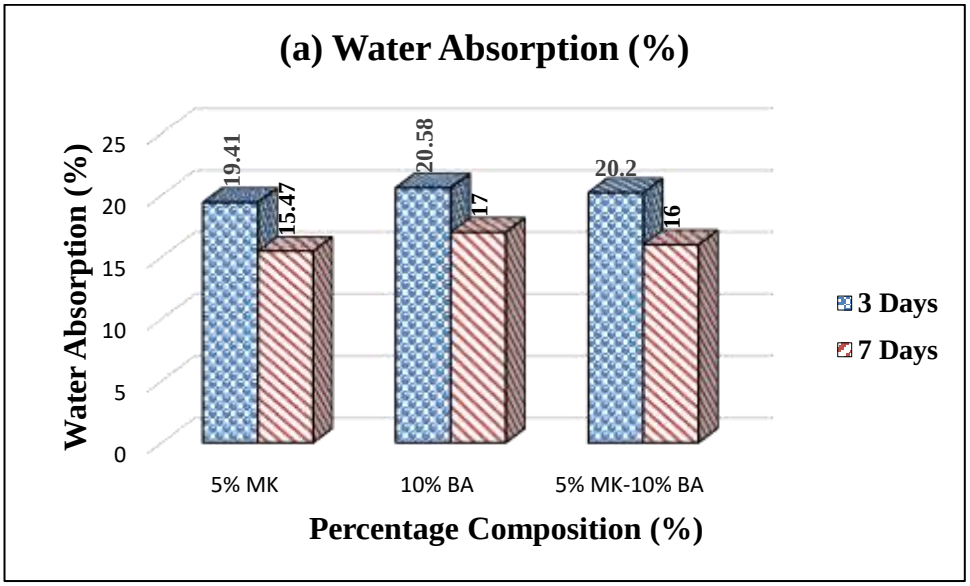

The apparent porosity for the composite show decrement this is the indication of the finer particle size filling the void space. Figure 4.32 b shows the decrease in the percentage of porosity. The possible reason for decreasing the porosity is the formation of densified structure CSH as can be confirmed by XRD results.

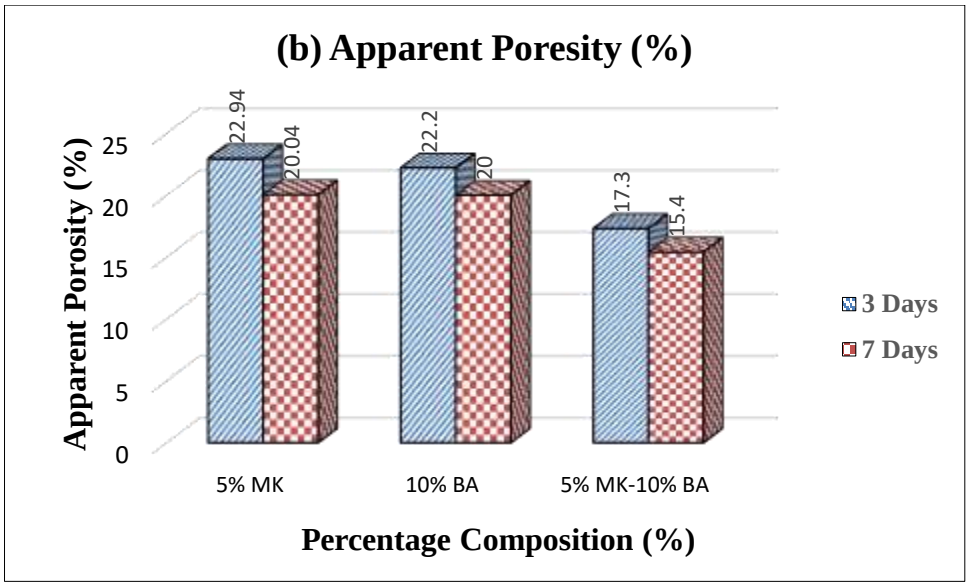

Figure 4.32 Blended OPC-paste; (a) Water absorption; (b) Apparent porosity

4.3.6 Potentiodynamic polarization curve of MK-BA Blended Mortar

A mix containing 5% MK showed the highest polarization resistance and resistivity. the lowest I_{corr}. This can be explained according to the higher binding capacity of MK in paste compared to ordinary paste which exhibited a positive effect on the mortar resistivity due to the formation of CSH gel that leads to a denser and more homogenous matrix. 5% MK shows the highest corrosion potential and the lowest corrosion current density. The result is also supported by previous studies (Nivin M Ahmed et al., 2021; J. Zhang et al., 2020). The chloride ion adversely affects 10% BA compared to 5% MK this is most probably due to the alkaline oxide found in the chemical composition.

Table 4.3 Parametr Obtained from Tafel Plot

Samples	E_{cor} (mV)	I_{corr} (µA/cm^2)	β_c (mV)	β_a (mV)	R_p
OPC	-292.300	3.283	4.140	282.600	0.540
5% MK	-137.500	3.183	91.500	131.300	7.356
10% BA	-231.300	3.596	89.270	135.000	6.489
MK-BA	-171.900	3.301	85.200	125.000	6.666

$$R_p = \frac{\beta_c \times \beta_a}{2.303 I_{corr}(\beta_c + \beta_a)} \quad (4.1)$$

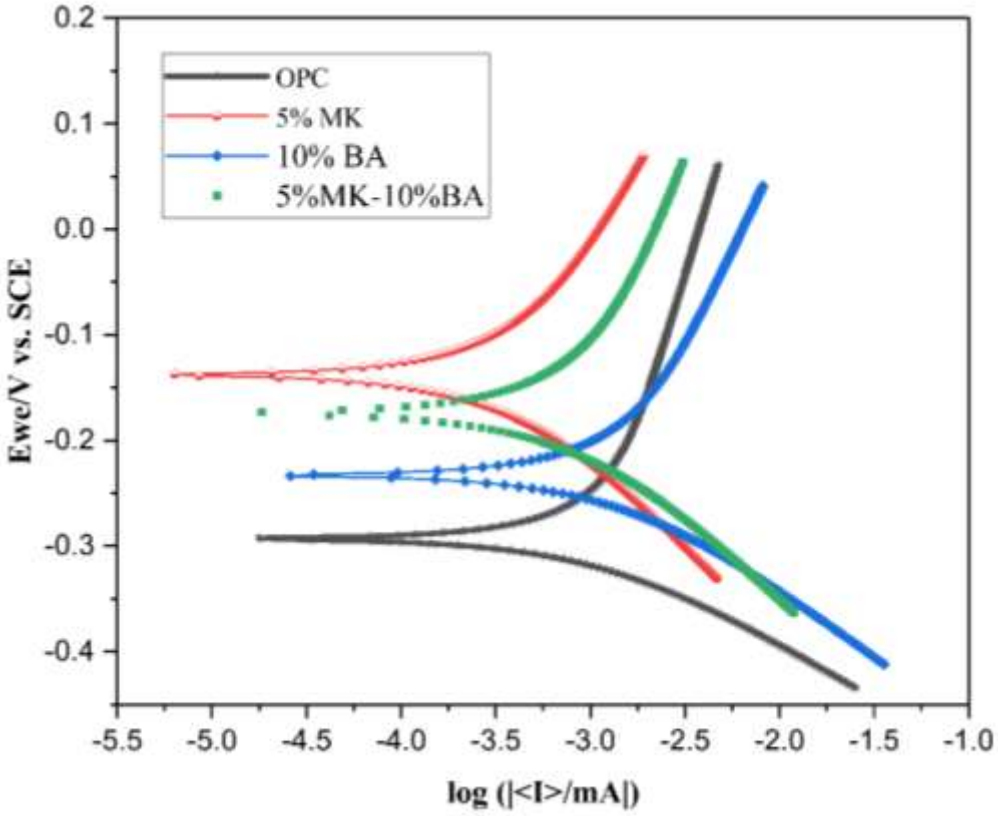

Figure 4.33 Tafel extrapolation plot of different blended mixed cement paste

4.3.7 Microstructure Characterization of Composite Blended Mortar

Figure 4.34 shows the microstructure of the metakaolin and bagasse ash blended paste. From the morphology result, we can see the densified structure due to the higher forms of CSH as Can be seen from XRD results. This is due to the mixed effect of the two most reactive pozzolanic materials.

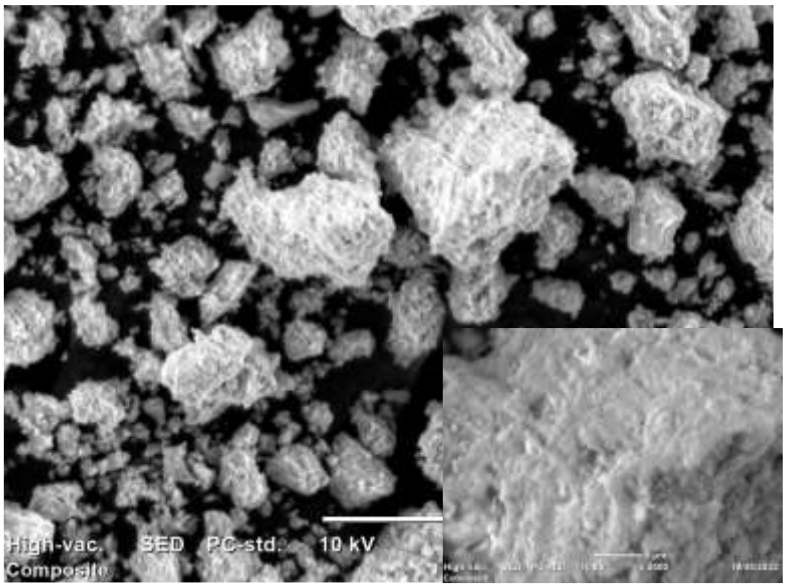

Figure 4.34 SEM image of 5% MK-10% BA blended composite paste

CHAPTER FIVE

5 CONCLUSIONS AND RECOMMENDATION

5.1 Conclusion

The amorphous reactive silica was successfully obtained by the calcination of filter cake (Kaolinite), and bagasse ash (300 ℃) at 600 ℃/2h in a muffle furnace. The synthesized amorphous pozzolanic materials were confirmed by XRF, XRD, FT-IR, TGA/DTA, and SEM. The XRF results show the pozzolanic oxide summation is greater than 70 percent which confirms the required pozzolanic composition. The XRD result for MK and BA shows aboard peaks between 15° and 30°. it confirms the amorphous nature of materials. The three important peak1089 cm^{-1} of Si-O-Si asymmetric stretching, 799 cm^{-1} of Al-O-Si, and 461 cm^{-1} of Si-O bending FT-IR result also another way to confirm the XRF and pozzolanic properties. The pozzolanic material was partially replaced with OPC and resulting in higher compressive strength at 10% MK replacement in all mechanical, physical, and chemical properties. The partially replaced 5% MK shows the best durability in chloride ion solution. So, it is better to use it in a saltwater environment. From the Potentiodynamic result, the 10% BA needs to treat to reduce alkaline.

5.2 Recommendation

The aim of producing partially replaced Metakaolin and Bagasse ash blended composite is to improve the mechanical properties of the individual replacement and to increase the chemical stability of BA replacement. Due to a huge amount of waste bagasse ash existing in a landfill on the open surface. It is also better to make cost analyses and put the use of waste materials to the ground in the practical work.

REFERENCE

Abdelmelek, N., S. Alimrani, N., Krelias, N., & Lubloy, E. (2021). Effect of Elevated Temperatures on Microstructure of High Strength Concrete Based-Metakaolin. *Journal of King Saud University - Engineering Sciences*. https://doi.org/https://doi.org/10.1016/j.jksues.2021.08.001

Abdullah, N., & El-Sokkary, T. (2022). Valorization of siliceous wastes of alum industry as an additive for geopolymer cement.

Adesanya, D., & Raheem, A. (2009). Development of corn cob ash blended cement. *Construction and Building Materials*, *23*(1), 347-352.

Ahmad, S., Wong, Y., & Veloo, K. (2018). Sugarcane bagasse powder as biosorbent for reactive red 120 removals from aqueous solution. IOP Conference Series: Earth and Environmental Science,

Ahmed, N. M., Mossalam, E. A., El-Sabbagh, B., & Souaya, E. M. (2021). Evaluation of synergic methods for corrosion protection of reinforced steel. *Pigment & Resin Technology*.

Ahmed, N. M., Mossalam, E. A., El-Sabbagh, B., & Souaya, E. M. R. (2021). Evaluation of synergic methods for corrosion protection of reinforced steel. *Pigment & Resin Technology*.

Aïtcin, P.-C. (2016). Portland cement. In *Science and Technology of Concrete Admixtures* (pp. 27-51). Elsevier.

Aïtcin, P. C. (2016). 3 - Portland cement. In P.-C. Aïtcin & R. J. Flatt (Eds.), *Science and Technology of Concrete Admixtures* (pp. 27-51). Woodhead Publishing. https://doi.org/https://doi.org/10.1016/B978-0-08-100693-1.00003-5

Akbar, A., Farooq, F., Shafique, M., Aslam, F., Alyousef, R., & Alabduljabbar, H. (2021). Sugarcane bagasse ash-based engineered geopolymer mortar incorporating propylene fibers. *Journal of Building Engineering*, *33*, 101492. https://doi.org/https://doi.org/10.1016/j.jobe.2020.101492

Al-Mansour, A., Chow, C. L., Feo, L., Penna, R., & Lau, D. (2019). Green concrete: By-products utilization and advanced approaches. *Sustainability*, *11*(19), 5145.

Aragaw, T. A., & Kuraz, F. (2018). Physico-chemical characterizations of Ethiopian kaolin for industrial applications: case study WDP propoxur formulations.

Araos Henríquez, P., Aponte, D., Ibáñez-Insa, J., & Barra Bizinotto, M. (2021). Ladle furnace slag as a partial replacement of Portland cement. *Construction and Building Materials*, *289*, 123106. https://doi.org/https://doi.org/10.1016/j.conbuildmat.2021.123106

Arif, E., Clark, M. W., & Lake, N. (2016). Sugar cane bagasse ash from a high efficiency co-generation boiler: Applications in cement and mortar production. *Construction and Building Materials*, *128*, 287-297.

ASTM, C. (2004). 191, Test Method for Time of Setting of Hydraulic Cement by Vicat Needle. *1995 Annual Book of ASTM Standards. Section*, *4*.

Astutiningsih, S., Sura, W., & Zakiyuddin, A. (2018). Comparison of the compressive strength and the microstructure of Metakaolin Metastar and Metakaolin Bangka as Additive in Ordinary Portland Cement.

Bahurudeen, A., Kanraj, D., Dev, V. G., & Santhanam, M. (2015). Performance evaluation of sugarcane bagasse ash blended cement in concrete. *Cement and Concrete Composites*, *59*, 77-88.

Bahurudeen, A., & Santhanam, M. (2015). Influence of different processing methods on the pozzolanic performance of sugarcane bagasse ash. *Cement and Concrete Composites*, *56*, 32-45.

Bahurudeen, A., Wani, K., Basit, M. A., & Santhanam, M. (2016). Assesment of pozzolanic performance of sugarcane bagasse ash. *Journal of Materials in Civil Engineering*, *28*(2), 04015095.

Baltakys, K., Jauberthie, R., Siauciunas, R., & Kaminskas, R. (2007). Influence of modification of SiO2 on the formation of calcium silicate hydrate. *Materials Science-Poland*, *25*(3), 663-670.

Barbhuiya, S., Chow, P., & Memon, S. (2015). Microstructure, hydration and nanomechanical properties of concrete containing metakaolin. *Construction and Building Materials*, *95*, 696-702. https://doi.org/https://doi.org/10.1016/j.conbuildmat.2015.07.101

Barger, G. M., Hulshizer, A. J., Popovics, S., Call, B. M., Jaber, T. M., Prusinski, J., Carrasquillo, R. L., Jensen, J. S., Ravina, D., & Cook, J. E. (2001). Use of Raw or Processed Natural Pozzolans in Concrete. In.

Barger, G. S., Hansen, E. R., Wood, Neary, T., Beech, D. J., & Jaquier, D. (2001). Production and Use of Calcined Natural Pozzolans in Concrete. *Cement Concrete and Aggregates - CEMENT CONCRETE AGGREGATES*, *23*. https://doi.org/10.1520/CCA10478J

Bergold, S., Goetz-Neunhoeffer, F., & Neubauer, J. (2013). Quantitative analysis of C–S–H in hydrating alite pastes by in-situ XRD. *Cement and Concrete Research*, *53*, 119-126.

Bourchy, A., Barnes-Davin, L., Bessette, L., & Torrenti, J. M. (2020). Effect of cement composition on fresh state and heat of hydration of Portland cement with limestone and slag. *ACI Materials Journal*, *117*(1), 153-165.

Bullard, J. W., Jennings, H. M., Livingston, R. A., Nonat, A., Scherer, G. W., Schweitzer, J. S., Scrivener, K. L., & Thomas, J. J. (2011). Mechanisms of cement hydration. *Cement and Concrete Research*, *41*(12), 1208-1223.

Caldarone, M. A., Gruber, K. A., & Burg, R. G. (1994). High reactivity metakaolin (HRM): a new generation mineral admixture for high performance concrete. *Concrete International*, *16*(11), 37-41.

Chen, P., Cao, Z.-f., Wen, X., Wang, J., Yang, F., Qiu, P., Yue, Y.-j., Liu, G.-y., Wang, S., & Zhong, H. (2017). A novel mesoporous silicate material (MS) preparation from dolomite and enhancing methylene blue removal by electronic induction. *Journal of the Taiwan Institute of Chemical Engineers*, *80*, 128-136.

Chindaprasirt, P., Sujumnongtokul, P., & Posi, P. (2019). Durability and mechanical properties of pavement concrete containing bagasse ash. *Materials Today: Proceedings*, *17*, 1612-1626.

Chusilp, N., Jaturapitakkul, C., & Kiattikomol, K. (2009a). Effects of LOI of ground bagasse ash on the compressive strength and sulfate resistance of mortars. *Construction and Building Materials*, *23*(12), 3523-3531.

Chusilp, N., Jaturapitakkul, C., & Kiattikomol, K. (2009b). Utilization of bagasse ash as a pozzolanic material in concrete. *Construction and Building Materials*, *23*(11), 3352-3358.

Cordeiro, G., Toledo Filho, R., & Fairbairn, E. (2009). Effect of calcination temperature on the pozzolanic activity of sugar cane bagasse ash. *Construction and Building Materials*, *23*(10), 3301-3303.

Cordeiro, G. C., Toledo Filho, R. D., & Fairbairn, E. M. R. (2009). Effect of calcination temperature on the pozzolanic activity of sugar cane bagasse ash. *Construction and Building Materials*, *23*(10), 3301-3303.

Cordeiro, G. C., Toledo Filho, R. D., Tavares, L. M., & Fairbairn, E. d. M. R. (2009). Ultrafine grinding of sugar cane bagasse ash for application as pozzolanic admixture in concrete. *Cement and Concrete Research*, *39*(2), 110-115.

Crossin, E. (2015). The greenhouse gas implications of using ground granulated blast furnace slag as a cement substitute. *Journal of Cleaner Production*, *95*, 101-108.

Cyr, M., Trinh, M., Husson, B., & Casaux-Ginestet, G. (2014). Effect of cement type on metakaolin efficiency. *Cement and Concrete Research*, *64*, 63-72.

de A. Mello, L. C., S. dos Anjos, M. A., V. A. de Sá, M. V., S. L. de Souza, N., & de Farias, E. C. (2020). Effect of high temperatures on self-compacting concrete with high levels of sugarcane

bagasse ash and metakaolin. *Construction and Building Materials*, *248*, 118715. https://doi.org/https://doi.org/10.1016/j.conbuildmat.2020.118715

de Oliveira, V. M., de Souza, F., da Cruz, R. T., Py, L. G., Kirchheim, A. P., & Braganca, S. R. (2021). Valorization of non-beneficiated clays as supplementary cementitious materials in the production of cement-based mortar. *Journal of Building Engineering*, *42*, 102474.

Deb, P. S., Nath, P., & Sarker, P. K. (2014). The effects of ground granulated blast-furnace slag blending with fly ash and activator content on the workability and strength properties of geopolymer concrete cured at ambient temperature. *Materials & Design (1980-2015)*, *62*, 32-39.

Deepika, S., Anand, G., Bahurudeen, A., & Santhanam, M. (2017). Construction products with sugarcane bagasse ash binder. *Journal of Materials in Civil Engineering*, *29*(10), 04017189.

Dinakar, P. (2011). High reactive metakaolin for high strength and high performance concrete.

Dinakar, P., Sahoo, P. K., & Sriram, G. (2013). Effect of metakaolin content on the properties of high strength concrete. *International Journal of Concrete Structures and Materials*, *7*(3), 215-223.

Dineshkumar, R., & Balamurugan, P. (2021). Behavior of high-strength concrete with sugarcane bagasse ash as replacement for cement. *Innovative Infrastructure Solutions*, *6*(2), 1-12.

Ding, J.-T., & Li, Z. (2002). Effects of metakaolin and silica fume on properties of concrete. *Materials Journal*, *99*(4), 393-398.

Dunuweera, S. P., & Rajapakse, R. M. G. (2018). Cement Types, Composition, Uses and Advantages of Nanocement, Environmental Impact on Cement Production, and Possible Solutions. *Advances in Materials Science and Engineering*, *2018*, 4158682. https://doi.org/10.1155/2018/4158682

Elsayed, A. (2011). Influence of silica fume, fly ash, super pozz and high slag cement on water permeability and strength of concrete. *Jordan Journal of Civil Engineering*, *5*(2), 245-257.

Embong, R., Shafiq, N., Kusbiantoro, A., & Nuruddin, M. F. (2016). Effectiveness of low-concentration acid and solar drying as pre-treatment features for producing pozzolanic sugarcane bagasse ash. *Journal of Cleaner Production*, *112*, 953-962.

Fairbairn, E. M., Americano, B. B., Cordeiro, G. C., Paula, T. P., Toledo Filho, R. D., & Silvoso, M. M. (2010). Cement replacement by sugar cane bagasse ash: CO2 emissions reduction and potential for carbon credits. *Journal of environmental management*, *91*(9), 1864-1871.

Fapohunda, C., Akinbile, B., & Shittu, A. (2017). Structure and properties of mortar and concrete with rice husk ash as partial replacement of ordinary Portland cement–A review. *International Journal of Sustainable Built Environment*, *6*(2), 675-692.

Fernández, Á., Calvo, J. L. G., & Alonso, M. C. (2018). Ordinary Portland Cement composition for the optimization of the synergies of supplementary cementitious materials of ternary binders in hydration processes. *Cement and Concrete Composites*, *89*, 238-250.

Fernandez, R., Martirena, F., & Scrivener, K. L. (2011). The origin of the pozzolanic activity of calcined clay minerals: A comparison between kaolinite, illite and montmorillonite. *Cement and Concrete Research*, *41*(1), 113-122. https://doi.org/https://doi.org/10.1016/j.cemconres.2010.09.013

Galitsky, C., & Worrell, E. (2008). Energy Efficiency Improvement and Cost Saving Opportunities for Cement Making. An ENERGY STAR Guide for Energy and Plant Managers. *Lawrence Berkeley National Laboratory*.

Ganesan, K., Rajagopal, K., & Thangavel, K. (2007). Evaluation of bagasse ash as supplementary cementitious material. *Cement and concrete composites*, *29*(6), 515-524.

Gao, L., Zheng, Y., Tang, Y., Yu, J., Yu, X., & Liu, B. (2020a). Effect of phosphoric acid content on the microstructure and compressive strength of phosphoric acid-based metakaolin geopolymers. *Heliyon*, *6*(4), e03853.

Gao, L., Zheng, Y., Tang, Y., Yu, J., Yu, X., & Liu, B. (2020b). Effect of phosphoric acid content on the microstructure and compressive strength of phosphoric acid-based metakaolin geopolymers. *Heliyon*, *6*(4). https://doi.org/10.1016/j.heliyon.2020.e03853

Gartner, E. (2004). Industrially interesting approaches to “low-CO2” cements. *Cement and Concrete Research*, *34*(9), 1489-1498.

Givi, A. N., Rashid, S. A., Aziz, F. N. A., & Salleh, M. A. M. (2010). Assessment of the effects of rice husk ash particle size on strength, water permeability and workability of binary blended concrete. *Construction and Building Materials*, *24*(11), 2145-2150.

Gollakota, A. R. K., Volli, V., & Shu, C.-M. (2019). Progressive utilisation prospects of coal fly ash: A review. *Science of the Total Environment*, *672*, 951-989.

Gupta, V. K., Jain, C. K., Ali, I., Chandra, S., & Agarwal, S. (2002). Removal of lindane and malathion from wastewater using bagasse fly ash—a sugar industry waste. *Water research*, *36*(10), 2483-2490.

Hela, R., Tazky, M., & Bodnarova, L. (2016). Possibilities of determination of optimal dosage of power plant fly ash for concrete. *Jurnal Teknologi*, *78*(5-3).

Helsel, M. M. A., Ferraris, C. F., & Bentz, M. D. (2016). Comparative study of methods to measure the density of Cementious powders. *Journal of testing and evaluation*, *44*(6).

Hendriks, C. A., Worrell, E., De Jager, D., Blok, K., & Riemer, P. (1998). Emission reduction of greenhouse gases from the cement industry.

Ibrahim, S., Hagrass, A., Boulos, T. R., Youssef, S., El-Hossiny, F., & Moharam, M. (2018). Metakaolin as an Active Pozzolan for Cement That Improves Its Properties and Reduces Its Pollution Hazard. *Journal of Minerals and Materials Characterization and Engineering*, *06*, 86-104. https://doi.org/10.4236/jmmce.2018.61008

Ibrahim, S. S., Hagrass, A. A., Boulos, T. R., Youssef, S. I., El-Hossiny, F. I., & Moharam, M. R. (2017). Metakaolin as an active pozzolan for cement that improves its properties and reduces its pollution hazard. *Journal of Minerals and Materials Characterization and Engineering*, *6*(1), 86-104.

Jagadesh, P., Ramachandramurthy, A., Murugesan, R., & Sarayu, K. (2015). Micro-Analytical studies on sugar cane bagasse ash. *Sadhana*, *40*(5), 1629-1638.

Jaishankar, P., Murali, G., Salaimanimagudam, M. P., Amran, Y. H. M., Fediuk, R., & Karthikeyan, K. (2021). Study of topology optimized hammerhead pier beam made with novel preplaced aggregate fibrous concrete. *Periodica Polytechnica Civil Engineering*, *65*(1), 287-298.

Jiang, G., Rong, Z., & Sun, W. (2015). Effects of metakaolin on mechanical properties, pore structure and hydration heat of mortars at 0.17 w/b ratio. *Construction and Building Materials*, *93*, 564-572. https://doi.org/https://doi.org/10.1016/j.conbuildmat.2015.06.036

Jo, B. W., Sikandar, M. A., Chakraborty, S., & Baloch, Z. (2017). Strength and durability assessment of portland cement mortars formulated from hydrogen-rich water. *Advances in Materials Science and Engineering*, *2017*.

Jokar, Z., & Mokhtar, A. (2018). Policy making in the cement industry for CO2 mitigation on the pathway of sustainable development-A system dynamics approach. *Journal of Cleaner Production*, *201*, 142-155.

Kabir, H., Hooton, R. D., & Popoff, N. (2020). Evaluation of cement soundness using the ASTM C151 autoclave expansion test. *Cement and Concrete Research*, *136*, 106159.

Kalpokaitė-Dičkuvienė, R., Baltušnikas, A., Levinskas, R., & Čėsnienė, J. (2019). Incinerator residual ash–metakaolin blended cements: effect on cement hydration and properties. *Construction and Building Materials*, *206*, 297-306.

Kasaniya, M., Thomas, M. D. A., & Moffatt, E. G. (2019). Development of rapid and reliable pozzolanic reactivity test method. *ACI Materials Journal*, *116*(4), 145-154.

Kasaniya, M., Thomas, M. D. A., & Moffatt, E. G. (2021a). Efficiency of natural pozzolans, ground glasses and coal bottom ashes in mitigating sulfate attack and alkali-silica reaction. *Cement and Concrete Research*, *149*, 106551. https://doi.org/https://doi.org/10.1016/j.cemconres.2021.106551

Kasaniya, M., Thomas, M. D. A., & Moffatt, E. G. (2021b). Pozzolanic reactivity of natural pozzolans, ground glasses and coal bottom ashes and implication of their incorporation

on the chloride permeability of concrete. *Cement and Concrete Research*, *139*, 106259. https://doi.org/https://doi.org/10.1016/j.cemconres.2020.106259

Katare, V. D., & Madurwar, M. V. (2017). Experimental characterization of sugarcane biomass ash–A review. *Construction and Building Materials*, *152*, 1-15.

Khan, M. I., Khan, H. U., Azizli, K., Sufian, S., Man, Z., Siyal, A. A., Muhammad, N., & ur Rehman, M. F. (2017). The pyrolysis kinetics of the conversion of Malaysian kaolin to metakaolin. *Applied Clay Science*, *146*, 152-161.

Khatib, J. M., Baalbaki, O., & ElKordi, A. A. (2018). 15 - Metakaolin. In R. Siddique & P. Cachim (Eds.), *Waste and Supplementary Cementitious Materials in Concrete* (pp. 493-511). Woodhead Publishing. https://doi.org/https://doi.org/10.1016/B978-0-08-102156-9.00015-8

Koutnik, P., Soukup, A., Bezucha, P., Šafář, J., Hájková, P., & Čmelík, J. (2019). Comparison of kaolin and kaolinitic claystones as raw materials for preparing meta-kaolinite-based geopolymers. *Ceramics–Silikáty*, *63*(1), 110-123.

Kumar, A., & Lingfa, P. (2020). Sodium bentonite and kaolin clays: Comparative study on their FT-IR, XRF, and XRD. *Materials Today: Proceedings*, *22*, 737-742. https://doi.org/https://doi.org/10.1016/j.matpr.2019.10.037

Kumar, M. L., & Revathi, V. (2020). Microstructural Properties of Alkali-Activated Metakaolin and Bottom Ash Geopolymer. *Arabian Journal for Science and Engineering*, *45*(5), 4235-4246. https://doi.org/10.1007/s13369-020-04417-6

Kumar, R., & Dhaka, J. (2016). Review paper on partial replacement of cement with silica fume and its effects on concrete properties. *International Journal for Technological Research in Engineering*, *4*(1).

Lagier, F., & Kurtis, K. E. (2007). Influence of Portland cement composition on early age reactions with metakaolin. *Cement and Concrete Research*, *37*(10), 1411-1417.

Larissa, C. d. A., dos Anjos, M. A., de Sá, M. V., de Souza, N. S., & de Farias, E. C. (2020). Effect of high temperatures on self-compacting concrete with high levels of sugarcane bagasse ash and metakaolin. *Construction and Building Materials*, *248*, 118715.

Le, D.-H., Sheen, Y.-N., & Lam, M. N.-T. (2018). Fresh and hardened properties of self-compacting concrete with sugarcane bagasse ash–slag blended cement. *Construction and Building Materials*, *185*, 138-147.

Li, G. (2004). Properties of high-volume fly ash concrete incorporating nano-SiO2. *Cement and Concrete Research*, *34*(6), 1043-1049.

Li, L., Zhang, Y., Liu, Y., & Ling, T.-C. (2022). Upcycling coal-and soft-series metakaolin in blended cement with limestone. *Construction and Building Materials*, *327*, 126965.

Lima, S. A., Sales, A., Almeida, F. d. C. R., Moretti, J. P., & Portella, K. F. (2011). Concretes made with sugarcane bagasse ash: evaluation of the durability for carbonation and abrasion tests. *Ambiente Construído*, *11*, 201-212.

Lothenbach, B., Scrivener, K., & Hooton, R. D. (2011). Supplementary cementitious materials. *Cement and Concrete Research*, *41*(12), 1244-1256. https://doi.org/https://doi.org/10.1016/j.cemconres.2010.12.001

Malagavelli, V., Angadi, S., Prasad, J. S. R., & Joshi, S. (2018). Influence of metakaolin in concrete as partial replacement of cement. *Int J Civil Eng Technol*, *9*(7), 105-111.

Maliger, V. R., Doherty, W. O., Frost, R. L., & Mousavioun, P. (2011). Thermal decomposition of bagasse: effect of different sugar cane cultivars. *Industrial & engineering chemistry research*, *50*(2), 791-798.

MESERET, M. T. INVESTIGATION ON QUALITY CONTROL FOR CONCRETE MAKING MATERIALS USED IN COST EFFICIENT HOUSING PROJECT.

Meyer, C. (2009). The greening of the concrete industry. *Cement and concrete composites*, *31*(8), 601-605.

Mobili, A., Belli, A., Giosuè, C., Bellezze, T., & Tittarelli, F. (2016). Metakaolin and fly ash alkali-activated mortars compared with cementitious mortars at the same strength class.

Cement and Concrete Research, *88*, 198-210. https://doi.org/https://doi.org/10.1016/j.cemconres.2016.07.004

Mohd Nasir, N. A., Abu Bakar, N., Safiee, N. A., & Abdul Aziz, F. N. A. (2021). Permeation-durability properties of metakaolin blended concrete containing rubber. *European Journal of Environmental and Civil Engineering*, 1-16. https://doi.org/10.1080/19648189.2021.1885499

Mohomane, S. M., Motaung, T. E., & Revaprasadu, N. (2017). Thermal Degradation Kinetics of Sugarcane Bagasse and Soft Wood Cellulose. *Materials (Basel, Switzerland)*, *10*(11), 1246. https://doi.org/10.3390/ma10111246

Motahari Karein, S. M., Ramezanianpour, A. A., Ebadi, T., Isapour, S., & Karakouzian, M. (2017). A new approach for application of silica fume in concrete: Wet granulation. *Construction and Building Materials*, *157*, 573-581. https://doi.org/https://doi.org/10.1016/j.conbuildmat.2017.09.132

Moumin, G., Ryssel, M., Zhao, L., Markewitz, P., Sattler, C., Robinius, M., & Stolten, D. (2020). CO2 emission reduction in the cement industry by using a solar calciner. *Renewable energy*, *145*, 1578-1596.

Nadeem, A., Memon, S. A., & Lo, T. Y. (2013). Mechanical performance, durability, qualitative and quantitative analysis of microstructure of fly ash and Metakaolin mortar at elevated temperatures. *Construction and Building Materials*, *38*, 338-347. https://doi.org/https://doi.org/10.1016/j.conbuildmat.2012.08.042

Narmluk, M., & Nawa, T. (2011). Effect of fly ash on the kinetics of Portland cement hydration at different curing temperatures. *Cement and Concrete Research*, *41*(6), 579-589.

Nasir, M., & Al-Kutti, W. (2018). Performance of date palm ash as a cementitious material by evaluating strength, durability, and characterization. *Buildings*, *9*(1), 6.

Nežerka, V., Slížková, Z., Tesárek, P., Plachý, T., Frankeová, D., & Petráňová, V. (2014). Comprehensive study on mechanical properties of lime-based pastes with additions of metakaolin and brick dust. *Cement and Concrete Research*, *64*, 17-29. https://doi.org/https://doi.org/10.1016/j.cemconres.2014.06.006

Nicoara, A. I., Stoica, A. E., Vrabec, M., Šmuc Rogan, N., Sturm, S., Ow-Yang, C., Gulgun, M. A., Bundur, Z. B., Ciuca, I., & Vasile, B. S. (2020). End-of-life materials used as supplementary cementitious materials in the concrete industry. *Materials*, *13*(8), 1954.

Norsuraya, S., Fazlena, H., & Norhasyimi, R. (2016). Sugarcane bagasse as a renewable source of silica to synthesize Santa Barbara Amorphous-15 (SBA-15). *Procedia engineering*, *148*, 839-846.

Ou, Z. H., Ma, B. G., & Jian, S. W. (2011). Comparison of FT-IR, thermal analysis and XRD for determination of products of cement hydration. Advanced Materials Research,

Panda, L., Rath, S. S., Rao, D. S., Nayak, B. B., Das, B., & Misra, P. K. (2018). Thorough understanding of the kinetics and mechanism of heavy metal adsorption onto a pyrophyllite mine waste based geopolymer. *Journal of Molecular Liquids*, *263*, 428-441.

Panesar, D. K. (2019). 3 - Supplementary cementing materials. In S. Mindess (Ed.), *Developments in the Formulation and Reinforcement of Concrete (Second Edition)* (pp. 55-85). Woodhead Publishing. https://doi.org/https://doi.org/10.1016/B978-0-08-102616-8.00003-4

Papadakis, V., & Tsimas, S. (2002). Supplementary cementing materials in concrete: Part I: efficiency and design. *Cement and Concrete Research*, *32*(10), 1525-1532.

Pinheiro, D. d. R., Gonçalves, L. R., Sena, R. L. P. d., Martelli, M. C., Neves, R. d. F., & Ribeiro, N. F. d. P. (2020). Industrial kaolin waste as raw material in the synthesis of the SAPO-34 molecular sieve. *Materials Research*, *23*.

Pintér, F., & Gosselin, C. (2018). The origin, composition and early age hydration mechanisms of Austrian natural Portland cement. *Cement and Concrete Research*, *110*, 1-12.

Poon, C.-S., Kou, S. C., & Lam, L. (2006). Compressive strength, chloride diffusivity and pore structure of high performance metakaolin and silica fume concrete. *Construction and Building Materials*, *20*(10), 858-865.

Praveenkumar, S., & Sankarasubramanian, G. (2019). Mechanical and durability properties of bagasse ash-blended high-performance concrete. *SN Applied Sciences*, *1*(12), 1-7.

Priya, K. L., & Ragupathy, R. (2016). Effect of sugarcane bagasse ash on strength properties of concrete. *Int. J. Res. Eng. Technol*, *5*(4), 159-164.

Qian, X., & Li, Z. (2001). The relationships between stress and strain for high-performance concrete with metakaolin. *Cement and Concrete Research*, *31*(11), 1607-1611.

Qian, X., Wang, J., Wang, L., & Fang, Y. (2019). Enhancing the performance of metakaolin blended cement mortar through in-situ production of nano to sub-micro calcium carbonate particles. *Construction and Building Materials*, *196*, 681-691. https://doi.org/https://doi.org/10.1016/j.conbuildmat.2018.11.134

Ramezanianpour, A. A., & Jovein, H. B. (2012). Influence of metakaolin as supplementary cementing material on strength and durability of concretes. *Construction and Building Materials*, *30*, 470-479.

Rashad, A. M. (2013). Metakaolin as cementitious material: History, scours, production and composition–A comprehensive overview. *Construction and Building Materials*, *41*, 303-318.

Raslan, H. A., Fathy, E. S., & Mohamed, R. M. (2018). Effect of gamma irradiation and fiber surface treatment on the properties of bagasse fiber-reinforced waste polypropylene composites. *International Journal of Polymer Analysis and Characterization*, *23*(2), 181-192.

Ravina, D., & Mehta, P. K. (1986). Properties of fresh concrete containing large amounts of fly ash. *Cement and Concrete Research*, *16*(2), 227-238.

Revathi, V. (2021). Durability studies in alkaline activated systems (metakaolin–bottom ash): A prospective study. *Boletín de la Sociedad Española de Cerámica y Vidrio*.

Rimaz, S., Kosari, M., Zarinejad, M., & Ramakrishna, S. (2022). A comprehensive review on sustainability-motivated applications of SAPO-34 molecular sieve. *Journal of Materials Science*, 1-39.

Rukzon, S., & Chindaprasirt, P. (2012). Utilization of bagasse ash in high-strength concrete. *Materials & Design*, *34*, 45-50. https://doi.org/https://doi.org/10.1016/j.matdes.2011.07.045

Saafan, M. A., Etman, Z. A., & El lakany, D. M. (2021). Microstructure and Durability of Ground Granulated Blast Furnace Slag Cement Mortars. *Iranian Journal of Science and Technology, Transactions of Civil Engineering*, *45*(3), 1457-1465. https://doi.org/10.1007/s40996-020-00533-3

Sabir, B. (1995). High-strength condensed silica fume concrete. *Magazine of Concrete Research*, *47*(172), 219-226.

Sabir, B., Wild, S., & Bai, J. (2001). Metakaolin and calcined clays as pozzolans for concrete: a review. *Cement and Concrete Composites*, *23*(6), 441-454.

Sabir, B. B., Wild, S., & Bai, J. (2001). Metakaolin and calcined clays as pozzolans for concrete: a review. *Cement and concrete composites*, *23*(6), 441-454. https://doi.org/https://doi.org/10.1016/S0958-9465(00)00092-5

Saillio, M., Baroghel-Bouny, V., Pradelle, S., Bertin, M., Vincent, J., & de Lacaillerie, J.-B. d. E. (2021). Effect of supplementary cementitious materials on carbonation of cement pastes. *Cement and Concrete Research*, *142*, 106358.

Sales, A., & Lima, S. A. (2010). Use of Brazilian sugarcane bagasse ash in concrete as sand replacement. *Waste management*, *30*(6), 1114-1122.

Saravanakumar, R., & Revathi, V. (2017). Some durability aspects of ambient cured bottom ash geopolymer concrete. *Archives of Civil Engineering*, *63*(3).

Schwanke, A. J., Silveira, D. R., Puton, B. M. S., Cansian, R. L., & Bernardo-Gusmão, K. (2022). Sustainable conversion of Brazilian Amazon kaolin mining waste to zinc-based Linde Type A zeolites with antibacterial activity. *Journal of Cleaner Production*, 130659.

Segura, J. C. F., Cruz, V. E. R., Bueno, J. d. J. P., Ascencio, E. M. L., & García, F. L. (2017). Characterization and electrochemical treatment of a kaolin. *Applied Clay Science*, *146*, 264-269.

Sekhar, D. C., & Nayak, S. (2018). Utilization of granulated blast furnace slag and cement in the manufacture of compressed stabilized earth blocks. *Construction and Building Materials*, *166*, 531-536.

Seyoum, R., Tesfamariam, B. B., Andoshe, D. M., Algahtani, A., Ahmed, G. M. S., & Tirth, V. (2021). Investigation on Control Burned of Bagasse Ash on the Properties of Bagasse Ash-Blended Mortars. *Materials*, *14*(17), 4991.

Shreyas, K. (2017). Characteristics of GGBS as an alternate material in conventional concrete. *Int J Creat Res Thoughts (IJCRT)*, *5*(4), 3174-3184.

Siddique, R. (2011). Utilization of silica fume in concrete: Review of hardened properties. *Resources, Conservation and Recycling*, *55*(11), 923-932. https://doi.org/https://doi.org/10.1016/j.resconrec.2011.06.012

Singh, N., Singh, V., & Rai, S. (2000). Hydration of bagasse ash-blended portland cement. *Cement and Concrete Research*, *30*(9), 1485-1488.

Soler, J. M. (2007). Thermodynamic description of the solubility of CSH gels in hydrated Portland cement. Literature review.

Song, H.-W., Pack, S.-W., Nam, S.-H., Jang, J.-C., & Saraswathy, V. (2010). Estimation of the permeability of silica fume cement concrete. *Construction and Building Materials*, *24*(3), 315-321.

Souri, A., Golestani-Fard, F., Naghizadeh, R., & Veiseh, S. (2015). An investigation on pozzolanic activity of Iranian kaolins obtained by thermal treatment. *Applied Clay Science*, *103*, 34-39. https://doi.org/https://doi.org/10.1016/j.clay.2014.11.001

Standard, A. (2015). Standard test methods for apparent porosity, water absorption, apparent specific gravity, and bulk density of burned refractory brick and shapes by boiling water. *West Conshohocken, PA.: ASTM C20-00*.

Subedi, S., Arce, G., Hassan, M., Kumar, N., Barbato, M., & Gutierrez-Wing, M. T. (2019). Influence of Production Methodology on the Pozzolanic Activity of Sugarcane Bagasse Ash. *MATEC Web Conf.*, *271*, 07003. https://doi.org/10.1051/matecconf/201927107003

Sun, J., Sun, X., Zhao, H., & Sun, R. (2004). Isolation and characterization of cellulose from sugarcane bagasse. *Polymer degradation and stability*, *84*(2), 331-339.

Tan, H., Nie, K., He, X., Deng, X., Zhang, X., Su, Y., & Yang, J. (2019). Compressive strength and hydration of high-volume wet-grinded coal fly ash cementitious materials. *Construction and Building Materials*, *206*, 248-260.

Tang, Y.-J., Zuo, X.-B., Yin, G.-J., He, S.-L., & Ayinde, O. (2017). Influence of slag on leaching behavior of cement mortar lined in ductile iron pipe under a flowing solution. *Materials & Design*, *114*, 612-622. https://doi.org/https://doi.org/10.1016/j.matdes.2016.11.096

Tawfik, T. A., Metwally, K. A., Zaki, W., & Faried, A. S. (2019). Hybrid effect of nanosilica and metakaolin on mechanical properties of cement mortar. *Int. J. Eng. Res. Technol*, *8*(3).

Tech, J. E. T. (2019). Utilization Potential of Waste from Sugarcane Factory of Bangladesh as Partial Replacement of Cement in Concrete. *Journal of Environmental Treatment Techniques*, *7*(1), 109-112.

Tekleab, A. M. (2016). *Analyzing Social Responsibility Towards Improving Labor Practice Issues in Ethiopia-A Focus on Metahara Sugar Factory* NTNU].

Testing, A. S. f., & Materials. (2012). ASTM C 618-Standard specification for coal fly ash and raw or calcined natural pozzolan for use in concrete.

Thomas, M. (2007). *Optimizing the use of fly ash in concrete* (Vol. 5420). Portland Cement Association Skokie, IL.

Tippayasam, C., Keawpapasson, P., Thavorniti, P., Panyathanmaporn, T., Leonelli, C., & Chaysuwan, D. (2014). Effect of Thai Kaolin on properties of agricultural ash blended geopolymers. *Construction and Building Materials*, *53*, 455-459. https://doi.org/https://doi.org/10.1016/j.conbuildmat.2013.11.079

Topçu, İ. B., & Ünverdi, A. (2017). Properties of high content ground granulated blast furnace slag concrete.

Trifunovic, P. D., Marinkovic, S. R., Tokalic, R. D., & Matijasevic, S. D. (2010). The effect of the content of unburned carbon in bottom ash on its applicability for road construction. *Thermochimica acta*, *498*(1-2), 1-6.

Tripathi, D., Kumar, R., Mehta, P. K., & Singh, A. (2020). Silica fume mixed concrete in acidic environment. *Materials Today: Proceedings*, *27*, 1001-1005. https://doi.org/https://doi.org/10.1016/j.matpr.2020.01.311

Turner, L. K., & Collins, F. G. (2013). Carbon dioxide equivalent (CO2-e) emissions: A comparison between geopolymer and OPC cement concrete. *Construction and building materials*, *43*, 125-130.

Varma, D., Garikipati, V., Raju, P., & Kumar, M. P. (2019). *Compressive strength and durability of Metakaolin blended concrete exposed to acid and sulphate attack* (Vol. 1025). https://doi.org/10.1088/1757-899X/1025/1/012004

Wang, H., Li, C., Peng, Z., & Zhang, S. (2011). Characterization and thermal behavior of kaolin. *Journal of Thermal Analysis and Calorimetry*, *105*(1), 157-160.

Wang, H., Li, H., & Yan, F. (2005). Synthesis and mechanical properties of metakaolinite-based geopolymer. *Colloids and Surfaces A: Physicochemical and Engineering Aspects*, *268*(1), 1-6. https://doi.org/https://doi.org/10.1016/j.colsurfa.2005.01.016

Wen, Q., Yu, Z., & Riedel, R. (2020). The fate and role of in situ formed carbon in polymer-derived ceramics. *Progress in Materials Science*, *109*, 100623.

Wild, S., Khatib, J. M., & Jones, A. (1996). Relative strength, pozzolanic activity and cement hydration in superplasticised metakaolin concrete. *Cement and Concrete Research*, *26*(10), 1537-1544.

Worrell, E., Price, L., Martin, N., Hendriks, C., & Meida, L. O. (2001). Carbon dioxide emissions from the global cement industry. *Annual review of energy and the environment*, *26*(1), 303-329.

Yager, T. R. (2010). The Mineral Industry of Ethiopia. *Minerals Yearbook*, *3*, 13.

Yao, Z. T., Ji, X. S., Sarker, P. K., Tang, J. H., Ge, L. Q., Xia, M. S., & Xi, Y. Q. (2015). A comprehensive review on the applications of coal fly ash. *Earth-Science Reviews*, *141*, 105-121.

Yu, L., Zhou, S., & Ou, H. (2015). Determining the pozzolanic activity component of volcanic rock. *Materials Research Innovations*, *19*(sup8), S8-881-S888-888. https://doi.org/10.1179/1432891715Z.0000000001830

Yu, P., Kirkpatrick, R. J., Poe, B., McMillan, P. F., & Cong, X. (1999). Structure of calcium silicate hydrate (C-S-H): Near-, Mid-, and Far-infrared spectroscopy. *Journal of the American Ceramic Society*, *82*(3), 742-748.

Zareei, S. A., Ameri, F., & Bahrami, N. (2018). Microstructure, strength, and durability of eco-friendly concretes containing sugarcane bagasse ash. *Construction and Building Materials*, *184*, 258-268.

Zemri, C., & Bachir Bouiadjra, M. (2020). Comparison between physical–mechanical properties of mortar made with Portland cement (CEMI) and slag cement (CEMIII) subjected to elevated temperature. *Case Studies in Construction Materials*, *12*, e00339. https://doi.org/https://doi.org/10.1016/j.cscm.2020.e00339

Zhang, J., Yang, J., & Ying, Z. (2020). Study on Mechanical Properties of Metakaolin-Based Concretes and Corrosion of Carbon Steel Reinforcement in 3.5% NaCl. *Int. J. Electrochem. Sci*, *15*, 2883-2893.

Zhang, P., Liao, W., Kumar, A., Zhang, Q., & Ma, H. (2020). Characterization of sugarcane bagasse ash as a potential supplementary cementitious material: Comparison with coal combustion fly ash. *Journal of Cleaner Production*, *277*, 123834.

Zhao, D., & Khoshnazar, R. (2020). Microstructure of cement paste incorporating high volume of low-grade metakaolin. *Cement and concrete composites*, *106*, 103453. https://doi.org/https://doi.org/10.1016/j.cemconcomp.2019.103453

Zhao, S., & Zhang, Q. (2019). Effect of Silica Fume in Concrete on Mechanical Properties and Dynamic Behaviors under Impact Loading. *Materials*, *12*(19), 3263. https://www.mdpi.com/1996-1944/12/19/3263

Zheng, Q., Jiang, J., Xu, G., Yu, J., Tang, L., & Li, S. (2020). New Insights into the Role of Portlandite in the Cement System: Elastic Anisotropy, Thermal Stability, and Structural Compatibility with C-S-H. *Crystal Growth & Design*, *20*(4), 2477-2488. https://doi.org/10.1021/acs.cgd.9b01644

Acknowledgments: This research thesis was funded by Adama Science and Technology University under the grant number of ASTU/SM- R/436/22, Adama, Ethiopia.

Appendix

Blended cement pastes for Potentiodynamic test

Humudity curing cabinet

curing room

Mortar under curing condition

3 hr boiling water bath

Mortar under mixing

0.5 water to cement ratio

Mortar sample to select the best proportion of Composite formation

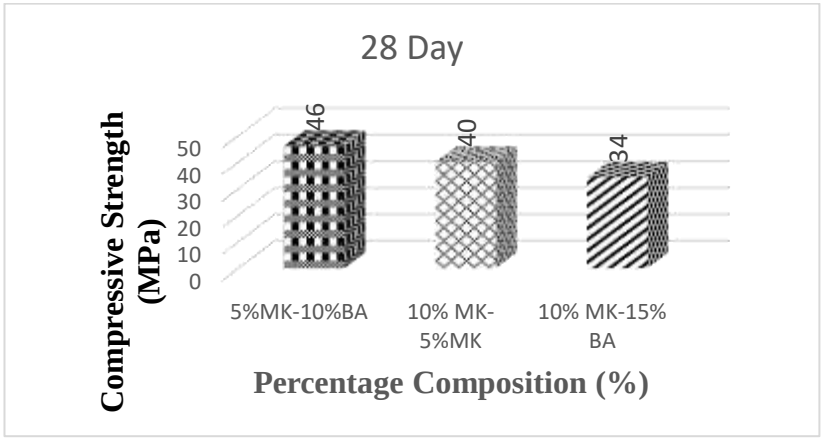

3.5% NaCl solution blended cement paste cured